Dark Energy and Modified Theories of Gravity

Nelson Daniel de Aguiar Lima

Doctor of Philosophy
The University of Edinburgh
November 2016

Abstract

It is now a consolidated fact that our Universe is undergoing an accelerated expansion. According to Einstein's General Relativity, if the main constituents of our Universe were ordinary and cold dark matter, then we would expect it to be contracting and collapsing due to matter's attractive nature. The simplest explanation we have for this acceleration is in the form of a component with a negative ratio of pressure to density equal to -1 known as cosmological constant, Λ, presently dominating over baryonic and cold dark matter.

However, the Λ Cold Dark Matter (ΛCDM) model suffers from a well known fine-tuning problem. This led to the formulation of dark energy and modified gravity theories as alternatives to the problem of cosmic acceleration. These theories either include additional degrees of freedom, higher-order equations of motion, extra dimensionalities or imply non-locality.

In this thesis we focus on single field scalar tensor theories embedded within Horndeski gravity. Even though there is currently doubt on their ability to explain cosmic acceleration without having a bare cosmological constant on their action, the degree of freedom they introduce mediates an additional fifth force. And while this force has to suppressed on Solar system scales, it can have interesting and observable effects on cosmological scales.

Over the next decade there is a surge of surveys that will improve the understanding of our Universe on the largest scales. Hence, in this work, we take several different modified gravity theories and study their impact on cosmological observables. We will analyze the dynamics of linear perturbations on these theories and clearly highlight how they deviate from ΛCDM, allowing to break the degeneracy at the background level. We will also study the evolution of the gravitational potentials on sub horizon scales and provide simplified expressions at this regime and, for some models, obtain constraints using the latest data.

Declaration

I declare that this thesis was composed by myself, that the work contained herein is my own except where explicitly stated otherwise in the text, and that this work has not been submitted for any other degree or professional qualification except as specified.

Parts of this work have been published in [1].

Parts of this work have been published in [2].

Parts of this work have been published in [3].

Parts of this work have been published in [4].

Parts of this work have been published in [5].

(*Nelson Daniel de Aguiar Lima, November 2016*)

Acknowledgements

Mom and Dad, first and foremost, thank you. I could not be prouder of the parents I have been blessed with. Without your love, infinite support and sacrifice I would not have had the opportunities that led to this. Amo-vos.

Ana, my everything and the person who fascinates me more than the Universe ever will. Amo-te.

Andrew, much more than my supervisor, you were my counselor and colleague throughout this journey, and there was never a time you did not have the right words for me. You have always guided me in the right direction while giving me the freedom to grow as an independent researcher. Thank you for believing in me and let me be your student. It was an honor.

Vanessa, my dear colleague and friend, these four years were a battle made easier with your support. Having you experiencing the same maddening hurdles and help me push through them definitely helped my sanity. Thank you.

Lucas, thank you so much for your help through these last stages of the PhD. You are never short of ideas, and your kind words and guidance were invaluable.

Guinness, my buddy, for always putting a smile on my face.

Lastly, I want to thank the Fundação para a Ciência e Tecnologia for providing me with the financial support that made this work possible.

Contents

List of Figures

List of Tables

Chapter 1

Introduction to general relativity

The theory of general relativity (GR) is, without question, one of the most complex and revolutionary mathematical formulations of the 20th century, being initially understood only by a handful of people. It is the product of the ingenious mind of Albert Einstein, who published it in 1916 [6], establishing itself the ultimate theory of gravitation during the 100 years that have passed since its publication.

Achieving this was no easy task, and the laborious work of Einstein had one particular objective in mind: to obtain a field equation that would relate the distribution of the gravitational source with the corresponding relativistic gravitational field or, in other words, the development of the relativistic generalization of the well known Newtonian Equation

$$\nabla^2\Phi = 4\pi G_{\rm N}\rho_{\rm m}. \tag{1.1}$$

Newtonian theory suffices to describe systems in which the gravitational interaction is weak and the relativistic effects negligible. However, when the focus of our study are very dense systems such as neutron stars, or extremely massive ones, like the whole of our Universe, then a relativistic approach is necessary. A way to have an estimate of the scale at which the relativistic effects become relevant is to take the ratio between the classical gravitational energy induced by a spherically symmetric source over a test object of mass $m_{\rm G}$ and its relativistic rest mass energy $m_{\rm I}c^2$

$$\frac{m_{\rm G}\Phi}{m_{\rm I}c^2} = \frac{G_{\rm N}M}{c^2 r} \tag{1.2}$$

where Φ is the gravitational potential produced by the mentioned source of mass M and radius r. When this ratio approaches unity Newtonian theory breaks down and General Relativity becomes necessary.

Note that, in Eq. (1.2), we have assumed an equality between a body's gravitational and inertial mass. This is the cornestorne of the Newtonian law of gravitation, according to which the acceleration produced by a gravitational source will simply be given by $\vec{a} = -\nabla\Phi$. Hence, the behavior of two free-falling test bodies (that are not acted upon by such forces as electromagnetism or are too small to be affected by tidal gravitational forces) should be the same independent of their composition. This is known as the weak equivalence principle (WP).

This principle became one of the pillars of Einstein's general relativity and the universality of gravitation, as he argued that one should not be able to distinguish between the effects of being in a gravitational field or in a frame of reference with constant acceleration (far from any massive sources). Hence, the Einstein equivalence principle (EEP) was born, as he postulated that the outcome of any non-gravitational experiment should be independent of when and where these were conducted, and the laws of physics in a freely-falling frame should be those of special relativity in an inertial frame.

In the context of special relativity (SR), mass is nothing more than an organized form of energy, corresponding to the rest energy of an object. This is translated in the iconic equation $E = \gamma m_0 c^2$, where γ is the Lorentz factor, c is the frame-invariant light velocity and m_0 is the rest mass of the object. Under this criteria, one could make the assumption that the simplest relativistic generalization of the newtonian field equation would be replacing the classical source of the gravitational field, $\rho_{\rm m}$, by the total energy density of the source, ρ.

However, what one learns from special relativity is that energy and momentum come up as being equivalent, since they can be transformed into each other according to generic Lorentz transformations when measured by different observers. Therefore, in GR and SR, they end up constituting a very important rank-two tensor, the energy-momentum or stress-energy tensor, T. Hence, in order to construct a frame invariant theory that does not favor a particular frame or observer over any other, one has to consider the whole energy-momentum tensor as the source of the gravitational field in the relativistic approach to Eq. 1.1.

The iconic Einstein equations can be easily derived from the gravitational

Einstein-Hilbert action

$$S = \int d^4x\sqrt{-g}\left[\frac{R}{2\kappa^2} + \mathcal{L}_{\rm m}\right] \tag{1.3}$$

where g is the determinant of the metric tensor $g^{\mu\nu}$; R is the Ricci scalar and $\mathcal{L}_{\rm m}$ is the matter lagrangian. In order for the Newtonian weak-field limit to be recovered, the constant κ^2 must be equal to $8\pi G_{\rm N}$. Varying the action with respect to the metric elements $g^{\mu\nu}$ we then obtain

$$G_{\mu\nu} \equiv R_{\mu\nu} - \frac{1}{2}R = \kappa^2 T_{\mu\nu}. \tag{1.4}$$

The Einstein field equations relate the curvature of spacetime through the Einstein tensor $G_{\mu\nu}$ with the matter-energy composition of the Universe described by the stress-energy tensor $T_{\mu\nu}$. They are a set of powerful and complex equations that dictate how an energy/mass source dynamically alters the geometry of spacetime around it, whose solution are the metric elements $g_{\mu\nu}$.

1.1 Solar system tests of general relativity

General relativity has endured a complete century of intensive scrutiny, and has emerged as the definitive local theory of gravitation. Several tests on solar system scales have proved its consistency on small scales. These include: the measurement of the deflection of light by the Sun [7–9]; the measurement of the delay of light signals reflected back to Earth from distant sources [10] and the triumphant measurement of the perihelion shift of Mercury [11]. And, recently, we have had the historical observation of the merger of two black holes and the emission of gravitational waves producing a signal accurately predicted by GR [12].

Differences between different theories of gravity can be described and tested in the limit of weak-gravitational fields and slowly-moving gravitational sources, known as the post-Newtonian limit. This should be accurate enough to encompass the majority of solar system tests to be performed in the foreseeable future [13].

In the post-Newtonian limit, the spacetime metric g can be expressed as an expansion around the Minkowskian flat-space metric $\eta_{\mu\nu} = \text{Diag}(-1, 1, 1, 1)$ in terms of dimensionless gravitational potentials that are weighted by coefficients

with different degrees of smallness. The parametrized post-Newtonian (PPN) formalism inserts parameters in place of these coefficients whose values depend on the theory under consideration [14, 15].

The deflection of light by gravitational sources that is predicted by general relativity is a test of the PPN parameter $\gamma_{\rm PPN}$, which measures how much space curvature is produced by a unit rest mass [13]. A light ray that passes the vicinity of the Sun at a distance d is deflected by an angle [16]

$$\delta\theta = \frac{1}{2}\left(1+\gamma_{\rm PPN}\right)\frac{4M_\odot}{d}\frac{1+\cos\mathcal{K}}{2}, \tag{1.5}$$

where $M_\odot$ is the mass of the Sun and $\mathcal{K}$ is the angle between the Earth-Sun line and the direction of the approaching photon. For a light ray passing very close to the surface of the Sun, such that $d \approx R_\odot$ and $\mathcal{K} \approx 0$ [13]

$$\delta\theta \approx \frac{1}{2}\left(1+\gamma_{\rm PPN}\right)1.''7505, \tag{1.6}$$

independent of the frequency of the incident light. The PPN parameter $\gamma_{\rm PPN}$ is equal to unity in standard GR.

The confirmation of the bending of optical starlight during a solar eclipse performed by the British astronomer Sir Arthur Eddington was the first victory of general relativity, one that projected Albert Einstein and his theory into fame. However, this measurement only had a 30% accuracy [13].

Fortunately, the advent of radio interferometery, and later of very-long-baseline radio interferometry (VLBI) now allows the measurement of angular separation with a precision better than 100 microarcseconds. More specifically, these devices measure the deflection of radio waves emanating from distant compact radio sources by the Sun with extraordinary precision. A 2004 analysis of almost 2 million VLBI observations of 541 radio sources, made by 87 VLBI sites yielded $(1+\gamma_{\rm PPN})/2 = 0.99992 \pm 0.00023$ or, equivalently, $(\gamma_{\rm PPN}-1) = (-1.7 \pm 4.5) \times 10^{-4}$ [7]. Subsequent analysis that incorporated data trough 2010 reported a measurement $(\gamma_{\rm PPN}-1) = (-0.8 \pm 1.2) \times 10^{-4}$ [8, 9].

Another test of the parameter $\gamma_{\rm PPN}$ is the measurement of the time-delay of signals emitted from the Earth across the Sun to a distant source (planet or satellite) that bounce back and are returned to the Earth. General relativity predicts that clocks will measure time differently depending on the strength of the gravitational field they experience: the stronger the gravitational source, the slower time shall

pass. Hence, as light passes close to the Sun, an observer on Earth will measure a longer flight travel for the light ray than if the Sun was not present. For a ray that passes close to the Sun, we have [13]

$$\delta t = \frac{1}{2}\left(1+\gamma_{\mathrm{PPN}}\right)\left[240 - 20\ln\left(\frac{d^2}{r}\right)\right]\,\mu\mathrm{s}, \tag{1.7}$$

where d is the distance of closest approach of the ray in solar radii, r is the distance of the target from the Sun, in astronomical units and δt is measured in microseconds. This effect was predicted in 1964 by Irwin Shapiro [17], with the most recent measurement performed by the Cassini spacecraft which concluded that the parameter $\left(1+\gamma_{\mathrm{PPN}}\right)/2$ must be within at most 0.0012 percent of unity [10].

Lastly, we have the measurement of the perihelion shift of Mercury. In a two body Newtonian problem consisting of a lone object orbiting a spherical mass, the object would trace out an ellipse with the massive body at a focus. If the massive body is the Sun, the point of closest approach is the perihelion. In an ideal system, the perihelion occurs at the same angular location from one orbit to the other.

However, in any complex gravitational system, the presence of neighboring planets and the fact the objects are not point-like and have mass distributions will introduce perturbations to the elliptic orbit that will induce a shift/precession of its perihelion. Newtonian theory predicted a value 43 arcseconds inferior to the observed value of the perihelion shift of Mercury. General relativity accounts for this discrepancy naturally and without disturbing the agreement with other planetary observations.

In the parameterized post-Newtonian formalism, the advance of Mercury's perihelion is given by [13]

$$\dot{\tilde{\omega}} = 42.''98\left(\frac{1}{3}\left(2+2\gamma_{\mathrm{PPN}}-\beta_{\mathrm{PPN}}\right)+3\times10^{-4}\frac{J_2}{10^{-7}}\right), \tag{1.8}$$

where β_{PPN} measures how much nonlinearity is there in the superposition law for gravity, being equal to unity in standard GR; J_2 depends upon solar quadrupole moment, with the latest helioseismology data yielding a value of $J_2 = (2.2 \pm 0.1)\times 10^{-7}$ [18].

Adopting the Cassini bound on $\gamma_{\rm PPN}$, the most recent fits to planetary data including data from the Messenger spacecraft that orbited Mercury yield $\beta - 1 = (-4.1 \pm 7.8) \times 10^{-5}$ [13]. Another, although slightly weaker bound on β comes from the perihelion advance of Mars from the Mars Reconnaissance Orbiter: $\beta - 1 = (0.4 \pm 2.4) \times 10^{-4}$ [19].

Despite the aforementioned successes, in Einstein's original formulation from the action 1.3), and in the presence of matter and radiation alone, general relativity fails to explain one feature of our Universe on the larger scales: its accelerated expansion. Observations of type Ia Supernova [20–23] have unquestionably shown that our Universe is expanding in an increasing rate. If the stress-energy tensor entering the Einstein field equations accounted only for the presence of ordinary matter and radiation, their gravitational attractive effect would be to counteract the expansion of our Universe following its violent beginning in the Big Bang. Therefore, in this scenario, our Universe's expansion rate should be decreasing.

Thus, a new paradigm was established with the addition of a Cosmological Constant to the Einstein-Hilbert action, Λ, that exerts the needed repulsive effect to accelerate the expansion of the Universe. This has become that standard cosmological model known as Λ Cold Dark Matter (ΛCDM).

1.2 The standard model of cosmology

The Cosmological Constant, Λ, was first considered by Einstein himself as a way of balancing the presence of matter and radiation in order to obtain a static Universe. Now, it is seen as the simplest and strongest explanation for the cosmic acceleration we observe.

Its presence modifies the Einstein-Hilbert action of Eq. (1.3) simply as

$$S = \int d^4x \frac{\sqrt{-g}}{2\kappa^2} \left[R + \Lambda + 2\kappa^2 \mathcal{L}_{\rm m} \right], \tag{1.9}$$

implying that the Einstein field equations will now read

$$G_{\mu\nu} = \kappa^2 T_{\mu\nu} + \Lambda g_{\mu\nu}. \tag{1.10}$$

In the absence of the regular stress-energy tensor $T_{\mu\nu}$, $\Lambda g_{\mu\nu}$ can be seen as the energy-momentum tensor of the vacuum. And it is quite appropriate that such

tensor is proportional to the metric one, since this is the only rank-2 symmetric tensor that, in local coordinates, is lorentz invariant. Therefore, as expected, there will not be any privileged observers for vacuum.

In order to understand how the presence of Λ can alter the dynamics of the Universe, it is necessary to study the Friedmann equations. And, to do so, one has to make some assumptions about the Universe we live in:

- Our Universe is, on the largest scales, homogeneous and isotropic, whereas on small scales it exhibits a great variety of highly non-linear and inhomogeneous structure. Galaxy redshift surveys determine the two-point correlation function, which gives the excess probability, relative to a random distribution, of finding pairs of galaxies separated by a distance r. The Fourier transform of this function corresponds to the power spectrum $P(k)$ which is related to the square of Fourier coefficients of the fluctuations in density as compared to an unperturbed Universe: the root mean square of the fluctuations can be roughly written as $\langle(\delta\rho/\rho)^2\rangle \propto k^3 P(k)$. Hence, proving the homogeneity of the Universe is no easy task, but galaxy clustering surveys such as the Sloan Digital Sky Survey [24] or the 2-degree Field Galaxy Redshift (2dFGRS) [25] provide pictures of the cosmos that exhibit an homogeneous Universe as we approach the largest scales [26]. Also, recent analysis of the SDSS catalog and the blue galaxies of the WiggleZ survey point to a homogeneity scale roughly above 100 h^{-1}Mpc [27–29]. The isotropy and homogeneity of the Universe is also supported by observations of the temperature anisotropies of the cosmic microwave background (CMB) [30]. This first assumption implies that the evidence available for all observers should be the same, independently of their location and direction of observation;

- Our Universe is geometrically flat, meaning that light rays shall propagate in a straight line from the point of their emission. This is supported by the position of the primary peak of the CMB [31, 32].

Under these assumptions, we adopt the flat Friedmann-Lemaître-Robertson-Walker (FLRW) metric, $g_{\mu\nu} = -dt^2 + a(t)^2 d\vec{x}^2$, with a being the normalized scale factor, and we take the stress energy-tensor to be given by $T^\mu_\nu = \mathrm{Diag}(-\rho, p, p, p)$, with ρ and p representing the energy density and pressure of matter and radiation

combined. The Friedmann equations will then read

$$3H^2 = \kappa^2\rho + \Lambda \tag{1.11}$$

$$\frac{\ddot{a}}{a} = -\frac{\kappa^2}{6}(\rho + 3p) + \frac{\Lambda}{3}, \tag{1.12}$$

which correspond to the $0-0$ and $i-i$ components of the Einstein field equations respectively. $H \equiv \dot{a}/a$ is the Hubble parameter. We take the present-day value of the scale factor to be 1, tending to smaller values in the past.

From the conservation of stress-energy tensor, $T^{0\nu}{}_{;\nu} = 0$, we know that the energy densities of matter and radiation evolve as a function of the scale factor, respectively, like

$$\rho_{\rm m} \propto a^{-3}, \quad \rho_{\rm r} \propto a^{-4}. \tag{1.13}$$

These results are a direct consequence of considering pressureless baryonic and cold dark matter homogeneously distributed throughout our Universe, hence $p_{\rm m} = 0$. Also, from relativistic considerations, we know that $p_{\rm r} = 1/3\,\rho_{\rm r}$. Therefore, presently, one can only consider the much less diluted presence of matter in the calculations.

In order to have an accelerated expansion, we see in Eq. (1.11) we must have $\ddot{a} > 0$, which is only attainable if

$$\kappa^2\rho_{\rm m} + \Lambda + 3\kappa^2 p_{\rm m} - 3\Lambda < 0 \leftrightarrow -\frac{\rho_{\rm m} + \rho_\Lambda}{3p_\Lambda} > 1, \tag{1.14}$$

where we defined $\rho_\Lambda \equiv \Lambda/\kappa^2$ and $p_\Lambda \equiv -\Lambda/\kappa^2$. The last condition is only achievable if the cosmological constant has negative pressure, which is guaranteed if $\Lambda > 0$. We actually have $p_\Lambda/\rho_\Lambda \equiv w_\Lambda = -1$, and such a simple modification is in fact capable of yielding cosmic acceleration since, presently, we have $\rho_{\rm m}/\rho_\Lambda \approx 0.4$ [33].

However, not all is perfect with this picture. The value that is observed for the cosmological constant is approximately 120 orders of magnitude smaller than the value we can predict from quantum field theory (QFT) calculations. These estimate the energy density of vacuum by summing the zero-point energies of quantum fields with mass m,

$$\rho_{\Lambda{\rm QFT}} = \int_0^\infty \frac{d^3k}{(2\pi)^3}\sqrt{k^2+m^2} = \frac{1}{4\pi^2}\int_0^\infty \sqrt{k^2+m^2}k^2dk \tag{1.15}$$

With the current limits, this integral is bound to diverge. However, QFT should be valid up to the Planck scale, $m_{\rm Pl} = 1.22 \times 10^{19}$ GeV. Hence, setting a cutoff for the upper limit of the integral, $k_{\rm cutoff} = m_{\rm Pl}$, we are able to solve the integral (assuming $k_{\rm cutoff} \gg m$), obtaining

$$\rho_{\Lambda \rm QFT} \approx \frac{k_{\rm cutoff}^4}{16\pi^2} \approx 10^{74}\ {\rm GeV}^4. \tag{1.16}$$

The observed value for Λ is of order of the present-day value of the Hubble parameter, $\Lambda \approx H_0^2 \approx (10^{-42})^2$ GeV. Hence, the measured value of $\rho_\Lambda = \Lambda/\kappa^2 = \Lambda m_{\rm Pl}^2/8\pi \approx 10^{-47}$ GeV^4 and we see that $\rho_{\Lambda \rm QFT}/\rho_\Lambda \approx 10^{121}$. This is known as the 'fine-tuning' problem.

Not only that, but there is the 'coincidence' problem that questions the moment in cosmic history the accelerated expansion occurs. We just happen to exist in an epoch where the cosmological constant energy density is comparable to the matter energy density, just slightly dominating over the latter and leading cosmic acceleration. For reviews on the cosmological constant and attempts to solve its problems see ([34–36]).

Hence, in light of these issues, the nature of the cosmological constant and the origin of cosmic acceleration has become one of the most active topics of research in Physics, leading to the appearance of alternative theories to explain the accelerated expansion of the Universe.

1.3 Dark energy and modified theories of gravity

One of the most common alternatives to the cosmological Constant is to introduce dark energy within the framework of General Relativity (for a review see [37]). Dark energy will behave as a fluid with an equation of state $w_{\rm DE} = p_{\rm DE}/\rho_{\rm DE}$ that has to be negative in order to produce cosmic acceleration. Within dark energy theories, we can have a wide array of models. Possibly the most studied ones are the quintessence models [38], which consist in treating dark energy as a scalar field with a canonical kinetic term slowly-rolling in a potential,

$$S = \int d^4x \frac{\sqrt{-g}}{2\kappa^2} \left[R - g^{\mu\nu}\partial_\mu\phi\partial_\nu\phi - 2V(\phi) + 2\kappa^2 \mathcal{L}_{\rm m}[g_{\mu\nu}, \psi_{\rm i}] \right], \tag{1.17}$$

where we made explicit the dependence of the matter lagrangian on the metric elements and different matter fields $\psi_{\rm i}$.

In quintessence, one can have models that are presently slightly deviating from the cosmological constant with $w_{\rm DE} \simeq -1$, known as thawing models; or models with a slightly diverging behavior in the past and that are currently approaching $w_{\rm DE} \simeq -1$, known as freezing quintessence. [39].

Then, one can also have quintessence models that track the Universe's dominating matter component in the distant past until recently, leading cosmic acceleration in the present. These are known as tracking models [40, 41] and could provide a possible explanation to the coincidence problem, as the density of dark energy will be insensitive to the initial conditions. One of the prime examples is the Ratra-Peebles model with a potential of the form [42]

$$V(\phi) = \frac{M^{4+n}}{\phi^n}, \tag{1.18}$$

with $n > 0$.

Lastly, we can have an even richer phenomenology when considering quintessence models with non-canonical kinetic terms known as k-essence [43, 44]. These models are particularly interesting as they predict a structure formation that can be significantly different with respect to the canonical quintessence models, while reproducing their background history.

There are, however, other alternatives to explain cosmic acceleration that introduce infrared modifications to general relativity, assuming that the theory of GR fails on cosmological scales. These are known as modified gravity theories. While dark energy explicitly adds a new fluid with negative dark energy to the stress-energy on the right-hand side of Einstein equations, modified theories of gravity modify the gravitational sector and, consequently, the Einstein tensor.

A modification of gravity carries non-trivial implications, which is expected from Lovelock's theorem. The latter states that any modification introduced to the geometrical part of the Einstein-Hilbert action will add to your gravitational theory additional degrees of freedom, higher derivatives, extra dimensionalities or imply non-locality. Thus, the standard Einstein-Hilbert action is the only one capable of producing second order local equations of motion in four dimensions.

One then has to ensure the theoretical stability and consistence of the new theory.

Just as an example, one needs to guarantee that the effective mass of the scalar field is positive in order for it to not be tachyonic. This may not necessarily be catastrophyc though, as long as the associated time scale is long enough. Other examples would be ensuring that the kinetic and gradient terms have the right sign and that possible non-linear interactions involving the new degree of freedom are well understood and controlled. These may become relevant beyond a certain energy scale, meaning one may have to treat the model as an effective theory.

One of the most well-known models that consider additional dimensions is the Dvali-Gabadadze-Porrati (DGP), according to which we live in a four dimensional membrane of a five dimensional spacetime, and is described by the action [45]

$$S = \frac{1}{2M_{(5)}^3}\int d^5x\sqrt{-{}^{(5)}g}\,{}^{(5)}R + \frac{1}{2M_{(4)}^2}\int d^4x\sqrt{-{}^{(4)}g}\left[{}^{(4)}R + 2M_{(4)}^2\mathcal{L}_{\rm m}\right], \quad (1.19)$$

where ${}^{(5)}R$ and ${}^{(4)}R$ are the five and four dimensional Ricci scalars, respectively, while $M_{(5)}^3$ and $M_{(4)}^2$ are the respective Newton constants. Despite being able to produce self-accelerating solutions absent of a bare cosmological constant [46, 47], the reality is that the theory suffers from ghost instabilities [48–50].

Another interesting alternative theory is that of massive gravity. In Einstein's general relativity, the graviton is a massless spin-2 particle. In massive gravity, the graviton is allowed to be a massive particle, under the assumption that massive fields can induce Yukawa-type potentials

$$V(r)\ \frac{e^{-mr}}{r}, \quad (1.20)$$

and therefore leads to cosmic acceleration by a weakening of gravity at large scales with $m \sim H_0$, where H_0 is the present-day value of the Hubble parameter. This idea has garnered much interest recently with the development of a ghost-free theory by de Rham-Gabadadze-Tolley [51–53].

In this work we will be focusing on possibly the best-studied modification of general relativity, the scalar-tensor theories (for a comprehensive review on many other modified theories of gravity see [54]). Considering only canonical scalar

fields, these theories can be expressed in the Einstein frame[1] as

$$S = \int d^4x \frac{\sqrt{-\tilde{g}}}{2\kappa^2} \left(\tilde{R} - \tilde{g}^{\mu\nu}\partial_\mu\phi\partial_\nu\phi - 2V(\phi) + 2\kappa^2\mathcal{L}_{\rm m}[A^2(\phi)\tilde{g}_{\mu\nu}, \psi_{\rm i}] \right), \qquad (1.21)$$

where tilde quantities refer to the Einstein frame. In this formulation the coupling of the matter fields to the Jordan frame metric is given by $g_{\mu\nu} = A^2(\phi)\tilde{g}_{\mu\nu}$[2]. This coupling implies that the scalar degree of freedom will mediate an additional fifth force that is also present in the Newtonian regime as

$$\vec{a} = -\vec{\nabla}\left(\tilde{\Phi} + \ln A(\phi)\right), \qquad (1.22)$$

sourced by the Einstein frame potential $\tilde{\Phi}$ and the coupling $A(\phi)$. Also, if the additional scalar field has a mass of order H_0, then it can also mediate long range interactions and possibly source cosmic acceleration. Examples of well known scalar-tensor theories are Brans-Dicke gravity [56] and metric $f(R)$ theories [57], which will be the focus of some part of this work.

Of course, locally, any modification of gravity that introduces additional forces are strongly constrained by solar system tests. Thus, these theories must have a mechanism that ensures their viability on small scales. This is usually attainable with a proper choice of the potential $V(\phi)$ and the coupling $A(\phi)$, since the scalar field will evolve in an effective potential $V_{\rm eff} = V(\phi) + A(\phi)\rho_{\rm m}$ [58] that responds to the external matter sources in the Einstein frame.

Hence, a modified gravity theory should have a screening mechanism that suppresses any additional interaction it may mediate on solar system scales. One of the most popular examples is the chameleon mechanism [59, 60] with the Ratra-Peebles potential and a simple linear coupling $A(\phi)$. In this mechanism, the effective mass of the scalar field will increase in regions of high density, suppressing the additional Yukawa-type additional fifth force. The chameleon mechanism is employed to guarantee the viability of metric $f(R)$ theories, for instance.

Another example that is very similar to the previous one is the symmetron

[1] In the Einstein frame the field equations take the same form as in GR with a modified matter sector due to non-minimal coupling to matter fields. Usually, one can re-cast the theory in the Jordan frame where the metric satisfies a modified field Einstein field equation with a conventional stress-energy tensor. Cosmological observations are implicitly made in the Jordan frame where the masses of particles are constant.

[2] The presence of a non-minimal coupling in modified gravity theories can be used as an argument to draw a boundary between these and dark energy, as the former lead to a violation of the strong equivalence principle (for an interesting discussion on this topic see [55])

mechanism [61] in which the potential and coupling are given by

$$V(\phi) = -\frac{\mu^2}{2}\phi^2 + \frac{\lambda}{4}\phi^4, \quad A(\phi) \simeq 1 + \frac{\phi^2}{M^2}. \tag{1.23}$$

In regions of low density, the symmetry of the model is spontaneously broken and the scalar field will mediate an additional force, while in regions of high density the symmetry is restored and the fifth force is suppressed. These two last examples have the common property that the screening of the fifth force will happen when the gravitational potential exceeds some critical value. Thus, regions of small gravitational potential should exhibit the largest deviations from general relativity and can be used to test and impose tight constraints on these models.

We then have a screening mechanism that relies on the kinetic function of the scalar field becoming large, as this will effectively suppress the coupling to matter. This can be realized by ensuring that the first derivative of the scalar field becomes large, and is known by k-mouflage [62] as it is usually displayed in models with non-canonical kinetic terms. One can also have a screening method where the focus is on nonlinearities in second derivatives of the scalar field, such that $\nabla^\mu \nabla_\mu \phi$ is larger than some critical value. This is known as the Vainsthein mechanism [63] and is employed in Galileon theories [64].

Lastly, we note that the models represented by the action in Eq. (1.21) will produce second order equations of motion. In fact, they fall within the most general second order scalar tensor action one can write, which is given by the Horndeski theory [65]. It has been recently argued that there is always enough freedom within these theories to recover a background evolution that is indistinguishable from ΛCDM's [66, 67].

In an epoch where so many surveys are being designed to test gravity on larger scales, it is particularly relevant to know how to break the degeneracy between these theories at the background level. This can be achieved by a deeper understanding of modified gravity theories at the linear level of perturbations, which comprises the rich phenomenology these theories produce on the linear structure of the Universe. And even though it has been shown that genuine self-accelerating [3] Horndeski theories can not be made compatible with current

[3]Self-accelerating solutions should yield acceleration in the Jordan frame that is driven by the actual modifications of gravity introduced by the theory and not by the contribution of a cosmological constant or dark energy in the matter sector. This a sensible definition that involves both the Jordan and Einstein frames. See Ref. [68] for a discussion on this topic.

cosmological observations [69], these models are still worthwhile exploring and adopting to conduct tests of gravity.

1.4 Cosmological tests of general relativity

As stated in the previous section, there is a degeneracy between modified gravity theories and the standard model of cosmology at the background level. The Friedmann equation of a modified gravity model can always be recast as in standard general relativity with a dark energy component

$$H^2 = \frac{\kappa^2}{3}\left(\rho + \rho_{\rm DE}\right), \tag{1.24}$$

which, by tuning of the effective dark energy equation of state, should allow to reproduce any background history predicted by a dark energy model or ΛCDM. Hence, geometrical probes that measure the expansion history of the Universe do not suffice to cleanly distinguish between modified gravity and the standard model of cosmology (or even dark energy for that matter).

Possibly the strongest geometrical probe available presently is the use of high and low-redshift Type Ia supernova, serving as standard candles. Comparing their absolute magnitudes yields a measurement of the evolution of the luminosity distance which, for a flat Universe, is just $d_L = (1+z)\chi(z)$, where $\chi(z) \equiv \int_0^z dz'/H(z')$ is the comoving radial distance. The background history H can also be measured from the cosmic microwave background and the imprint of its acoustic peaks on large scale structure of the Universe, the baryon acoustic oscillations feature observed in galaxy clustering (for reviews on these see [70–72]).

The early Universe consisted of a hot and dense plasma of electrons and baryons, with the photons trapped in the primordial fluid, unable to travel any considerable length due to Thomson scattering. In regions of overdensity in this fluid, matter would tend to collapse, while the tremendous radiative outward pressure of the CMB photons opposed this, leading to the establishment of acoustic modes. At recombination, when the baryons and electrons combine into the first atoms, the photons are released from the plasma, but on both of them are left imprints of these acoustic oscillations with a characteristic scale given by the distance that a sound wave could travel in the age of the Universe to that point, corresponding to the sound horizon in the early Universe. Neglecting the presence of dark energy,

the comoving sound horizon at recombination can be determined by

$$r_{\rm s}\left(z,\Theta\right)=\frac{1}{\sqrt{3}}\int_0^{a_{\rm r}(z)}\frac{dz'}{H\left(z',\Theta\right)\sqrt{1+\frac{3\rho_{\rm b}}{4\rho_\gamma}}}, \tag{1.25}$$

where $a_{\rm r}(z)$ is the scale factor of recombination, and $\rho_{\rm b}$ and ρ_γ are, respectively, the baryon and photon energy density.

These imprints provide a new opportunity to measure distances at different redshifts. Indeed, the length scale that was imprinted by the sound waves, referred to as the acoustic scale, persists to the present time as wiggles in the power spectrum $P(k)$ of galaxy redshift surveys at a characteristic comoving length of $100\,h^{-1}$ Mpc. The latest generation of galaxy redshift surveys is able to probe the length scales required to make a precision measurement of the BAO signal, and this method has therefore been proposed as a new geometrical probe to constrain the physics of cosmic acceleration [73–75]. The BAO were first detected in the Luminous Red Galaxies (LRG) sample of the Sloan Digital Sky Survey (SDSS) [76], followed by measurements in the 6dF Galaxy Redshift Survey (6dFGRS) at low redshift [77], and by BOSS CMASS DR9 [78].

Therefore, complementary probes are needed to study modified gravity theories on large scales. As we have seen, the appearance of an additional scalar degree of freedom in modified gravity theories introduces an extra force that will impact the large scale structure of the Universe. This becomes clear when we perturb the metric and explicitly compute the perturbed Einstein equations in any modified gravity theory, as these will relate the gravitational potentials to the components of the perturbed stress-energy tensor. The latter includes the matter density fluctuations $\delta_{\rm m}$ that source the linear structure.

In standard GR, considering the perturbed FLRW metric in the newtonian conformal gauge

$$ds^2=-\left(1+2\Psi\right)dt^2+a^2\left(1-2\Phi\right)d\vec{x}^2, \tag{1.26}$$

one can combine the $0-0$ and $0-i$ components of Einstein's equations to obtain the Poisson equation

$$k^2\Phi=-4\pi G_{\rm N}a^2\rho_{\rm m}\delta_{\rm m}, \tag{1.27}$$

where we work in Fourier space since the different k-modes of the perturbations will evolve separately at linear order. We also restrict the analysis to wavemodes

that are well within the horizon, $k \gg aH$[4]. On the other hand, the anisotropy component ($i \neq j$) yields

$$k^2 (\Phi - \Psi) = 12\pi G_{\rm N} a^2 \rho \sigma, \tag{1.28}$$

where σ is the radiation shear. In epochs where radiation can be neglected, $\sigma = 0$ and the anisotropy equation becomes a simple constraint equation, $\Phi = \Psi$. Lastly, combining the continuity and Euler equations one obtains a second order equation describing the growth of $\delta_{\rm m}$

$$\ddot{\delta}_{\rm m} + 2H\dot{\delta}_{\rm m} = -\frac{k^2}{a^2}\Psi. \tag{1.29}$$

In ΛCDM, the growth of $\delta_{\rm m}$ can be accurately parametrized by the following function [82]

$$f = \frac{d\log\delta_{\rm m}}{d\log a} = \Omega_{\rm m}^{\bar{\gamma}}(a), \tag{1.30}$$

with $\bar{\gamma}_{\Lambda\rm CDM} \approx 0.55$. This formula also works remarkably well for smooth quintessence, since the evolution of the density perturbation will be determined by the background history, and then $\bar{\gamma}$ will be given by the dark energy equation of state $w_{\rm DE}$.

However, modified gravity theories tend to exhibit a more complex behavior due to the additional degree of freedom they introduce. Generally, this will source the anisotropic equation and the slip between the newtonian potentials with an extra dynamical term. Then, the growth of the matter perturbation $\delta_{\rm m}$ can no longer be solely determined by the background history. Thus, this would lead to inconsistencies when fitting different observations including measurements of the background history and the growth of structure of the Universe if it were described by a modified gravity model [82, 83].

Hence, finding a value $\bar{\gamma} \neq 0.55$ would provide evidence for new physics beyond smooth quintessence and ΛCDM (if the effective equation of state were also to be constrained to be -1, which it pretty much is [33]) such as clustering dark energy or modified gravity theories. On the reverse, finding consistency with ΛCDM or smooth DE using the previous test does not rule out modifications of gravity,

[4]This is known as the subhorizon approximation. In these scales, the time evolution of the newtonian potentials is negligible compared to the their gradients, which is known as the quasi-static approximation [79, 80]. On superhorizon scales ($k \ll aH$), the superhorizon adiabatic modes behave like a separate, curved universe, such that its evolution is determined by the background expansion solution in the given theory [81]

as the considered parameters do not encompass the entire space of possible dark energy and modified gravity models.

This is generally overcome by providing two functions of time (scale factor a) and scale k, $\mu(a,k)$ and $\gamma(a,k)$, that are used to parametrize the relation between the Newtonian potential and the matter density perturbation and the ratio between the gravitational potentials [84, 85]

$$-\frac{k^2}{a^2}\Psi = 4\pi G_{\rm N}\rho_{\rm m}\mu(a,k)\delta_{\rm m} \tag{1.31}$$

$$\frac{\Phi}{\Psi} = \gamma(a,k). \tag{1.32}$$

The parameter γ can be useful to constrain modified gravity theories on solar system scales as well. From its definition, it marks deviations from standard GR on the amount of spacial curvature produced from a unit rest mass. Hence, it can be identified with the PPN parameter $\gamma_{\rm PPN}$ defined in Sec. 1.1. For instance, in Brans-Dicke theory for a massless scalar field, we have

$$\gamma = \frac{1+\omega_{\rm BD}}{2+\omega_{\rm BD}}, \tag{1.33}$$

and the solar system constraints on the PPN parameter $\gamma_{\rm PPN}$ from the Cassini experiment allow to place constraints on the Brans-Dicke parameter $\omega_{\rm BD} > 4\times 10^4$.

Another useful parametrization that can be built from the previous two equations relates the lensing potential $(\Phi_+ \equiv \Phi+\Psi)/2$ with the matter density perturbation

$$k^2\left(\Phi+\Psi\right) = 8\pi G_{\rm N}\Sigma(a,k)a^2\rho_{\rm m}\delta_{\rm m}, \tag{1.34}$$

where $\Sigma = \mu\left(1+\gamma\right)/2$. Since the three functions are related, providing any two of them is sufficient for solving the evolution of linear perturbations [86]. General Relativity and non-clustering quintessence is recovered when $\mu=\gamma=\Sigma=1$ (for a very interesting discussion of the consequences of measurements different than the standard value on several modified gravity theories see [87]).

This choice of parametrization is motivated by two reasons. The first is that μ can be directly constrained by the growth of structure, which becomes clear when Eq. (1.29) is modified to

$$\ddot{\delta}_{\rm m} + 2H\dot{\delta}_{\rm m} = 4\pi G_{\rm N}\rho_{\rm m}\mu(a,k)\delta_{\rm m}. \tag{1.35}$$

Secondly, the parameter γ appears in the lensing potential $\Phi_+ \equiv (1+\gamma)\,\Psi$. This potential affects the propagation of photons in an effect known as weak lensing (WL) that impacts, for instance, the CMB power spectrum. Therefore, weak lensing surveys will be sensitive to the both μ and γ, which combine into Σ. It has been shown that Σ is the parameter better constrained from upcoming WL and large scale structure surveys [88, 89].

Thus, it is of paramount importance to know which observables are capable of constraining the previous parameters. The CMB anisotropies power spectrum is, as stated before, affected by the weak lensing of its photons due to the intervening matter structure between the observer and the surface of last scattering. Within the CMB, one also has the Integrated Sachs Wolf (ISW) effect [90] at the larger scales of the spectrum, which is due to the time evolution of the lensing potential $\dot{\Phi}_+$.

Next-generation weak lensing surveys (such as Euclid [91]) will measure the WL signal with unprecedented precision, allowing the improvement of already existing constraints. Gravitational lensing corresponds to the distortion of the shapes of distant sources, such as galaxies, due to the intervening matter structure between the source and the observer. The gravitational field of a massive object will extend far into space, and cause light rays passing close to that object to be bent and refocused somewhere else. This effect will be stronger the stronger the gravitational field is.

If the distortions can be resolved by eye, then we have strong gravitational lensing. However, this is not so common, and most galaxies have their shapes altered by 1%, and so we have weak lensing. Both are particularly valuable probes as they are sensitive to the growth of structure (as the photons experience a combination of the gravitational potentials Φ and Ψ) and the geometry of the Universe, as it is an integrated effect along the line of sight between the source and the observer: the longer the path length, the longer the distortion. Not only that, the Hubble parameter also enters the equation of the growth of structure, as seen in Eq. (1.35).

Weak gravitational lensing is measured by working out the average lensing effect on a set of galaxies, which is dubbed as cosmic shear (for a review see [92]). In order to do so, one assumes that all galaxies are roughly elliptical in overall shape and are randomly orientated in the sky. In the presence of weak lensing, one would expect the galaxies to show a systematic alignment, and any deviation

from a random distribution of galaxy shape orientations is a direct measure of the lensing signal in a specific patch of the sky. The most basic non-trivial cosmic shear observable is the real-space shear two-point correlation function (2PCF), since it can be estimated by simply multiplying the ellipticities of galaxy pairs and averaging. This cosmic shear distortion can be used to directly probe dark matter, and, when analyzed in tomographic redshift bins, can also reveal the growth of structure. Hence, it can also act as a useful tool for testing the laws of gravity [93–95].

The WL signal is thus simultaneously dependent on Σ and μ (since this affects the growth of structure). In order to break this degeneracy, it is important to combine WL surveys with observations of redshift space-distortions (RSD) that measure the peculiar velocities of galaxies, $\theta_{\rm m}$ [96]. The redshift space-distortions arise in maps made from galaxies if distances are determined from measured redshifts assuming that they are only caused by the Hubble flow. Because of gravitational growth, the galaxies tend to infall towards high-density regions and flow away from low-density regions, such that the clustering is enhanced in the line-of-sight direction compared to the perpendicular direction. Due to the RSD, the observed two-point statistics tend to exhibit a strong anisotropy with respect to the line-of sight direction. The measurement of RSD provide constraints on the amplitude of peculiar velocities induced by structure growth, thereby allowing tests of the theory of gravity governing the growth of those perturbations [96–100]. These are dependent on Ψ (as the velocity potential, in the Newtonian gauge, depends on Ψ) and hence, on μ, thus breaking the degeneracy. The E_G parameter relating these two observables was introduced in [101]

$$E_G = -\frac{2}{3}\frac{\nabla^2\Phi_+}{H_0^2 a^{-1}\theta_{\rm m}}, \tag{1.36}$$

which can be constructed directly from observations [102].

Lastly, it would be extremely useful to be able to measure the matter density perturbation $\delta_{\rm m}$. This can, in principle, be reconstructed from measurements of the galaxy distribution $\delta_{\rm g} \equiv \delta_{\rm m}/b$ from surveys such as the LSST [103]. However, it proves extremely difficult due to large uncertainties in the galaxy bias b. If such a measurement was made, it would allow for a very strong consistency test of ΛCDM from the relation [101, 104]

$$\alpha(a,k) \equiv \frac{2k^2}{3a^2H^2}\frac{(\Phi+\Psi)-\Psi}{\delta_{\rm m}} = 1. \tag{1.37}$$

Any accurate measurement of $\alpha \neq 1$ would be a strong indication of a deviation from ΛCDM and the presence of modified gravity.

There have already been several attempts at constraining the parameters μ and γ [105–108], the latest if which was performed by the Planck collaboration [109], where a significant tension was found when combining the Planck data with weak lensing and redshift space distortions data, even though this may be attenuated with a better understanding of the systematic effects [110].

In this work we provide some light on the phenomenology of different modified gravity theories, focusing on their impact on the large scale structure of the Universe and relevant cosmological observables. For that effect, we study the evolution of their linear perturbations, predicting the behavior of the lensing potential for some of the models. When relevant, we will inspect the simplified subhorizon regime and, for instance, provide analytical solutions for μ for the well known Brans-Dicke model. We also provide constraints on the models not only from geometrical probes, but also from the latest Planck data.

Chapter 2

On the phenomenology of extended Brans-Dicke gravity

Over the next decade, we expect a step change in our understanding of gravity on cosmological scales. Surveys of large scale structure should be able to pin down the expansion of the Universe and the growth of structure with exquisite precision [91, 103, 111, 112]. These new data sets should allow us to constrain modifications to general relativity at a level which may be comparable to those obtained on astrophysical scales.

If we are to fully take advantage of these data sets, it is essential to have a detailed and accurate understanding of how different observables depend on our assumptions about gravity. In particular, we should know how deviations from general relativity will affect our observations: whether the effects are large or small (given what we know on astrophysical scales) and how correlations between the observables themselves might be indicative of some underlying structure.

There has been a formidable campaign to develop methods for studying the effects of modified gravity on large scales (for a compendium of theories, see [54]). A different approach has been to develop a unified method of parameterizing all possible theories at the linearized level (for a selection of methods, see [113–116]). Yet, while there is an inexorable momentum that should lead to a battery of effective techniques for extracting useful information from the data, we do not have yet a firm understanding of what to expect. By this we mean that, given certain theoretical assumptions, what our observables should look like, i.e. what values should they take and how should they be interrelated as a function of

whatever fundamental parameters we might consider.

In principle, the step from taking the parameters, α_i (with $i = 1, \cdots N$), of some underlying theory and working out the resulting phenomenological parameters, β_j (with $j = 1, \cdots M$) tied to observations, should be straightforward. In practice, the process can be complicated, highly non-linear, degenerate and normally obscures the relationship between the prior assumptions on α_i and the resulting theoretical priors on β_j. One way around this is to develop an approximate mapping between the two sets of parameters and, wherever possible, analytic relations between the two. Furthermore, if one can find a method for restricting the range of α_i given some assumptions about a subset of the β_i, one can quickly surmise what correlations and covariance one should expect for the remaining phenomenological parameters. In this work we propose an approach to do so, considering a restricted model for cosmological modifications to gravity.

Our starting point is a well known theory, the Brans-Dicke (BD) theory of gravitation [117]. This theory is the simplest scalar-tensor theory one can envisage [118–122] and is considered a viable alternative to GR, one which respects Mach's Principle. This principle was also at the basis of general relativity as, according to Einstein, inertial forces observed locally in an accelerated laboratory may be interpreted as gravitational effects having their origin in distant matter accelerated relative to the laboratory. Along these lines, Robert Dicke suggested that inertial forces are, in fact, due to a force field interaction between the mass distribution in the universe and local test masses and the gravitational coupling should be a function of the mass distribution of the Universe. This led to the formulation of the Brans-Dicke theory with a coupling $G_{\rm eff} = G/\phi$ and $\Box\phi \simeq \rho$. One should note that, while the scalar field evolution is linked to the mass distribution, its effect on matter is indirect, as ϕ determines the space-time metric. Hence, the equivalence principle is preserved.

Since its formulation, this theory has been exhaustively studied as a possible alternative solution for the accelerated expansion of the Universe.

It has been shown that Brans-Dicke theory can produce accelerated solutions for small, negative values of the BD parameter $\omega_{\rm BD}$ [123, 124]. Given that one recovers standard GR in the limit where $\omega_{\rm BD} \to \infty$, such values of the $\omega_{\rm BD}$ clash with solar system constraints [125, 126]; furthermore, recent constraints with the latest CMB data are also not compatible with such low values of $\omega_{\rm BD}$ [127, 128]. Several modifications of this theory try to include self-interacting potentials [129–

131] or consider a field-dependent Brans-Dicke parameter $\omega(\phi)$ [132], without solving this problem successfully. Also, models with a non-minimal coupling of the scalar field have been considered in Refs. [133–136].

In this work we construct a theory of *designer*, extended Brans-Dicke gravity and use it to characterize the form of the observables we might measure. This theory is "extended" because we include a potential for the Brans-Dicke field and we dub it "designer" (the term "designer" was first used in models of inflation that attempted to match observations by designing the density fluctuation spectra [137]) because we reconstruct the potential (which might not have an analytic form) from a desired background evolution. While such a theory does not seem fundamental, it might be seen as an approximation to a scalar-tensor theory which has a particular, a priori, form of the background evolution. Our construction allows us to find a number of analytic approximations and, in doing so, lets us gain a firmer understanding of the phenomena we want to study.

Our designer approach for the extended Brans-Dicke gravity is novel. It allows us to retrieve the evolution of the scalar field, ϕ, by fixing the background evolution and is robust for high values of the BD parameter, which is the regime we are interested in. This method not only works for a ΛCDM like evolution with an effective equation of state $w_{\text{eff}} = -1$, but is also applicable for models with $w_{\text{eff}} > -1$ as in a wCDM scenario. And, for both cases, we are able to retrieve analytical approximations for ϕ as a function of the scale factor a which could prove useful for a faster and more efficient fitting of models to data.

This chapter is structured as follows. In Sec. 2.1 we introduce the Brans-Dicke theory with a constant ω_{BD} parameter. In Sec. 2.2 we describe the designer approach, motivated by an analysis of the behavior of this theory when we have a constant potential $V(\phi)$. In Sec. 2.3 find approximate analytic solutions to the evolution of the scalar field and use it to infer the shape of the potential. We then use these results in Sec. 2.4 to construct analytical approximations to the phenomenological parameter which can be constrained by data. In Sec. 2.5 we discuss our results.

I would like to state that the work presented in this chapter can be seen in [1]. It is the result of a collaboration with Professor Pedro Ferreira, who advised me and suggested corrections to parts of the scientific text.

2.1 Extended Brans-Dicke gravity: background equations

The action for extended Brans-Dicke theory in the Jordan frame, is given by

$$S = \frac{1}{2\kappa^2}\int d^4x\sqrt{-g}\left(\phi R - \frac{\omega_{\rm BD}}{\phi}\left(\partial\phi\right)^2 - 2V(\phi)\right) + S_{\rm m}, \tag{2.1}$$

where $S_{\rm m}\left[\Psi_{\rm m}; g_{\mu\nu}\right]$ is the minimally coupled matter Lagrangian and $\kappa^2 = 8\pi G$, where G is Newton's gravitational constant measured today. Varying the action with respect to the metric elements, we find the Einstein equations,

$$G_{\mu\nu} = \frac{\kappa^2}{\phi}T^{\rm m}_{\mu\nu} + \frac{\omega_{\rm BD}}{\phi^2}\left[\phi_{,\mu}\phi_{,\nu} - \frac{1}{2}g_{\mu\nu}\phi_{,\alpha}\phi^{,\alpha}\right] + \frac{1}{\phi}\left[\phi_{,\mu;\nu} - g_{\mu\nu}\Box\phi\right] - \frac{V(\phi)}{\phi}g_{\mu\nu}, \tag{2.2}$$

where $T^{\rm m}_{\mu\nu}$ is the matter stress-energy tensor.

By varying the action (2.1) with respect to the field, one gets the field's equation of motion

$$\Box\phi = \frac{\kappa^2 T}{3+2\omega_{\rm BD}} - \frac{2}{3+2\omega_{\rm BD}}\left[2V(\phi) - \phi V_\phi\right], \tag{2.3}$$

where $V_\phi \equiv dV/d\phi$. Considering a flat Friedmann-Lemaitre-Robertson-Walker (FLRW) metric, $ds^2 = -dt^2 + a^2(t)d\vec{x}^2$, this equation reads

$$\ddot{\phi} + 3H\dot{\phi} = \frac{\kappa^2\rho_{\rm m}}{3+2\omega_{\rm BD}} + \frac{4V(\phi) - 2\phi V_\phi}{3+2\omega_{\rm BD}}, \tag{2.4}$$

where $\rho_{\rm m}$ is the matter's energy density and $H \equiv \dot{a}/a$ is the Hubble parameter. The latter is determined by the two Friedmann equations, which are written as

$$\begin{aligned} 3H^2\phi &= \kappa^2\rho_{\rm m} - 3H\dot{\phi} + \frac{\omega_{\rm BD}}{2}\frac{\dot{\phi}^2}{\phi} + V(\phi) \equiv \kappa^2\left(\rho_{\rm m} + \rho_{\rm eff}\right) \qquad (2.5)\\ 2\dot{H}\phi + 3H^2\phi &= -\kappa^2 p_{\rm m} - \frac{\omega_{\rm BD}}{2}\frac{\dot{\phi}^2}{\phi} - 2H\dot{\phi} - \ddot{\phi} + V(\phi) \equiv -\kappa^2\left(p_{\rm m} + p_{\rm eff}\right), \end{aligned}$$

where the effective dark energy density and pressure are given by

$$\begin{aligned} \kappa^2\rho_{\rm eff} &= \frac{\omega_{\rm BD}}{2}\frac{\dot{\phi}^2}{\phi} - 3H\dot{\phi} + V(\phi) \qquad (2.6)\\ \kappa^2 p_{\rm eff} &= \frac{\omega_{\rm BD}}{2}\frac{\dot{\phi}^2}{\phi} + 2H\dot{\phi} + \ddot{\phi} - V(\phi) \qquad (2.7) \end{aligned}$$

Lastly, from the previous equations, one can define an effective equation of state for the dark energy component of our model, which is given by

$$w_{\text{eff}} = \frac{\dot{\phi}^2\omega(\phi) + 4H\dot{\phi} + 2\ddot{\phi} - 2V(\phi)}{\dot{\phi}^2\omega(\phi) - 6H\dot{\phi} + 2V(\phi)}, \tag{2.8}$$

where $\omega(\phi) = \omega_{\text{BD}}/\phi$ and, even more straightforwardly, one can define the fractional effective dark energy density parameter,

$$\Omega_\phi = \frac{\rho_\phi}{3H^2\phi}, \tag{2.9}$$

where the effective energy density is given by

$$\rho_\phi = \frac{\omega_{\text{BD}}}{\phi}\frac{\dot{\phi}^2}{2} - 3H\dot{\phi} + V(\phi). \tag{2.10}$$

2.1.1 Constant potential V(ϕ)

Before proceeding to the designer approach, we can get an idea of the different effects at play in extended Brans-Dicke gravity by considering the case of a constant potential $V(\phi)$. For all our calculations in this section, we have $V(\phi) = 3H_0^2\left(1 - \Omega_{\text{m}}\right) \equiv V$, where Ω_{m} is the fractional present-day energy density of matter. For a perfect ΛCDM scenario we should have an effective dark energy equation of state equal to -1 during the whole cosmological evolution, with the scalar field remaining perfectly still and showing no evolution at all. However, in the Brans-Dicke paradigm, the field should always evolve even if its dynamics are subdominant (in "slow roll") compared to the potential V. Hence, effectively, we will have a quasi-ΛCDM evolution.

We start by numerically solving the scalar field evolution using Eqs. (2.4) and (2.5) considering a constant potential as defined in the previous paragraph. We set the initial conditions for the scalar field deep within the matter dominated regime at a redshift around $z_{\text{i}} \approx 1000$. For this, we consider a known solution of Brans-Dicke gravity given by [138–140]

$$\phi = \phi_0 a^{1/(\omega_{\text{BD}}+1)}, \tag{2.11}$$

where $\phi_0 = \left(2\omega_{\text{BD}} + 4\right)/\left(2\omega_{\text{BD}} + 3\right)$. This solution is, in fact, an attractor solution of the system derived in the absence of a potential $V(\phi)$ and for a

Universe dominated by matter alone [138–140]. The scale factor, on the other hand, evolves as [138–140]

$$a(t) = \left(\frac{t}{t_0}\right)^{(2\omega_{\rm BD}+2)/(3\omega_{\rm BD}+4)}, \tag{2.12}$$

and we see that, in the GR limit of $\omega_{\rm BD} \to \infty$, $\phi = 1$ and $a(t) \propto t^{2/3}$ throughout the matter dominated regime; t_0 is related to the inverse of the present-day value of the Hubble parameter, H_0, such that $t_0 H_0 = (2\omega_{\rm BD} + 2) / (3\omega_{\rm BD} + 4)$. The value of ϕ_0 ensures that, in a matter dominated Universe, we would measure an effective gravitational constant today, $G_{\rm eff}$, equal to the actual Newton's gravitational constant, G, in Cavendish-like experiments. This assumes, of course, that the solar system value of ϕ is representative of the Universe as a whole, which may not be entirely accurate [141].

Let us also point out that, in a matter dominated flat Universe, the matter density will not be precisely equal to the critical density due to a very small, negative, and almost negligible contribution from the scalar field dynamics. It is possible to rescale the matter density (as in Ref. [142]), but we opt not to do so, since the correction is negligible in the $\omega_{\rm BD} >> 1$ regime we are mostly interested in this work.

In Fig. 2.1, we have the numerical evolution of the scalar field plotted against the power-law solution given by Eq. (2.11). We can clearly observe that, even in the presence of a constant potential V, the Brans-Dicke scalar field evolves according Eq. (2.11) at early-times, during the matter dominated epoch. Only at late-times, close to $a = 1$, we see a slight departure from the power-law of Eq. (2.11), when the dark energy component begins to dominate and accelerates the scalar field.

Still in Fig. 2.1 we can observe the numerical evolution of the dark energy effective equation of state $w_{\rm eff}$ as given by Eq. (2.8). We observe a very sharp transition from -0.4 to -1 that we will explain later on. For now, we can conclude that, even though the scalar field is accelerated by the presence of the constant potential V, its dynamics remain subdominant (the aforementioned slow roll evolution) and allow for a late-time potential dominated epoch with $w_{\rm eff} = -1$.

Having shown in Fig. 2.1 that we recover the power-law solution given Eq. (2.11) at early-times, we now extend its application by using it in the effective equation of state $w_{\rm eff}$ given by Eq. (2.8) in the presence of a constant potential V. Hence,

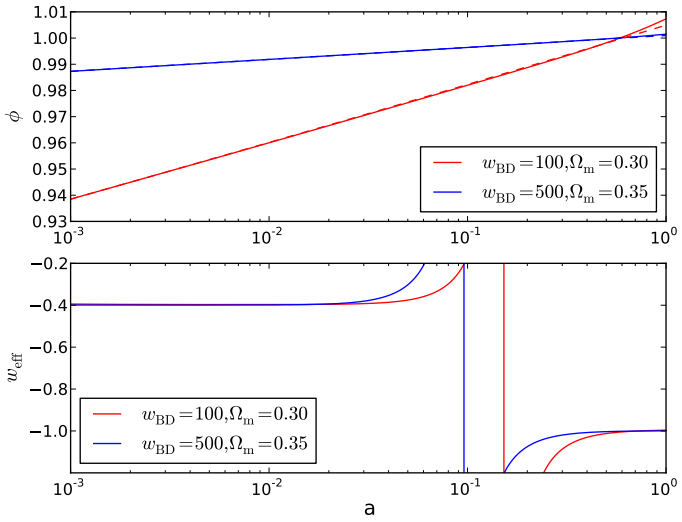

Figure 2.1 *We plot the numerical evolution (solid lines) of the scalar field evolution and the effective dark energy equation of state, $w_{\rm eff}$ in the presence of a constant potential. We note that, in the matter dominated regime, ϕ evolves according to a known power-law solution given by Eq. (2.11), which we also plot (dashed lines).*

we approximately obtain

$$w_{\rm eff} \approx \frac{4 - 4\omega_{\rm BD} V a^3/H_0^2}{-10 + 4\omega_{\rm BD} V a^3/H_0^2}, \tag{2.13}$$

in the limit of $\omega_{\rm BD} >> 1$, and where we have also used Eq. (2.12). Hence, in the matter dominated regime, the potential contribution is suppressed by the scale factor leading to $w_{\rm eff} \approx -0.4$ (unless $\omega_{\rm BD} \to \infty$ and $V \neq 0$). Thus, for values of $\omega_{\rm BD}$ which are consistent with solar system constraints, it is impossible to get an accelerated solution without adding a potential $V(\phi)$, that may not necessarily be constant. However, with a constant potential $V(\phi)$, one gets $w_{\rm eff} = -1$ at late times after a sharp, non-smooth transition from $w_{\rm eff} \approx -0.4$, which we have seen in Fig. 2.1.

An effective equation of state $w_{\rm eff} \approx -0.4$ at early times could constitute a problem, eventually compromising the extension of the matter dominated regime and rendering the model inviable. However, calculating Ω_ϕ, given by Eq. (2.9), explicitly during the matter dominated regime using Eqs. (2.11) and (2.12), one gets

$$\Omega_\phi \approx \frac{1}{3}\left[-\frac{5}{2\omega_{\rm BD}} + \frac{V(\phi)}{H_0^2}a^3\right], \tag{2.14}$$

which, for large values of $\omega_{\rm BD}$ is negligible at early times.

Also, we note that the discontinuity in $w_{\rm eff}$ happens due to a zero crossing of the denominator of Eq. (2.8). If we change from physical time t to the natural logarithm of the scale factor, $dt \rightarrow d\ln a$, we have that $d/dt \rightarrow Hd/d\ln a$. Therefore, neglecting the ϕ'^2 (the prime denotes a derivative with respect to $\ln a$) term because this is proportional to $(1+\omega_{\rm BD})^{-2}$ before the transition and for large $\omega_{\rm BD}$, the denominator of $w_{\rm eff}$ can be approximated to just $-3\phi' + V(\phi)/H^2$. Therefore, given that, in the matter dominated regime, $V(\phi)/H^2 \propto V(\phi)a^3/H_0^2$ is an increasing function of the scale factor, there will come a point at which this term will be equal to $3\phi'$, leading to the discontinuity in $w_{\rm eff}$. For the constant potential, the scale factor of the discontinuity is apprximately

$$a_{\rm disc} \approx \left(\frac{\Omega_{\rm m}}{1-\Omega_{\rm m}}\frac{1}{1+\omega_{\rm BD}}\right)^{1/3}. \tag{2.15}$$

The discontinuity in $w_{\rm eff}$ has no impact on the background expansion of the model: if we take the second Friedmann equation and $p_{\rm m} = 0$, we have

$$\frac{\ddot{a}}{a} = -\frac{H^2}{2}\left(1 + 3\frac{w_{\rm eff}}{\rho_{\rm m}/\rho_\phi + 1}\right). \tag{2.16}$$

Since the divergence in $w_{\rm eff}$ happens due to ρ_ϕ crossing zero, as we just discussed, no divergence is seen in the evolution of $\ddot{a}$ because the term $\rho_{\rm m}/\rho_\phi$ follows the behavior of $w_{\rm eff}$.

Finally, only when $\omega_{\rm BD} \rightarrow \infty$ (the general relativity limit) does one get $w_{\rm eff} = -1$ throughout the whole evolution, as seen in Fig. 2.1. Here the potential $V(\phi)$ will dominate and the scalar field dynamics is heavily suppressed. The discontinuity in $w_{\rm eff}$ will now happen at a much earlier time, as is clear from Eq. (2.15), leading to a smooth $w_{\rm eff} = -1$ in the case of a constant potential.

2.2 Designer extended Brans-Dicke gravity

Having presented the general form for extended Brans Dicke gravity, we now proceed to construct an algorithm that will lead to a particular expansion rate or, more specifically, to an effective equation of state. Hence, effectively, we design and impose the background history we wish for our model which in turn determines the dynamical evolution of the Brans-Dicke scalar field. We note that

the authors of Ref. [143] suggested the designer method we will describe further, but did not fully explore its consequences.

Following the previous section, we have shown that, at early-times, the scalar field will follow the matter domination attractor solution irrespective of the presence of a scalar potential $V(\phi)$. At late-times, its evolution should be dominated by $V(\phi)$, leading to a departure from the matter dominated attractor solution. Therefore, we now try fixing the background evolution to match that of a standard flat wCDM scenario, such that

$$H^2(a) = \frac{H_0^2 E(a)}{\phi} \equiv \frac{H_0^2}{\phi}\left[\Omega_{\rm m} a^{-3} + E_{\rm eff}(a)\right], \tag{2.17}$$

where $\Omega_{\rm m}$ is the present-day fractional matter energy density, and the dark energy component will be fixed as

$$E_{\rm eff}(a) = (1-\Omega_{\rm m})\, e^{3\int_a^1 (1+w_{\rm eff}) {\rm d}\ln {\rm a}}. \tag{2.18}$$

We will be assuming that the effective dark energy equation of state $w_{\rm eff}$ is a constant such that $w_{\rm eff} \geq -1$. We should be clear, however, that this is not a limitation of this procedure: it can be easily extended to a varying $w_{\rm eff}$ by providing a $w_{\rm eff}$ as a function of the scale factor a. We merely choose to do so in hope of finding analytic expressions for some of the observables in terms of the fundamental parameters of the theory. Therefore, we can now numerically evolve the scalar field just by using Eq. (2.4) without evolving the Hubble parameter using Eq. (2.5). We are also effectively parameterizing Eq. (2.10) so that our dark energy component's energy density matches a wCDM type and are not worried with its exact numerical evolution.

We then take the approximation of considering the scalar field potential to be determined by,

$$V(\phi) = 3H_0^2\,(1-\Omega_{\rm m})\, e^{3\int_a^1 (1+w_{\rm eff}) {\rm d}\ln {\rm a}}, \tag{2.19}$$

meaning that we are considering that the main contribution to the effective dark energy density comes from the scalar field potential, with the scalar field dynamics being sub-dominant. With this approximation we also don't expect to affect the matter domination attractor solution at early times since, as seen before, the potential contribution to Ω_ϕ is not relevant in the matter dominated regime.

To generate our numerical results we have fixed the initial value of the scalar field $\phi(z_i)$ and $\phi'(z_i)$ to match the matter dominated attractor solution value

at a redshift of $z_i = 1000$. In Fig. 2.2 we plot the evolution of ϕ and $w_{\rm eff}$ for different values of $\Omega_{\rm m}$, $w_{\rm eff}$, and $\omega_{\rm BD}$ by numerically solving Eq. (2.4) and fixing the evolution of H with Eq. (2.17). In order to compute the first derivative of the potential with respect to the scalar field, V_ϕ, we consider the chain differentiation, $V_\phi = 1/\phi' dV/d\ln a$.

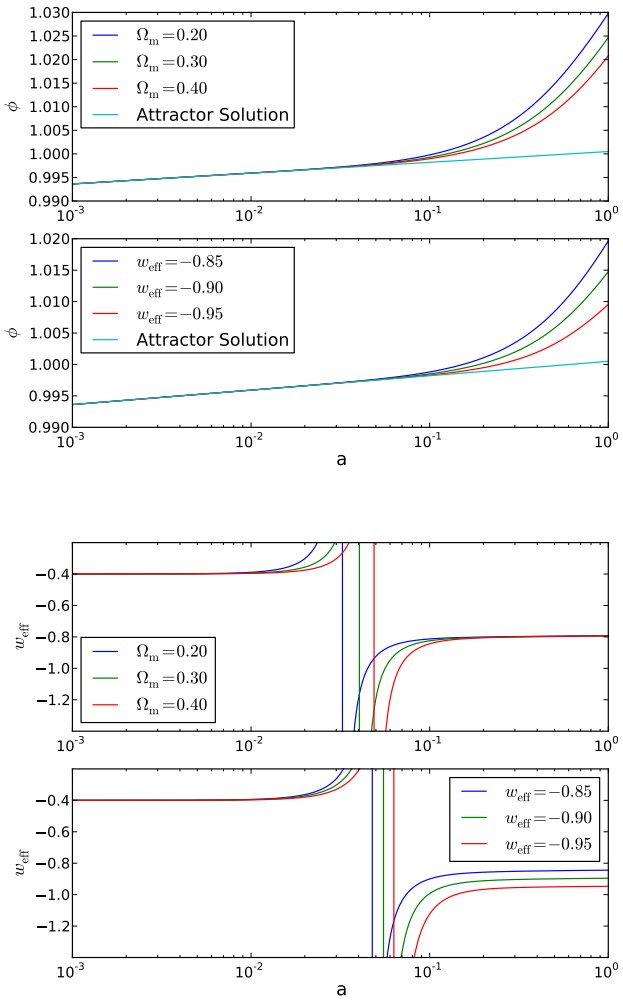

Figure 2.2 *We show the evolution of ϕ and $w_{\rm eff}$ as a function of the scale factor, for $\omega_{\rm BD} = 1000$. On the top plot, the top panel has $w_{\rm eff} = -0.80$ today, while the bottom panel has $\Omega_{\rm m} = 0.30$ and different values of $w_{\rm eff}$ today. On the bottom plot we show the respective evolution of $w_{\rm eff}$.*

We note that, similarly to what we observed in the constant potential case, the presence of the dark energy component leads to a departure of ϕ from the matter domination attractor solution at late times, leading to a scalar field value higher than ϕ_0 at the present. And Fig. 2.2 makes it clear that this departure happens

earlier in time and is more significant the earlier the dark energy component starts to dominate at late-times (which happens the bigger w_{eff} is or the smaller Ω_{m} is). This means that, the higher w_{eff} is, the more relevant the scalar field dynamics becomes. Hence, our designer approach breaks down if w_{eff} is much higher than -1.

Looking at Eq. (2.10), one might be concerned about the numerical evolution of the effective dark energy density which we parameterized by Eq. (2.18); we would probably not recover a flat cosmology today due to the contribution of the scalar field dynamics to the overall critical density of the Universe. If we were to compute ρ_ϕ numerically with Eq. (2.10), one could adjust the weight of the potential $V(\phi)$ to compensate for the dynamics of the scalar field and recover $\Omega_\phi = 1 - \Omega_{\text{m}}$ today. Hence, in effect, $V(\phi) = 3H_0^2\overline{\Omega}_\phi a^{-3(1+w_{\text{eff}})}$, where $\overline{\Omega}_\phi \neq (1 - \Omega_{\text{m}})$ could be found by performing a simple binary search, for example. We will provide an approximation for this factor using our analytical solutions for ϕ in Appendix A.

We can also study the evolution of w_{eff} in Fig. 2.2. We see that we again have a sharp transition from the matter domination attractor regime $w_{\text{eff}} = -0.4$ value at early times to the value we fix w_{eff} to at late-times. The scale factor at which this transition happens can be estimated from

$$a_{\text{disc}} \approx \left(\frac{\Omega_{\text{m}}}{1 - \Omega_{\text{m}}} \frac{1}{1 + \omega_{\text{BD}}} \right)^{-\frac{1}{3w_{\text{eff}}}} , \tag{2.20}$$

making it clear that, the larger w_{eff} is and the earlier our dark energy component becomes relevant, the earlier this transition happens. Also, even though we don't show that explicitly, we recover the GR plus wCDM limit when we take $\omega_{\text{BD}} \to \infty$, and w_{eff} should then be equal to the value we fix it to be throughout the whole evolution, since the discontinuity now happens earlier or may even be completely avoided.

2.3 Analytical solutions for ϕ

With our designer approach in hand, we can now proceed to find analytical approximations to the scalar field evolution which, in turn, can be used to construct approximations to our observables. We first consider the ΛCDM-like case and then generalize to an arbitrary (but constant) effective equation of state

$w_{\rm eff}$.

2.3.1 $w_{\rm eff} = -1$

We start by expressing the scalar field equation of motion, given by Eq. (2.4), in terms of ln a. We then simultaneously neglect the ϕ'' and ϕ'^2 terms. We know that, in the matter dominated regime, $\phi' \propto \omega_{\rm BD}^{-1}$ and $\phi'' \propto \omega_{\rm BD}^{-2}$. Also, from Section 2.2, we have learned that, at late-times, the scalar field departs from the matter domination attractor solution, but not in a significant way such that the dynamics of the scalar field would become relevant. Therefore, neglecting these terms is a valid approximation and, as we will see, it will not hinder the accuracy of the solutions we obtain. Hence, Eq. (2.4) becomes

$$\frac{\phi'}{\phi}\left(1-\frac{1}{2}\frac{\Omega_{\rm m}a^{-3}}{1-\Omega_{\rm m}+a^{-3}\Omega_{\rm m}}\right)=\frac{4\left(1-\Omega_{\rm m}\right)+a^{-3}\Omega_{\rm m}}{d\left(1-\Omega_{\rm m}\right)+a^{-3}\Omega_{\rm m}}, \tag{2.21}$$

where $d = (2\omega_{\rm BD} + 3)$. The solution for the scalar field will be a fully analytical expression, given by

$$\phi(a) = \phi(a_i)g(a_i)^{-1}g(a), \tag{2.22}$$

where $\phi(a_i)$ is the scalar field value at a high redshift z_i set by the matter dominated attractor solution, or can be fixed to be ϕ_0 at $a_i = 1$. The function $g(a)$ is given by

$$g(a) = a^{\frac{2}{d}}\left(2a^3\left(1-\Omega_{\rm m}\right)+\Omega_{\rm m}\right)^{\frac{2}{3d}} \tag{2.23}$$

We show the evolution of ϕ predicted by this solution in Fig. 2.3. It exhibits a tendency to overestimate the deviation from the matter domination attractor solution at late-times. However, its errors are small, specially when considering the considerable simplification we have found to the full numerical analysis of our designer approach.

2.3.2 $w_{\rm eff} \neq -1$

We now extend our analytical approximation for cosmologies with $w_{\rm eff} \neq -1$. In these circumstances, we expect the dark energy component to become relevant earlier, and hence produce larger deviations from the matter dominated attractor prediction. We will focus mainly in the late-time evolution of ϕ, when the dark energy component comes to dominate. For that effect, we re-express Eq. (2.4) in

terms of $\ln a$, and assuming $V_\phi = 1/\phi' \, dV/d\ln a$, we approximate it as

$$\phi \frac{12\phi'\,(1-\Omega_{\rm m}) + 18\phi\,(1-\Omega_{\rm m})\,(1+w_{\rm eff})}{d\,(1-\Omega_{\rm m}+\Omega_{\rm m}a^{3w_{\rm eff}})} \approx 3\phi'^2, \tag{2.24}$$

where $d = (2\omega_{\rm BD}+3)$ and we have also neglected terms proportional to ϕ'', ϕ'^3 and $(1+w_{\rm eff})(1-\Omega_{\rm m})$, the last two arising with the derivative of H. We have not included the matter driving term that dominates at early-times. Assuming that the driving term from the potential slope is much more significant than the $V(\phi)$ one- which effectively means ϕ' is much smaller than unity for large $\omega_{\rm BD}$- we take the square root of this equation and perform a Taylor expansion of the left-hand side, obtaining:

$$\frac{6\phi'\sqrt{(1-\Omega_{\rm m})}}{\sqrt{18\,(1+w_{\rm eff})}} + \sqrt{18\,(1-\Omega_{\rm m})\,(1+w_{\rm eff})}\phi - \phi'\sqrt{3d\,(1-\Omega_{\rm m}+\Omega_{\rm m}a^{3w_{\rm eff}})} \approx 0 \tag{2.25}$$

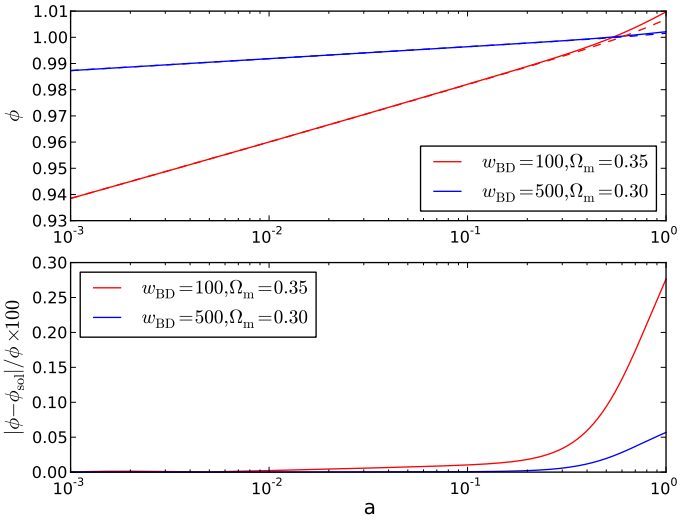

Figure 2.3 *We show the analytical solution for the scalar field, $\phi_{\rm sol}$, predicted by Eq. (2.22) (in solid lines) for different values of $\omega_{\rm BD}$ and $\Omega_{\rm m}$ in the upper plot. We compare the analytical solutions to the numerical evolution of ϕ (in dashed lines) predicted by our designer method, and show the relative error in the bottom plot. The errors are shown in %.*

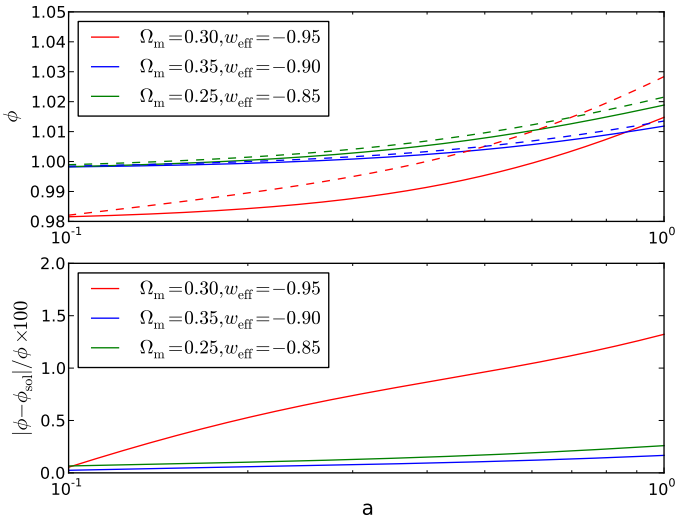

Figure 2.4 *We show the late-time analytical solution (solid lines) of the scalar field predicted by Eq. (2.26), $\phi_{\rm sol}$, when $w_{\rm eff} \neq -1$ for different values of $\omega_{\rm BD}$ and $\Omega_{\rm m}$. We compare it to the numerical solution (dashed lines) predicted by our designer approach in the top plot. We show the relative errors in the bottom plot, in %. The red lines are for $\omega_{\rm BD} = 100$, while the green and blue lines are for $\omega_{\rm BD} = 1000$.*

With these approximations, the solution for this equation is given by

$$\phi(a) = \phi(a_i) f(a) f(a_i)^{-1}, \tag{2.26}$$

where $\phi(a_i)$ is the value of the scalar field at a desired scale factor a_i. This can either be set to the matter dominated attractor solution at a redshift $z_i \approx 10$ or to ϕ_0 at $a = 1$ if one wants to fix the present-day value of the scalar field to recover $G_{\rm eff}/G = 1$ today. The function $f(a)$ is given approximately by

$$f(a) \approx \left(\frac{1+x}{x-1}\right)^{-\frac{\sqrt{6}\sqrt{d}(1+w_{\rm eff})^{3/2}}{w_{\rm eff}(-2+3d(1+w_{\rm eff}))}}, \tag{2.27}$$

where $x = \sqrt{1 + \frac{\Omega_{\rm m}}{1-\Omega_{\rm m}} a^{3w_{\rm eff}}}$ and we have neglected similar terms whose exponents were proportional to d^{-1}. In Fig. 2.4 we compare the late-time evolution of ϕ predicted by Eq. (2.26) with the numerical evolution found in our designer approach. We do so by fixing $\phi(a_i)$ to the matter domination attractor solution at $z_i = 10$ for all the cases. We see that this solution works better for larger $\omega_{\rm BD}$. Nevertheless, even if the agreement with the numerical solution is not perfect, the errors are small, and the overall form of ϕ is excellent for such a simple

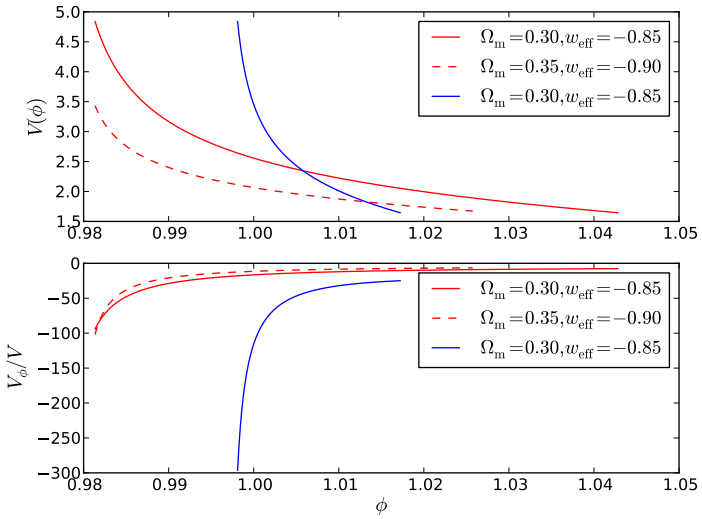

Figure 2.5 *We show the reconstructed functional form of $V(\phi)$. The red lines have $\omega_{\rm BD} = 100$, while the blue line has $\omega_{\rm BD} = 1000$.*

approximation.

We are now also in a position to reconstruct the effective form of the self-interaction potential $V(\phi)$ across the entire cosmological evolution. For that, we invert the solutions for ϕ to get the scale factor as a function of the scalar field. We use the field's matter dominated attractor solution at early-times and our analytical approximation at late-times. Hence, the potential will be given by

$$V(\phi) = \begin{cases} 3H_0^2(1-\Omega_{\rm m})\,(\phi/\phi_0)^{-3(1+w_{\rm eff})(1+\omega_{\rm BD})}\,, & \text{during matter domination} \\ 3H_0^2(1-\Omega_{\rm m}) \left[\dfrac{2^{2/3}(1-\Omega_{\rm m})^{1/3}(\phi/c)^{\frac{(-2+3d(1+w_{\rm eff}))w_{\rm eff}}{3\sqrt{6}\sqrt{d}(1+w_{\rm eff})^{3/2}}}}{\Omega_{\rm m}^{1/3}\left(1-(\phi/c)^{\frac{(-2+3d(1+w_{\rm eff}))w_{\rm eff}}{\sqrt{6}\sqrt{d}(1+w_{\rm eff})^{3/2}}}\right)^{2/3}} \right]^{\frac{-3(1+w_{\rm eff})}{w_{\rm eff}}}, & \text{at late-times,} \end{cases} \tag{2.28}$$

where $c = \phi(a_i)f(a_i)^{-1}$, as defined in Eq. (2.26). We plot the late-time form of the potential $V(\phi)$ and V_ϕ/V in Fig. 2.5 for different values of $\omega_{\rm BD}$, $w_{\rm eff}$ and $\Omega_{\rm m}$. We can observe that $V(\phi)$ exhibits a simple form, as in a standard run-away potential, with the slope decreasing at higher values of ϕ or, equivalently, close to the present. We see as well that V_ϕ/V takes significantly high, absolute values. This justifies our assumption in considering just the effect of the slope of the potential in the evolution of ϕ when $w_{\rm eff} \neq -1$. Indeed, this is the term that

will have the most effect on the scalar field dynamics, leading to a significant departure from the attractor solution at late-times for $w_{\rm eff} > -1$.

In Fig. 2.5 we can also observe that the slope of the potential becomes more significant for higher values of $\omega_{\rm BD}$. This seem to contradict what we have seen in Fig. 2.4, where the scalar field dynamics seem to be more relevant, the smaller $\omega_{\rm BD}$ is. However, the source terms for the evolution of ϕ are suppressed by a factor proportional to $\omega_{\rm BD}^{-1}$. Hence, for a larger value of $\omega_{\rm BD}$, the only way to have significant field dynamics at late-times, and hence induce a significant departure from the matter dominated attractor solution that produces a $w_{\rm eff} \neq -1$, is to have a very large source term. Finally, we can also see how, for larger $w_{\rm eff}$, we recover a more tilted potential: the more relevant we set our dark energy component to be, the more significant we expect the scalar field dynamics to be at late-times.

2.3.3 A global solution

In the previous two sections, we presented solutions for the evolution of the scalar field that worked well for $w_{\rm eff} = -1$ and $w_{\rm eff} > -1$ separately. We will now propose an approximate global solution:

$$\phi_{\rm global}(a) = \phi(a_i) f(a) g(a) f(a_i)^{-1} g(a_i)^{-1}, \tag{2.29}$$

which is just the product of the solutions we previously found for $w_{\rm eff} = -1$ and for $w_{\rm eff} > -1$.

Note that when $w_{\rm eff} = -1$, we have that $f(a_i) = f(a) = 1$. Hence, $\phi_{\rm global}(a)$ will be the exact solution for the scalar field equation of motion under the assumptions we discussed in Sec. 2.3.1. When $w_{\rm eff} > -1$, we note that the main contribution will come from the $f(a)$ and $f(a_i)$ terms; we already have seen in Section 2.3.2 how the scalar field dynamics are more significant when $w_{\rm eff} > -1$. Not only that, but we note that $dg(a)/d\ln a \propto d^{-1}$, whereas $df(a)/d\ln a$ produces terms proportional to $\left(\sqrt{d}\right)^{-1}$. Hence, assuming $dg(a)/d\ln a << df(a)/d\ln a$ when $w_{\rm eff} > -1$, $\phi_{\rm global}(a)$ will be a solution of Eq. (2.25). We will use this full solution in the following sections for the phenomenological parameters, and show that it is indeed a good approximation for the overall behavior of the scalar field.

2.4 A model for the phenomenological parameters.

It has been shown that, at the level of the background and linear cosmological perturbation theory, it is possible to completely characterize any modified theory of gravity in terms of a handful of time dependent functions [113]. We proceed to do so with our designer extended Brans-Dicke gravity. We have already discussed two of our time dependent functions: the time varying Newton's constant (at the level of the background), $G_0 = G/\phi$ and the effective equation of state, $w_{\rm eff}$.

For linear perturbations, following the notation of Ref. [144], we consider a perturbed metric about the FLRW background in the Newtonian gauge,

$$ds^2 = -(1+2\Psi)dt^2 + a^2(t)(1-2\Phi)\delta_{ij}dx^i dx^j, \tag{2.30}$$

where Ψ and Φ are the scalar perturbations that we will refer to as Newtonian potentials and are decomposed as a series of Fourier modes of scale k (h/Mpc).

If we are interested in the the impact of matter perturbations on galaxy and weak lensing surveys, we can focus on the modes that are well within the Hubble radius, i.e. such that the condition $k^2/a^2 \gg H^2$ is respected. In this *quasi-static* regime the evolution equation for the matter density perturbation $\delta_{\rm m}$ can be approximated as [145]

$$\delta_{\rm m}'' + \left(2 + \frac{H'}{H}\right)\delta_{\rm m}' - \frac{3}{2}\frac{G_{\rm eff}}{G}\Omega_{\rm m}(a)\delta_{\rm m} \simeq 0, \tag{2.31}$$

where $\Omega_{\rm m}(a) = \rho_{\rm m}/3H^2$, and $G_{\rm eff}/G$ will be dependent on the model. The primes represent derivatives with respect to $\ln a$. In the extended Brans-Dicke theory, $G_{\rm eff}$ is given by [144]

$$\frac{G_{\rm eff}}{G} = \frac{1}{\phi}\frac{4 + 2\omega_{\rm BD} + 2\phi\,(Ma/k)^2}{3 + 2\omega_{\rm BD} + 2\phi\,(Ma/k)^2}, \tag{2.32}$$

where the M term is [144]

$$M^2 = V_{\phi\phi} + \frac{\omega_{\rm BD}}{\phi^3}\left[\dot{\phi}^2 - \phi\left(\ddot{\phi} + 3H\dot{\phi}\right)\right]. \tag{2.33}$$

At late times, when the dark energy component starts to become relevant, the mass term can be simplified and expressed in terms of the potential alone using

the scalar field equation of motion, such that $M^2 \approx V_{\phi\phi} + \frac{V_\phi}{\phi}$ [144], where $V_{\phi\phi}$ and V_ϕ correspond to the second and first order derivatives of the potential with respect to the scalar field, respectively.

One can also define the gravitational slip γ corresponding to the ratio between the two Newtonian potentials [144]

$$\frac{\Phi}{\Psi} \equiv \gamma = \frac{1 + \omega_{\rm BD} + \phi\,(Ma/k)^2}{2 + \omega_{\rm BD} + \phi\,(Ma/k)^2} \tag{2.34}$$

which, again, should depend on the specifics of the scalar-tensor model. Lastly, the sub-horizon version of the Poisson equation can be written as [144]

$$\frac{k^2}{a^2}\Psi \simeq -4\pi G_{\rm eff}\rho_{\rm m}\delta_{\rm m}. \tag{2.35}$$

In standard GR, when we neglect matter shear, the anisotropy equation between the Newtonian potentials becomes a simple constraint equation, $\Psi = \Phi$, and γ should be 1 throughout the cosmological evolution, as should $G_{\rm eff}/G \equiv \xi$, where $\xi \equiv \mu$ in the notation of Sec. 1.4. Hence, in a modified gravity theory, a deviation in these parameters signals a departure from standard GR that can potentially be measured. From Eqs. (2.32) and (2.34) it is clear that the GR limit is recovered when $\omega_{\rm BD} \to \infty$, as expected, or when the field becomes supermassive and $M^2 \to \infty$. But we now wish to understand how these functions depend on time. To do so, it is convenient to study

$$\xi_{QS} \equiv \lim_{k\to\infty}\frac{G_{\rm eff}}{G} = \frac{1}{\phi}\frac{4 + 2\omega_{\rm BD}}{3 + 2\omega_{\rm BD}} \tag{2.36}$$

$$\gamma_{QS} \equiv \lim_{k\to\infty}\gamma = \frac{1 + \omega_{\rm BD}}{2 + \omega_{\rm BD}} \tag{2.37}$$

and the inverse length scale

$$k_M \equiv \sqrt{\frac{\phi}{1 + \omega_{\rm BD}}}Ma. \tag{2.38}$$

From Eq. (2.37), we see that $\gamma_{\rm QS}$ is constant throughout the cosmological evolution, independently of the scalar field dynamics [143–145]. Its GR limit is trivially recovered when we take $\omega_{\rm BD} \to \infty$.

On the other hand, the late-time evolution of the mass scale parameter, k_M, can

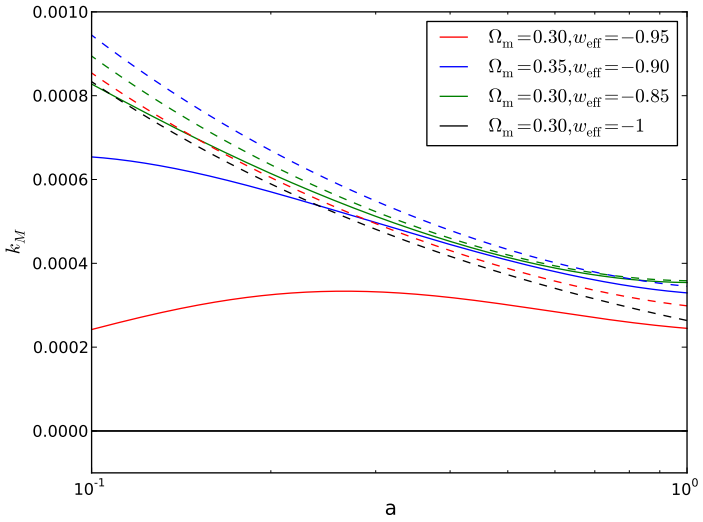

Figure 2.6 *We show the evolution of k_M. The solid lines are the numerical evolution obtained using the global solution for ϕ given by Eq. (2.29), while the dashed lines show the evolution predicted by the approximation given by Eq. (2.39). The red lines have $\omega_{\rm BD} = 1000$, the blue lines are for $\omega_{\rm BD} = 10000$ and the green lines have $\omega_{\rm BD} = 1 \times 10^5$. We have fixed $H_0 = 1/2997.9\ h/\mathrm{Mpc}$, with $h = 0.68$. The black lines are for $w_{\rm eff} = -1$, and the results shown are independent of $\omega_{\rm BD}$.*

be written as:

$$k_M(a) \approx \frac{3}{\sqrt{2}} H_0 \sqrt{2\,(1-\Omega_{\rm m})\,(1+w_{\rm eff})\,a^{-(1+3w_{\rm eff})} + a^{-1}\Omega_{\rm m}\,(2+w_{\rm eff})} \qquad (2.39)$$

which is valid for $w_{\rm eff} > -1$ and large $\omega_{\rm BD}$. In the limit $w_{\rm eff} = -1$, this equation predicts a non-zero value for k_M, whereas it should be exactly zero throughout, as predicted by explicitly using our global solution for ϕ in Eq. (2.38). This should be evident as $V_\phi = V_{\phi\phi} = 0$ when $w_{\rm eff} = -1$. This approximation works fairly well for small redshifts and better for larger $\omega_{\rm BD}$, as can be seen in Fig. 2.6.

We can also observe that k_M is a fairly negligible quantity, corresponding to scales which are of order or greater than the cosmological scale. To do so we compare k_M to the comoving horizon, $aH = H_0\sqrt{\Omega_{\rm m}a^{-1} + (1-\Omega_{\rm m})a^{-(1+3w_{\rm eff})}}$. It is not hard to see that $k_M/(aH) \lesssim 1$. Hence, the scale at which k/k_M becomes relevant is approximately the same at which the perturbations k-modes become sub-horizon, which is at the basis of our assumptions. Therefore, taking $k/k_M >> 1$ is an

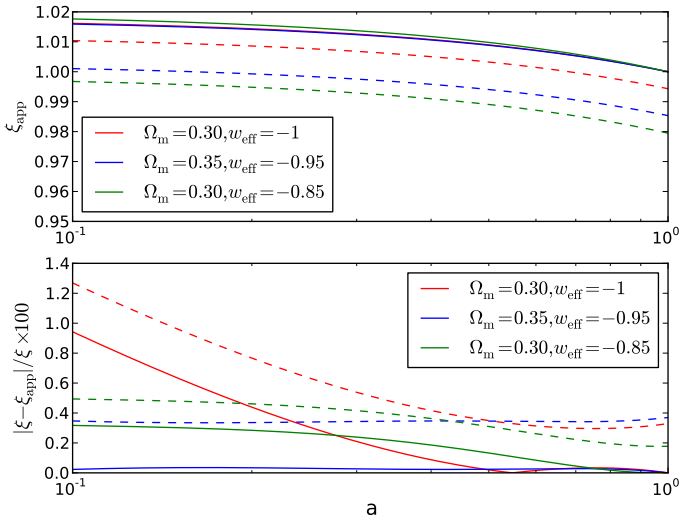

Figure 2.7 *We show the late-time evolution of $G_{\rm eff}/G$ in the quasi-static regime using Eq. (2.29) in the upper plot. The solid lines show $G_{\rm eff}/G$ with $\phi = \phi_0$ today, while the dashed lines do not have that restriction. The red lines are for $\omega_{\rm BD} = 100$, the blue lines for $\omega_{\rm BD} = 500$ and the green lines have $\omega_{\rm BD} = 1000$. The bottom plot shows the relative error of our approximations to the exact numerical solutions in %.*

excellent approximation on quasi-static scales.

To understand the parameter dependence of ξ_{QS} we perform a Taylor expansion around $a = 1$ using our approximate global solution for the scalar field. We further simplify our functions by considering the two regimes of interest we observe in our models: one where we will have $\phi = \phi_0$ today if we intend to recover $G_{\rm eff} = G$ at the present; and another one where we do not recover ϕ_0 at the present, meaning that, essentially, we instead recover the matter domination attractor solution for ϕ at early times given by Eq. (2.11). For the first case, we obtain:

$$\xi_{QS_1}(a) \approx 1 + (1-a)\left[\frac{8-6\Omega_{\rm m}}{d\,(2-\Omega_{\rm m})} + \frac{3\sqrt{6}\sqrt{d\,(1-\Omega_{\rm m})}\,(1+w_{\rm eff})^{3/2}}{3d\,(1+w_{\rm eff})-2}\right] \tag{2.40}$$

while for the second case we find

$$\xi_{QS_2}(a) \approx \left(\frac{\Omega_{\rm m}}{2-\Omega_{\rm m}}\right)^{\frac{2}{3d}} \left(\frac{\sqrt{\frac{1}{1-\Omega_{\rm m}}}-1}{1+\sqrt{\frac{1}{1-\Omega_{\rm m}}}}\right)^{-\frac{\sqrt{6}\sqrt{d}(1+w_{\rm eff})^{3/2}}{(-2+3d(1+w_{\rm eff}))w_{\rm eff}}} \xi_{QS_1}(a) \tag{2.41}$$

The GR limit of $\xi_{QS} = 1$ is recovered in both situations when we take $\omega_{\rm BD} \to \infty$. For the first case, as expected, $\xi_{QS} = 1$ when $a = 1$ since we have $\phi = \phi_0$ today. In the second case, $\xi_{QS} < 1$ today since the present-day value of the scalar field in these circumstances will always be larger than ϕ_0. This can be observed in Fig. 2.7, where we compare these approximations to the exact numerical solution of ξ and we see they work considerably well. We note that using ϕ_0 to normalize the matter attractor is an arbitrary choice. In practice, one could generalize Eq. (2.41) to any value of the scalar field at the present-day by replacing the term multiplying $\xi_{\rm QS_1}$. This could then be a free parameter to test how much the data allows deviations from the standard GR value $\xi_{\rm QS_1} = 1$.

We can now try and understand the dependence of ξ_{QS} on the different parameters. Looking at $d = 2\omega_{\rm BD} + 3$, it becomes clear that increasing the Brans-Dicke parameter leads to ξ_{QS} becoming closer to 1 throughout the late-time cosmological evolution: its slope at $a = 1$, as given by Eq. (2.40), decreases since it depends on the inverse of d or $\sqrt{d}$. Then, looking at Eq. (2.41), we see that the present-day value of ξ_{QS} increases towards 1 due to the exponents of the terms shown becoming extremely small.

Looking at the dependence of ξ_{QS} on $\Omega_{\rm m}$, we realize it is similar to that on $\omega_{\rm BD}$. Increasing $\Omega_{\rm m}$ leads to both the slope of ξ_{QS} decreasing in Eq. (2.40) as well as the present day-value tending to 1 in Eq. (2.41). In Eq. (2.41) we also see that, remarkably, our approximation recovers the matter dominated attractor solution value of $\xi_{QS} = 1$ when $\Omega_{\rm m} \to 1$. Lastly, we have the effective equation of state parameter, $w_{\rm eff}$. Looking at Eq. (2.40), we see that the slope of ξ_{QS} will increase as $w_{\rm eff}$ becomes less negative, making its evolution more noticeable for larger $w_{\rm eff}$ when all other parameters remain fixed. Also, the exponent of the second term in Eq. (2.41) increases for large $w_{\rm eff}$, leading to a significant departure of ξ_{QS} today, producing values of $\xi_{QS}(a = 1)$ that are detectably smaller than 1 in a clear departure from standard GR. This is a reflection of the effect of increasing $w_{\rm eff}$ on the evolution of the scalar field ϕ: the higher $w_{\rm eff}$ is, the sooner ϕ departs from the matter domination attractor solution and the larger its present-day value will be.

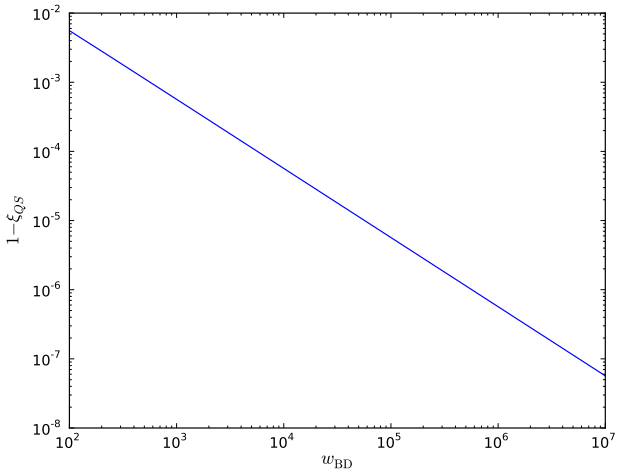

Figure 2.8 *We show the evolution of ξ_{QS} at $a = 1$ for $\Omega_{\rm m} = 0.308$ and $w_{\rm eff} = -1$ as a function of $\omega_{\rm BD}$. For this plot we have used Eq. (2.41), therefore assuming that $\phi(a = 1)$ may not be equal to ϕ_0.*

In Fig. 2.8, we plot ξ_{QS} as a function of $\omega_{\rm BD}$ at $a = 1$, using Eq. (2.41). We see that if we don't fix $\phi = \phi_0$ today, there is a significant, possibly detectable, deviation from the standard GR value, $\xi_{QS} = 1$, even for very large $\omega_{\rm BD}$. Of course, we also see that when $\omega_{\rm BD} \to \infty$, ξ_{QS} tends to 1. Therefore, in order to be competitive with solar system constraints $\omega_{\rm BD} > 10^4$ [125, 126], we would have to able to measure ξ_{QS} with a precision of around 10^{-4}.

2.5 Discussion

In this work we have applied the designer approach to the extended Brans-Dicke theory with the explicit presence of a self-interacting potential $V(\phi)$. By fixing the expansion history to that of an effective wCDM dark energy model, we are able to retrieve the scalar field evolution under the assumption that the main contribution to the effective dark energy density comes from the potential $V(\phi)$.

The numerical solutions we obtain have the property of respecting the matter domination attractor solution of Brans-Dicke models at early-times. At late-times, the scalar field departs from this solution and evolves more rapidly and towards larger values, yielding a value today larger than ϕ_0, where ϕ_0 is the present-day value of the matter regime attractor solution that ensures that one would measure $G_{\rm eff}$ today equal to the actual Newton's gravitational constant,

G, in a matter-dominated Universe. This transition from the attractor solution happens earlier whenever we take a larger dark energy equation of state, $w_{\rm eff}$. However, if we constrain the present-day value of ϕ to be equal to ϕ_0, our numerical solutions follow the power-law behavior of the attractor solution, shifted towards smaller values at early-times. When the evolution departs from the matter dominated behavior, we are then able to recover $\phi(a = 1) = \phi_0$ as intended.

We were able to obtain separate analytical approximations for the evolution of the scalar field when $w_{\rm eff} = -1$ and $w_{\rm eff} > -1$, which we then used to construct a global solution valid for $w_{\rm eff} \geq -1$. These approximations work remarkably well, with errors of sub-percent for large values of $\omega_{\rm BD}$. These approximations also allowed us to reconstruct the late-time functional form of the potential $V(\phi)$; we found a simple run-away potential whose slope is inevitably dependent on $w_{\rm eff}$ and $\omega_{\rm BD}$. We reiterate that we have limited our analysis to constant $w_{\rm eff}$ so as to obtain analytical solutions which will shed light on the parameter dependence of the various observables we are considering; a non-constant $w_{\rm eff}$ will severely complicate any attempts at doing so. However, we stress that the numerical implementation of the designer approach presented in Sec. 2.2 can be easily extended to a non-constant $w_{\rm eff}$.

With these analytic approximations in hand, we then focused on the phenomenological parameters that describe the sub-horizon evolution of the linear perturbations of the theory. We showed how the effective scale of the theory, which we designated by k_M, is of order the cosmological horizon; as a result we find that there is negligible scale dependence of the phenomenological parameters on observable scales. We found that the ratio between the Newtonian potentials, $\gamma = \Phi/\Psi$ is constant throughout the cosmological evolution, for large values of the Brans-Dicke parameter [144]. We also found simple analytical expression for $\xi = G_{\rm eff}/G$ which depend explicitly on the parameters of the theory, as seen in Eqs. (2.40) and (2.41).

One of the main features of this model is the possibility of having $\xi_{QS} \neq 1$ today; this is due to the departure of the scalar field from the matter dominated attractor solution at late-times such that its present-day value will be larger than ϕ_0. The present-day value of ξ_{QS} at $a = 1$, given in Eq. (2.41) tends to 1 as $\omega_{\rm BD} \to \infty$ since the exponent of the terms shown tend to zero. Also, as for $w_{\rm eff} > -1$, the exponent of one of the terms increases, leading to smaller values of ξ_{QS} today, even when $\omega_{\rm BD}$ is very large.

If, however, we impose ξ_{QS} to be 1 today, its evolution is predicted by Eq. (2.40). In these circumstances, the main distinguishing point between this model and standard GR will be the slope of ξ_{QS} at the present: for the extended Brans-Dicke theory it can be different from zero. We note that, even when $w_{\rm eff} = -1$, the predicted slope is different from zero. Hence, even the simple extended Brans-Dicke+ΛCDM model could be ruled out if ξ_{QS} is found to not vary close to the present.

Finally, we note that in order to attain constraints on $\omega_{\rm BD}$ that are competitive with those obtained in solar system tests [125, 126], ξ_{QS} and γ_{QS} would naively need to be constrained with a precision of around 10^{-4}. This is a formidable challenge, but one should bear in mind that $\gamma_{QS} \neq 1$ throughout (at least) the matter dominated era while the same is possible for ξ_{QS}. This means that there will be a cumulative effective (as shown in [146, 147]) which means that constraints on the growth rate (or weak lensing) of order 10^{-3} or even 10^{-2} might be sufficient to place competitive constraints on $w_{\rm BD}$.

Chapter 3

Linear perturbations in viable $f(R)$ theories

In this work, we focus on a well known modification of gravity, the metric $f(R)$ theory. This theory consists in a modification of the Einstein–Hilbert action through adoption of a general function $f(R)$ of the invariant Ricci scalar R. Even though this class of modified gravity theories (MGT) might be viewed as a toy model, it is interesting as it allows for fairly general modifications of the action and appears to be one of the few that avoids the potentially-fatal Ostrogradski instability [148]. According to Ostrogradski's theorem, there is a linear instability associated with non-degenerate Lagrangians that depend on more than one time derivative (for instance, such that $L = L(x, \dot{x}, \ddot{x})$ and $\partial^2 L/\partial^2 \ddot{x} \neq 0$). Such systems will lead to higher than second-order differential equations of motion that require more initial conditions than usual dynamical systems. This corresponds to the appearance of an additional degree of freedom whose Hamiltonian depends linearly on one canonical momentum and is thus (kinetically) unbounded from below [149, 150]. This could be problematic for $f(R)$ theories but, as it stands, these are one of the few modifications of gravity that are able to evade this powerful theorem as they are built solely from the Ricci scalar and can be recast as a scalar-tensor theory with a healthy propagating degree of freedom [149, 151].

Therefore, $f(R)$ has received a great deal of attention as, at the very least, the study of these models can provide information on how GR may be modified and the limits to such modifications, if they prove to be necessary. Since Starobinsky's first working model of inflation [152] which consisted of adding an R^2 term to

the action, there have been many more attempts to develop models that are cosmologically viable explanations of the Universe's acceleration [153–156]. In this work, we focus on Starobinsky's $f(R)$ model [157], the Hu–Sawicki model [158], and the exponential model [159], the reason being that these are models that provide viable cosmologies, while behaving like an effective cosmological constant in the high-curvature regime.

Due to the fourth-order nature of the equations of motion for $f(R)$, one can also apply the so-called designer approach to match any background history of the Universe [160]. However, respecting the stringent viability conditions, which we will describe later, one is usually restricted to a cosmological evolution almost indistinguishable from the ΛCDM. Nevertheless, one can always search for modifications in the gravitational potentials by analyzing the evolution of linear perturbations in $f(R)$ theories, which has been done extensively [160–167]. Due to the existence of an additional scalar degree of freedom that mediates an attractive 'fifth force', there can be detectable differences on the evolution of these potentials between these theories and ΛCDM. This renders the search for modifications in the growth dynamics one of the primary goals of upcoming dark energy projects, such as the Dark Energy Survey (DES) [168] and the *Euclid* mission [91], for instance.

In this work, we provide, for each of the chosen $f(R)$ models, two contrasting cases of the background evolution predicted by them for a choice of parameters that either substantially violate the viability conditions or are within the observational constraints. We then study the evolution of linear perturbations for these models on different scales, noting where this diverges from ΛCDM. We note differences in the evolution of the gravitational potentials between the different models which would possibly allow them to be distinguished. We also use the designer approach to present the evolution of the linear perturbations for an $f(R)$ model with an effective equation of state equal to ΛCDM's $w = -1$ and that completely respects the viability conditions.

This chapter is organized as follows. In Section 3.1, we present the cosmological equations in the context of $f(R)$ theories and discuss the chosen models as well as the viability conditions. In Section 3.2, we show the linearly-perturbed equations and examine some of their generic features. In Section 3.3, we present the results and conclude with a brief discussion in Section 3.4.

I would like to state that this chapter can be seen in [2]. It was done in

collaboration with my supervisor, Professor Andrew Liddle, who advised me throughout and extensively supervised the writing of the scientific text.

3.1 Cosmology in $f(R)$

3.1.1 Dynamical equations

Our treatment of the background dynamics closely follows Refs. [162, 169]. The action of $f(R)$ gravity in the Jordan frame is

$$S = \frac{1}{2\kappa^2} \int d^4x \sqrt{-g} \left[f(R) + 2\kappa^2 \mathcal{L}_{\rm m}(\chi_i, g_{\mu\nu}) \right] , \tag{3.1}$$

where $\kappa^2 = 8\pi G$, and $f(R)$ is a general function of the Ricci scalar, R, of the form $f(R) = R + \tilde{f}(R)$, where $\tilde{f}(R)$ will be the change to GR's Einstein–Hilbert action, effectively playing the role of DE. In this frame the matter fields, χ_i, will fall along the geodesics defined by the metric $g_{\mu\nu}$, since the respective Lagrangian, $\mathcal{L}$, is minimally coupled. The field equations are obtained by varying the action with respect to the metric, yielding

$$f_R R_{\mu\nu} - \frac{1}{2} f g_{\mu\nu} - (\nabla_\mu \nabla_\nu - g_{\mu\nu} \Box) f_R = \kappa^2 T_{\mu\nu} \, . \tag{3.2}$$

In this equation, $f_R \equiv \partial f / \partial R$ and $\Box \equiv g^{\mu\nu} \nabla_\mu \nabla_\nu$ is the covariant D'Alembertian. $T_{\mu\nu}$ is the energy–momentum tensor of matter, which is taken to be that of a perfect fluid

$$T_{\mu\nu} = (\rho + p) \, U_\mu U_\nu + p g_{\mu\nu} \, , \tag{3.3}$$

where U^μ is the fluid rest-frame four-velocity, ρ is the energy density and p is the pressure, related to the density by $w = p/\rho$, where w is the equation of state (w is 0 for pressureless matter and 1/3 for radiation). Due to the minimal coupling of matter to the metric, the energy–momentum tensor will obey the same conservation law as in standard GR. Adopting a flat Friedmann–Robertson–Walker (FRW) metric, $ds^2 = -dt^2 + a^2(t) d\mathbf{x}^2$, this has the well-known form

$$\dot{\rho} + 3H \left(\rho + p \right) = 0 \, , \tag{3.4}$$

where overdot is differentiation with respect to time t and $H = \dot{a}/a$ is the Hubble expansion factor.

The appearance of a new scalar degree of freedom in $f(R)$ theories can be seen by taking the trace of Eq. (3.2),

$$\Box\tilde{f}_R = \frac{1}{3}\left(R + 2\tilde{f} - R\tilde{f}_R\right) - \frac{\kappa^2}{3}(\rho - 3p) \equiv \frac{\partial V_{\rm eff}}{\partial \tilde{f}_R}\,, \tag{3.5}$$

which is a second-order differential equation for a field $\tilde{f}_R$, the scalaron [152], with a canonical kinetic term and an effective potential $V_{\rm eff}(\tilde{f}_R)$. This scalar degree of freedom can also be seen by transforming the action (3.1) into that of a scalar-tensor theory

$$S = \frac{1}{2\kappa^2}\int d^4x\sqrt{-g}\left[f(\varphi) + f'(\varphi)(R-\varphi) + 2\kappa^2\mathcal{L}_{\rm m}(\chi_{\rm i}, g_{\mu\nu})\right]. \tag{3.6}$$

Variation with respect to φ leads to the equation $\varphi - R = 0$ if $f'' \neq 0$, which reproduces the original action (3.1). With that, Eq. (3.6) can be recast as

$$S = \frac{1}{2\kappa^2}\int d^4x\sqrt{-g}\left[\phi R - V(\phi) + 2\kappa^2\mathcal{L}_{\rm m}(\chi_{\rm i}, g_{\mu\nu})\right], \tag{3.7}$$

where we have made the identification $\phi = f_R \equiv 1 + \tilde{f}_R$ and $V(\phi) = \phi R - f(R)$. This last equation renders $f(R)$ theories eqivalent to Brans–Dicke theories with $\omega_{\rm BD} = 0$ by comparison with action (2.1).

Further conformally transforming the metric so that the gravitational part of the action resembles that of GR allows to describe the model in the Einstein frame, where the Friedmann equations take their standard form and the scalar degree of freedom evolves as dark energy. Even though, in this frame, things might sometimes be conceptually simpler, the transformation also leads to a non-minimal coupling of the matter to the metric. Making explicit the dynamical equivalence between the approaches is beyond the scope of this work so, for the remainder we will stick to the Jordan frame, referring the reader to Ref. [170, 171] and references therein for a more detailed discussion of the subject.

In order to have consistency with our knowledge from the high-redshift Universe, which is well constrained by CMB observations [172, 173], one wants $|\tilde{f}| \ll R$ and $|\tilde{f}_R| \ll 1$ to recover standard GR with a negligible cosmological constant. In that regime, the extremum of the effective potential is located at the GR value $R = \kappa^2(\rho - 3p)$. The nature of that extremum is defined by the second derivative of the potential, which can also be interpreted as the effective mass of the scalaron

$$m^2_{\tilde{f}_R} \equiv \frac{\partial^2 V_{\rm eff}}{\partial \tilde{f}_R^2} = \frac{1}{3}\left[\frac{1+\tilde{f}_R}{\tilde{f}_{RR}} - R\right], \tag{3.8}$$

where $\tilde{f}_{RR}$ is the second partial derivative of $\tilde{f}$ with respect to R. One can then define the Compton wavelength that determines the range of the attractive fifth force mediated by the scalaron

$$\lambda_{\rm C} = \frac{2\pi}{m_{\tilde{f}_R}}. \tag{3.9}$$

One expects that on scales inside the Compton radius there is an enhancement in the gravitational potentials, which we will study later.

To obtain the background evolution relating to the different $f(R)$ models, we follow the approach taken in Ref. [169]. We start by re-writing Eq. (3.2) as a dynamical equation for R, yielding

$$\begin{aligned} f_R G_{\mu\nu} \quad & -f_{RR}\nabla_\mu\nabla_\nu R - f_{RRR}\left(\nabla_\mu R\right)\left(\nabla_\nu R\right) \\ +g_{\mu\nu} \quad & \left[\frac{1}{2}\left(Rf_R - f\right) + f_{RR}\Box R + f_{RRR}\left(\nabla R\right)^2\right] = \kappa^2 T_{\mu\nu}. \end{aligned} \tag{3.10}$$

Taking the trace one finds

$$\Box R = \frac{1}{3f_{RR}}\left[\kappa^2 T - 3f_{RRR}\left(\nabla R\right)^2 + 2f - Rf_R\right], \tag{3.11}$$

where T is the trace of the energy–momentum tensor. This can then be reinserted into Eq. (3.10) to give

$$\begin{aligned} G_{\mu\nu} \quad = \quad & \frac{1}{f_R}[f_{RR}\nabla_\mu\nabla_\nu R + f_{RRR}\left(\nabla_\mu R\right)\left(\nabla_\nu R\right) \\ & -\frac{g_{\mu\nu}}{6}\left(Rf_R + f + 2\kappa^2 T\right) + \kappa^2 T_{\mu\nu}], \end{aligned} \tag{3.12}$$

where $G_{\mu\nu}$ is Einstein's tensor.

Finally, the set of equations to retrieve the cosmology for particular $f(R)$ models will come from the t–t and i–i Einstein's equations, as well from Eq. (3.11). These are

$$\ddot{R} = -3H\dot{R} - \frac{1}{3f_{RR}}\left[3f_{RRR}\dot{R}^2 + 2f - f_R R + \kappa^2 T\right], \tag{3.13}$$

for R, the generalization of the usual first Friedmann equation,

$$H^2 + \frac{1}{f_R}\left[f_{RR}H\dot{R} - \frac{1}{6}\left(f_R R - f\right)\right] = -\frac{\kappa^2 T^t{}_t}{3f_R}\,, \tag{3.14}$$

and the second Friedmann equation,

$$\dot{H} = -H^2 + \frac{1}{f_R}\left(f_{RR}H\dot{R} + \frac{f}{6} + \frac{\kappa^2 T^t{}_t}{3}\right)\,. \tag{3.15}$$

From the last two equations, we can define an effective energy density and pressure for our $f(R)$ component behaving like DE. These correspond to Eqs. (30) and (31) in Ref. [169], from which one can define the $f(R)$ effective equation of state as

$$w_{\rm eff} = \frac{3H^2 - 3\kappa^2 p_{\rm rad} - R}{3\left(3H^2 - \kappa^2\rho\right)}\,, \tag{3.16}$$

which, contrary to the definition used in Chapter 2 for standard Brans-Dicke, explicitly includes f_R (or, equivalently, the scalar field ϕ) in the denominator of $\rho_{\rm eff}$ and $p_{\rm eff}$. It can also be written in purely geometrical terms as [162]

$$w_{\rm eff} = -\frac{1}{3} - \frac{2}{3}\frac{\left[H^2\tilde{f}_R - \frac{1}{6}\tilde{f} - H\dot{\tilde{f}}_R - \frac{1}{2}\ddot{\tilde{f}}_R\right]}{\left[-H^2\tilde{f}_R - \frac{1}{6}\tilde{f} - H\dot{\tilde{f}}_R + \frac{1}{6}\tilde{f}_R R\right]}\,. \tag{3.17}$$

Summing up, one can use Eqs. (3.13) and (3.15) to get the cosmology for a given model starting at an initial redshift, $z_{\rm c}$, using ΛCDM as reference to obtain the initial abundances of dark matter and radiation and the value for the Hubble parameter, $H_{\rm c}$. Setting $w_{\rm eff}(z_{\rm c}) \approx -1$, one can solve Eq. (3.16) for $R_{\rm c}$. The initial value for $\dot{R}$ is then obtained from Eq. (3.14). This is a very good approximation as in the high-redshift Universe one expects to have $f(R) \to R - 2\Lambda^{\infty}_{\rm eff}$ in realistic $f(R)$ models.

Due to the fourth-order nature of $f(R)$ theories, the initial value problem (or Cauchy problem) could be ill-defined, requiring one to provide initial conditions up to the third order in derivatives. However, the metric-affine $f(R)$ gravity including a matter source in the form of a perfect fluid has been shown to be equivalent to GR. Hence the initial-value problem is well formulated and well posed, as the system of equations of motion can be recast as a system of only first-order equations in time and space in the scalar field variables (see Ref. [174] and references therein for a detailed discussion).

3.1.2 Cosmological viability of $f(R)$ models

A great deal of work on the viability conditions of $f(R)$ theories has been done. This gives a set of restrictions that must be respected in order for $f(R)$ to have a consistent matter domination phase prior to the onset of acceleration [175, 176], to meet the strict solar system (SS) tests of gravity [177, 178], and to provide a stable high-curvature regime where one should recover standard GR. We will only make a brief overview of these conditions.

One immediate condition, from the definition of the scalaron's effective mass, is that $\tilde{f}_{RR} > 0$ for $|R\tilde{f}_{RR}| \ll 1$, so that the scalaron in non-tachyonic. This guarantees a stable high-curvature regime with a proper matter domination phase [179]. As we want to recover standard GR at early times, we need $\tilde{f} \ll R$ as R increases. Together with the $\tilde{f}_{RR} > 0$ condition, one can conclude that $\tilde{f}_R < 0$.

Another requirement is that $1 + \tilde{f}_R > 0$. Violating this can have several consequences, such as the graviton turning into a ghost [180], or the Universe rapidly becoming inhomogeneous and anisotropic [181]. A more straightforward interpretation is that this condition prevents the effective Newton's constant, rescaled from the original by $G_{\rm eff} = G/(1 + \tilde{f}_R)$, changing sign.

A variety of constraints have been placed on the absolute value of $\tilde{f}_R$ today, $|\tilde{f}_{R_0}|$, both on SS scales and Galactic scales. Hu and Sawicki argue that Galactic structure requires it to be smaller than about 10^{-6} [158], though we note this assumes galaxy formation in $f(R)$ proceeds the same way as in GR. The tightest current observational constraints from large-scale structure and distance indicators place upper bounds on $|\tilde{f}_{R_0}|$ between 10^{-3} and 10^{-7} at the 95% confidence level [182, 183]. Future constraints provided by 21cm intensity mapping are expected to place an upper limit on $|\tilde{f}_{R0}|$ around 10^{-5} at the same confidence level [184]. For our purposes we adopt the conservative view that $|\tilde{f}_{R0}|$ should not exceed 10^{-4}, in considering specific parameters within our models.

Lastly, there is the chameleon mechanism of $f(R)$ models [59], which is vital to pass SS tests and can also help produce a viable background expansion, as shown in Ref. [163]. This is deeply connected to the identification of $f(R)$ as a scalar–tensor theory, as stressed previously [170, 171]. It ensures that the additional scalar degree of freedom acquires a large mass in regions of high concentrations of matter, such as galaxies. The additional attractive fifth force is then largely suppressed. This mechanism, alongside the conditions mentioned in the previous

paragraphs, should be sufficient to get a cosmologically-viable model of $f(R)$ (for a detailed discussion of fifth-force solar system and Equivalence Principle tests in $f(R)$ gravity, see Ref. [185]).

3.1.3 Realistic models of $f(R)$

In this work, we focus on three particular $f(R)$ models that not only mimic Λ at early times, but also at late times. The first is Starobinsky's model [157], which is defined by the following $f(R)$ function,

$$f(R) = R + \lambda R_S \left[\left(1 + R^2/R_S^2\right)^{-q} - 1 \right] , \tag{3.18}$$

where $R_S = \sigma_\star H_0^2$ is a parameter of the model that can be adjusted to fit observations or give the right cosmological evolution. We will be using $q = 2$ throughout this work, and use two sets of values for the dimensionless parameters $\sigma_\star$ and λ in the cases we will be considering later. Note that this model, for $q > 0$, behaves like an effective cosmological constant for $R \gg R_S$, such that $\Lambda_{\rm eff}^{\infty} \approx -\lambda R_S/2$.

Furthermore, to understand the cosmological evolution predicted by this and the following models, one can define, from Eq. (3.11), an effective potential given by [169]

$$V(R) = -\frac{1}{3} R f(R) + \int^R f(x) dx \, . \tag{3.19}$$

If one finds a solution such that $V_R(R_1) = 0$, then Eq. (3.11) will admit the constant R_1 value as a solution in the regime of negligible matter contribution, e.g., outside a compact object or at late times in the evolution of the Universe. According to Eq. (3.12), $G_{\mu\nu} = -\Lambda_{\rm eff} g_{\mu\nu} \equiv -g_{\mu\nu} R_1/4$, meaning that $f(R)$ theories will mimic Λ if R approaches a critical point of $V(R)$ when the energy–momentum tensor contribution is negligible, i.e. $T_{\mu\nu} \approx 0$. This corresponds to the de Sitter point where the cosmological solution is expected to asymptotically settle.

In Starobinsky's model, the potential is given by

$$V(R) = \frac{1}{6} \left(R^2 - \lambda R R_S \frac{4R^4 + 5R^2 R_S^2 + 3R_S^4}{\left(R^2 + R_S^2\right)^2} \right) + \frac{\lambda R_S^2}{2} \arctan \frac{R}{R_S} \, , \tag{3.20}$$

which will be shown later when we study the background evolution predicted by the $f(R)$ models. We note that f_{RR} is not positive definite, since $f_{RR} = 0$ when

$R = \pm R_S\sqrt{2q+1}$.

The second model is that of Hu and Sawicki [158]. The $f(R)$ function is given by

$$f(R) = R - m^2 \frac{c\,(R/m^2)^n}{1 + d\,(R/m^2)^n}\,, \tag{3.21}$$

where m^2, c, d and $n > 0$ are parameters of the model. Following Ref. [169], we take $n = 4$. According to Ref. [158], m^2 is fixed from the length scales of the Universe and takes a value around $m^2 \approx 0.24H_0^2$, which we adopt in this work. As for c and d, these are dimensionless parameters which we fix according to Ref. [158] so that the predicted background evolution agrees closely with ΛCDM. In one of the two sets of parameters considered for this model, we also fix them so that $\tilde{f}_{R_0}$ is close to the viable range.

Again, we note that this model effectively behaves like a cosmological constant in the early high curvature Universe, such that $f(R) = R - 2\Lambda^{\infty}_{\rm eff} \equiv R - (1/2)(m^2 c/d)$. The corresponding potential, however, does not have a reasonable analytic form. We will show it later, and it will become evident that the Ricci scalar is able to settle into a minimum at the late-time evolution. Also, even though f_R and f_{RR} are not positive definite, we do not face that situation in the obtained expansion histories.

The last model analyzed is the $f(R)$ exponential model [159]. It is defined by

$$f(R) = R + \lambda R_\star \left(e^{-R/R_\star} - 1\right)\,, \tag{3.22}$$

where λ is a dimensionless parameter and $R_\star$ is a characteristic scale of the model, playing a similar role as m^2 and R_S in the previous models. Like the previous models, this has the property of developing an effective cosmological constant at early times, such that $\Lambda^{\infty}_{\rm eff} = \lambda R_\star/2$. For $\lambda > 0$, f_{RR} is positive definite, while $1 + \tilde{f}_R$ will be positive as long $R > R_\star \ln\lambda$, which is assured in the background evolutions obtained in this work. The potential, $V(R)$, is

$$V(R) = \frac{R_\star^2}{6}\left[\tilde{R}\left(\tilde{R} - 4\lambda\right) - 2\lambda\left(\tilde{R} + 3\right)e^{-\tilde{R}}\right]\,, \tag{3.23}$$

where $\tilde{R} \equiv R/R_\star$. Plots of this will be shown later but, as stated in Ref. [159], for $\lambda > 0$, this potential has a local maximum at $R = 0$ and a global minimum at $R_1 > 0$ needed to have a non-vanishing cosmological constant where our solution settles asymptotically in future time.

3.2 Linear perturbations in $f(R)$

The evolution of linear perturbations in $f(R)$ models has been derived and thoroughly analyzed in Refs. [161–164, 167]. Here, it will suffice to present the reader with the equations that are useful for this work and briefly overview their possible implications.

Working in the Jordan frame, we will be considering scalar perturbations of the metric given by the standard form

$$ds^2 = -a^2(\tau)\left[(1+2\Psi)\,d\tau^2 + (1-2\Phi)\,d\mathbf{x}^2\right]\,, \tag{3.24}$$

where τ is the conformal time, related to the coordinate time by $dt = a d\tau$; Ψ and Φ are small scalar perturbations of the FRW metric that are both time and space dependent. As for the energy–momentum tensor, we consider the usual first-order expansion given by

$$\begin{aligned} T^0{}_0 &= -\rho\,(1+\delta)\,; \\ T^0{}_i &= -\,(\rho+p)\,v_i\,; \\ T^i{}_j &= (p+\delta p)\,\delta^i_j + \pi^i{}_j\,, \end{aligned} \tag{3.25}$$

where $\delta \equiv \delta\rho/\rho$ is the density contrast, v_i is the velocity field, δp is the pressure perturbation, and $\pi^i{}_j$ is the traceless part of the energy–momentum tensor. The perturbed energy–momentum conservation equations, since matter is minimally coupled in the $f(R)$ Lagrangian, have the same form as in standard GR:

$$\delta' + \frac{k}{aH}V - 3\,(1+w)\,\Phi' + 3\left(\frac{\delta p}{\delta\rho} - w\right)\delta = 0\,, \tag{3.26}$$

for the t–t component, and

$$V' + (1-3w)\,V - \frac{k}{aH}\left(\frac{\delta p}{\delta\rho} - \frac{\Pi}{\delta}\right)\delta - \frac{k}{aH}\,(1+w)\,\Psi = 0\,, \tag{3.27}$$

for the individual matter components. V is the scalar velocity potential, whose gradient gives v_i, and Π is the scalar part of the anisotropic stress defined by $\rho\Pi \equiv (\hat{k}^i\hat{k}_j - 1/3\delta^i_j)\pi^i{}_j$. Primes denote derivatives with respect to $\log a$, and k is the comoving wavenumber of the expansion of the perturbed quantities in Fourier space, where the different modes evolve independently.

The full set of linearly-perturbed equations for $f(R)$ can be seen in Refs. [161, 162]. The anisotropy, or space-off diagonal equation is given by [161, 162]

$$\Phi - \Psi = \frac{9}{2}\frac{a^2}{k^2} E_n \Pi_n - \tilde{f}_R \left(\Phi - \Psi\right) + \tilde{f}_{RR} \delta R \,, \tag{3.28}$$

where δR is the linear perturbation of the Ricci scalar and E_n is the density of the n-th matter component as a fraction of the *present-day* critical density. The repeated indices denote a sum over the matter fields. Neglecting any anisotropic contribution from matter fields, hence setting $\Pi_n = 0$, one gets the following relation between the gravitational potentials

$$f_R \left(\Phi - \Psi\right) = \tilde{f}_{RR} \delta R \,, \tag{3.29}$$

where $f_R \equiv 1 + \tilde{f}_R$. This equation already presents a dynamical departure from standard GR, where the anisotropy equation just yields the constraint $\Psi = \Phi$. Note that this limit is recovered when $\tilde{f} = 0$, as expected.

The Poisson equation is given by [161, 162]

$$\begin{aligned} f_R \frac{k^2}{a^2}\Phi = & - \frac{3}{2} E_n \Delta_n + \frac{1}{2}\frac{k^2}{a^2}\tilde{f}_{RR}\delta R \\ & - \frac{3}{2} H^2 \tilde{f}'_R \left(\Psi + \Phi'\right) - \frac{3}{2} H H' \tilde{f}_{RR} \delta R \,, \end{aligned} \tag{3.30}$$

where it becomes clear that the presence of the modified gravity term in the action adds extra dynamical terms to the evolution equations of the Newtonian potentials. In standard GR, this would just be an algebraic relation between Ψ and the comoving matter density perturbation Δ_n. The latter is defined as

$$\Delta_n \equiv \delta_n + 3\frac{aH}{k}(1 + w_n) V_n \,. \tag{3.31}$$

Following Ref. [162], one may choose instead to evolve the following variables:

$$\chi = \tilde{f}_{RR} \delta R, \quad \Phi_+ = \frac{\Phi + \Psi}{2} \,, \tag{3.32}$$

where χ is the slip between the Newtonian potentials and Φ_+ is the lensing potential that is responsible for such effects as the Sachs–Wolfe effect in the CMB and weak lensing of distant galaxies. Hence, Eq. (3.29) becomes a simple constraint equation, and any $\chi \neq 0$ will indicate a departure from standard GR. The evolution equations for Φ and Ψ will then be obtained from the Poisson

equation and from the perturbed i–0 Einstein equation (or the momentum equation). Neglecting any contribution from the radiation component, these are given by [162]

$$\Phi'_{+} = \frac{3}{2}\frac{E_{\rm m}V_{\rm m}}{Hkf_R} - \left(1 + \frac{1}{2}\frac{f'_R}{f_R}\right)\Phi_{+} + \frac{3}{4}\frac{f'_R}{f_R^2}\chi\,, \tag{3.33}$$

and

$$\begin{aligned}\chi' = & - \frac{2E_{\rm m}\Delta_{\rm m}}{H^2}\frac{f_R}{f'_R} + \left(1 + \frac{f'_R}{f_R} - 2\frac{H'}{H}\frac{f_R}{f'_R}\right)\chi \\ & - 2f_R\Phi'_{+} - 2f_R\left(1 + \frac{2}{3}\frac{k^2}{a^2H^2}\frac{f_R}{f'_R}\right),\end{aligned} \tag{3.34}$$

where the subscript 'm' stands for ordinary matter.

At early times, the effect of $\tilde{f}(R)$ on the overall background evolution of the Universe is negligible. Therefore, for modes inside the horizon ($k > aH$) but way outside the Compton radius, $\lambda_{\rm C}$ (which is suppressed at this point since $\tilde{f}_{RR} \to 0$), one expects the evolution of the gravitational potentials to exhibit the same behavior as they do in standard GR. Hence, the lensing potential is expected to remain constant. Then, as $\lambda_{\rm C}$ increases, the Fourier mode eventually enters the radius defined by it and one should observe an enhancement in the perturbed potentials due to the attractive fifth force. Finally, at late times in the cosmological evolution, given the background expansion due to the presence of an effective cosmological constant, the Newtonian potentials should decay, as in GR.

Due to the oscillations of the linear perturbation of the Ricci scalar, δR, in $f(R)$ models [157], which can have catastrophic consequences relating to particle production, χ will oscillate as well with an amplitude and frequency proportional to the squared mass of the scalaron, $m^2_{\tilde{f}_R}$ [167]. Nonetheless, as will be seen in the next section, these oscillations are quite suppressed due to the very small values of $\tilde{f}_{RR}$, and their effect on the evolution of the gravitational potentials is practically negligible.

For completeness, we also show the form of the lensing potential in the sub-horizon quasi-static regime, i.e. $k^2 \gg a^2H^2$. As was mentioned in Sec. 1.3, $f(R)$ gravity is equivalent to a scalar-tensor theory with a null Brans-Dicke parameter.

Therefore, imposing $\omega_{\rm BD} = 0$ in Eqs. (2.32) and (2.34) we have,

$$\frac{G_{\rm eff}}{G} = \frac{1}{f_R}\frac{4+2f_R(Ma/k)^2}{3+2f_R(Ma/k)^2} \tag{3.35}$$

$$\gamma = \frac{1+f_R(Ma/k)^2}{2+f_R(Ma/k)^2} \tag{3.36}$$

where we have made the identification $\phi \equiv 1 + \tilde{f}_R \equiv f_R$. Following the notation of Ref. [144], $M^2 = 1/(2f_{RR})$, we can express the previous relations as [162]

$$\frac{G_{\rm eff}}{G} = \frac{1}{f_R}\frac{1+4Q}{1+3Q} \tag{3.37}$$

$$\gamma = \frac{1+2Q}{1+4Q}, \tag{3.38}$$

where we have defined $Q \equiv (k^2/a^2)f_{RR}/f_R$. From the last two expressions one can see that, in the high-redshift regime where, for viable $f(R)$ models, $f_{RR} \to 0 \Rightarrow Q \to 0$ and we recover $G_{\rm eff}/G \simeq 1$ and $\eta \simeq 1$ as in standard GR. Then, at late times, the mass term can become smaller as f_{RR} increases, and Q can become significant to the point where $G_{\rm eff}/G \simeq 4/3$ and $\eta \simeq 1/2$, and the growth rate of matter perturbations will then be larger than in GR+ΛCDM.

We can now write the sub-horizon expressions for $\Phi_+ \equiv (\Phi + \Psi)/2$ and $\chi = f_R\,(\Phi - \Psi)$:

$$\frac{k^2}{a^2}\Phi_+ \approx -\frac{3}{2}\frac{E_{\rm m}\delta_{\rm m}}{f_R} \tag{3.39}$$

$$\chi \approx -\frac{2Q}{1+3Q} f_R \Phi_+, \tag{3.40}$$

and these will help understand the results we will presenting in the following sections.

3.3 Results

Here we present the evolution of the background history and of the linear perturbations predicted by the three distinct $f(R)$ theories considered in this work. For each model, we will consider two cases:

1. We choose parameters to result in a $|\tilde{f}_{R_0}| \approx 1 \times 10^{-4}$, within the

observational constraints. We will use a numeral subscript 1 when referring to quantities obtained with this set of parameters.

2. The value obtained for $|\tilde{f}_{R_0}|$ is in disagreement with the corresponding theoretical and observational bounds, even though the predicted background evolution is very close to ΛCDM. The numeral subscript 2 will refer to this case.

Additionally, we present results for an $f(R)$ model with an effective equation of state equal to -1 throughout the cosmological evolution and $|\tilde{f}_{R0}| \approx 10^{-6}$ using the designer approach mentioned before and detailed in Ref. [160].

To obtain the background evolution predicted by each model, we have set the initial conditions at $z_{\rm c} = 10$, using a present-day value of $\Omega_{\rm m0} = 0.27$ and assuming a flat cosmology. We have ensured the numerical present-day value obtained for the Hubble parameter was in better than 1% agreement with the input $H_0 = 72$ km s^{-1}Mpc^{-1}. Reaching higher redshifts with exact integration is not possible due to the rapid oscillations in $w_{\rm eff}$ around the phantom divide $w_{\rm eff} = -1$, which complicates the numerical treatment [186, 187]. In order to start the evolution of perturbations at high redshift, we therefore assumed that between $z_{\rm i} = 1000$ and $z_{\rm c} = 10$ the equation of state can be replaced with its time-averaged value of -1. Then, from $z_{\rm c} = 10$ to the present time, we use the form for $w_{\rm eff}$ recovered from the full background evolution.

For the evolution of the linear perturbations, the initial conditions were defined as in Ref. [162], assuming again a flat cosmology with $\Omega_{\rm m0} = 0.27$. We started the evolution from $z_{\rm i} = 1000$ and the initial values of Φ_+ and χ were -1 and 0, respectively. Since the deviations from standard GR are small at this epoch, the initial conditions for $v_{\rm m}$ and $\Delta_{\rm m}$ are

$$v_{\rm m,i} = \frac{2k}{3aH}\Phi_+ \quad ; \quad \Delta_{\rm m,i} = -\frac{2k^2}{3a^2H^2}\Phi_+ \,. \tag{3.41}$$

3.3.1 Starobinsky model

For this model, we have chosen $R_{S1} = 0.83$ and $\lambda_1 = 5.3$, and $R_{S2} = 4.17$ and $\lambda_2 = 1.0$. The latter values were used in Ref. [169]. Using the formalism described in Section 3.1, we start by presenting, in Fig. 3.1, the evolution of the background Hubble expansion factor and Ricci scalar as a function of redshift z. We also plot

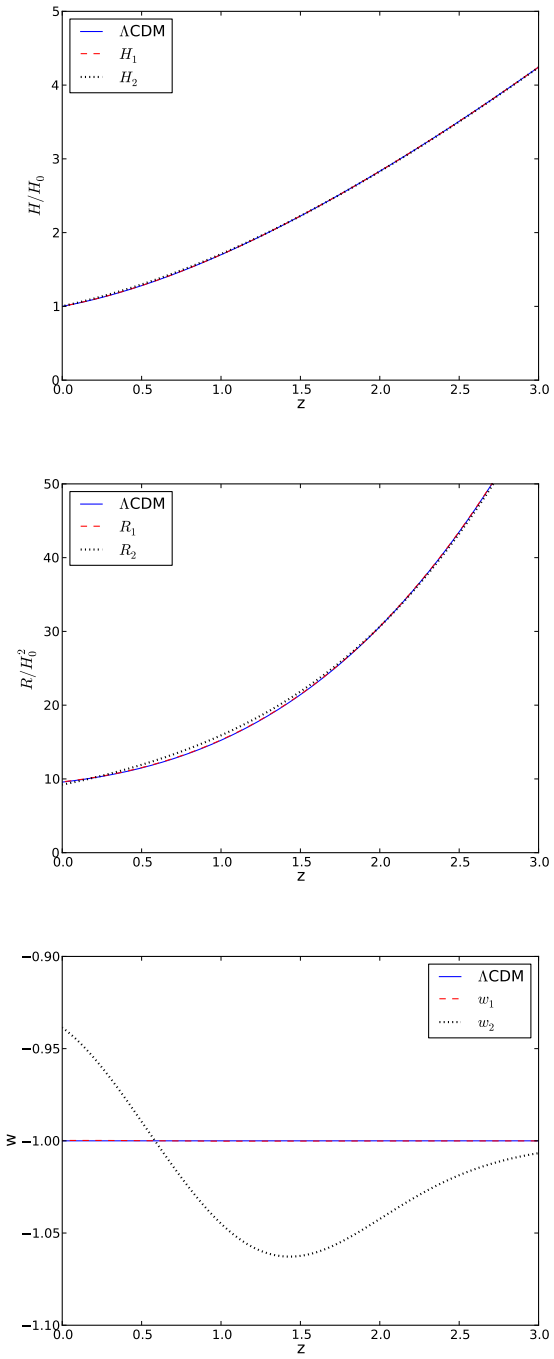

Figure 3.1 *The Hubble parameter, Ricci scalar, and $f(R)$ effective equation of state as a function of redshift, z, for the Starobinsky model, compared to the ΛCDM model.*

the evolution of this model's effective equation of state, as defined by Eqs. (3.16) or (3.17).

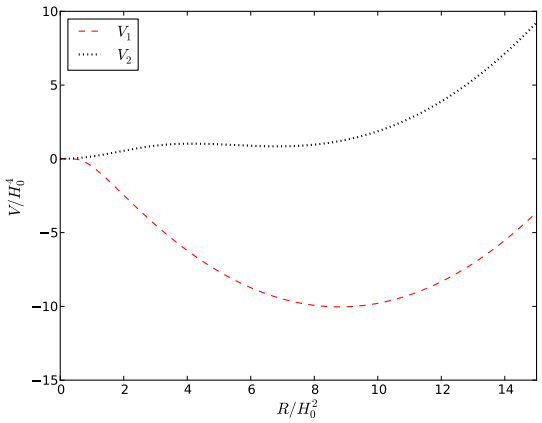

Figure 3.2 *The $V(R)$ potential as a function of the Ricci scalar for the Starobinsky model.*

In Fig. 3.1, we can see a typical feature of viable $f(R)$ models that satisfy $\tilde{f}_{RR} > 0$, which is the phantom crossing in the equation of state. This has been emphasized in several previous works [158, 169, 188], and is more easily seen in w_2. This also happens with w_1, though with a very much smaller amplitude, given the fact that this equation of state is practically indistinguishable from ΛCDM's.

It is interesting that two different sets of parameters yield such similar background histories, and that these are close to the cosmological evolution predicted by ΛCDM. This is expected, since the model is designed to yield a negligible cosmological constant in the high-redshift Universe and settle in a stable de Sitter point in the future. The sets yield present-day values of H and R that are very close to each other. However, as one can see in Fig. 3.2, they should disagree in the distant future, as R_{1_0} is already close to the de Sitter minimum of the $V(R)$ potential, where it will settle, while for the second set of parameters the solution is still moving towards the respective minimum, at a smaller value of R.

Despite the subtle differences in the background evolution, note that the values obtained for $\Lambda_{\rm eff}$ at the de Sitter limit and in the high-curvature regime are very close to each other for both sets of parameters. Hence, for the first set, we have $\Lambda_{\rm eff}^{\rm de\ Sitter} \approx 2.1H_0^2$ and $\Lambda_{\rm eff}^{\infty} \approx 2.2H_0^2$, while for the second set we have $\Lambda_{\rm eff}^{\rm de\ Sitter} \approx 1.7H_0^2$ and $\Lambda_{\rm eff}^{\infty} \approx 2.1H_0^2$ [169].

Throughout the evolution of this model, we have not reached a singular point where f_{RR} reached zero and then changed sign, hence the stability of the solutions is guaranteed. Also, we have obtained $\tilde{f}_{R0} \approx -1 \times 10^{-4}$ for the first set of

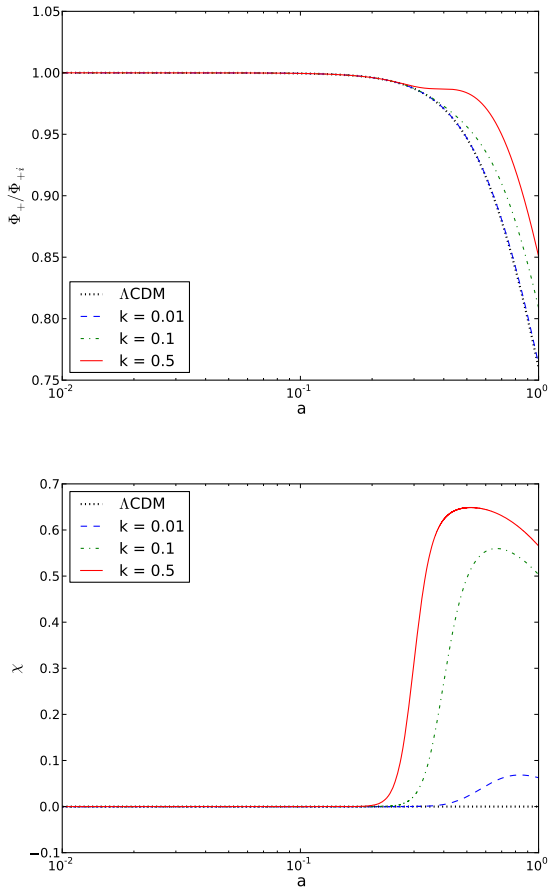

Figure 3.3 *The lensing potential Φ_+ and χ as a function of the scale factor, a, for the Starobinsky model, for the first set of parameters.*

parameters, and $\tilde{f}_{R0} \approx -4 \times 10^{-2}$ for the second set of parameters, in agreement with Ref. [169].

Figures 3.3 and 3.4 show the evolution of the linear perturbations in this model. In contrast to the ΛCDM case where the evolution is independent of scale, the potentials evolve differently depending on length scale. For both cases considered, the enhancement of the perturbations is stronger at smaller scales, i.e., higher wavenumber k.[1] This is because the modes corresponding to smaller scales enter the range of action of the fifth force, defined by the Compton wavelength in Eq. (3.9), sooner, the latter being dependent on the scalaron's mass defined by Eq. (3.8).

Hence, in the high-curvature/redshift regime, the fifth force is quite suppressed

[1] k is in units of h/Mpc, where h is $H_0/100$ and H_0 is the present-day value of the Hubble parameter. In this work, we have taken $H_0 = 72\,\mathrm{km\,s^{-1}Mpc^{-1}}$.

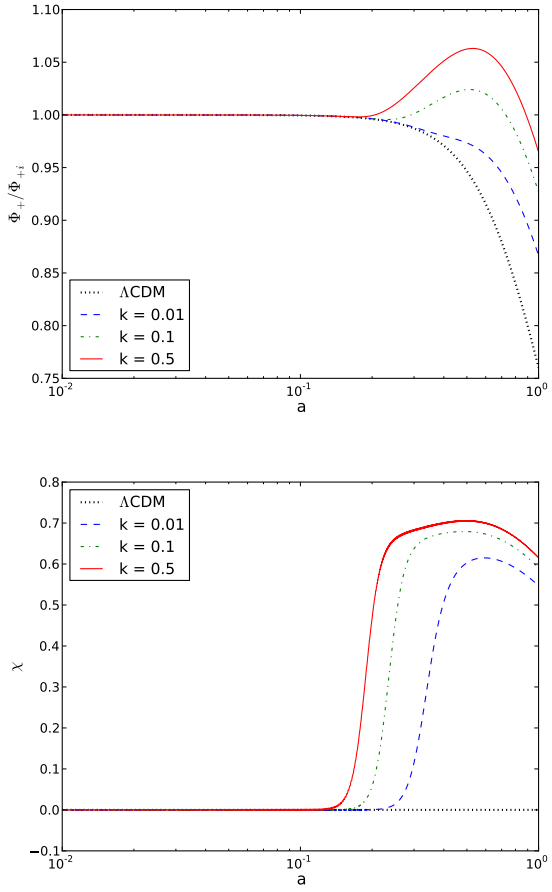

Figure 3.4 *The lensing potential Φ_+ and χ as a function of a for the Starobinsky model, for the second set of parameters.*

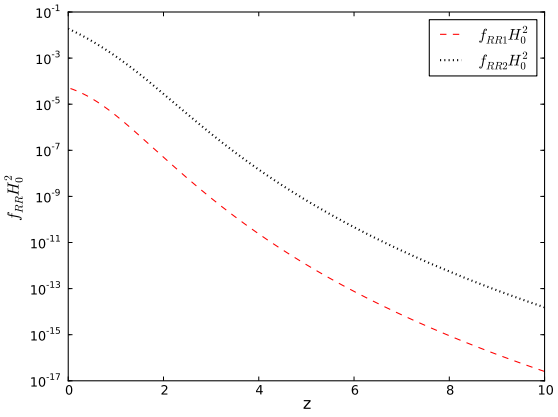

Figure 3.5 *The form of f_{RR} as a function of redshift for the two cases considered in the Starobinsky model.*

as the mass is very large, since $f_{RR} \equiv \tilde{f}_{RR} \to 0$, as one can observe in Fig. 3.5. Therefore, the evolution of the perturbed gravitational potentials is similar to that in scale-invariant ΛCDM with standard GR. The exception is the high-frequency oscillations in χ which depend on the mass of the scalaron, and which cannot be resolved by eye.

Later in the evolution, when f_{RR} starts to rise, the mass of the scalaron decreases, the Compton wavelength increases, and the modes start to enter it. This corresponds to the regime $Q \gg 1$ discussed for the subhorizon evolution of the perturbations at the end of Sec. 3.2, where we have an enhancement of the gravitational strength $G_{\rm eff}$ that shows as a growth of the Newtonian potentials. Correspondingly, the lensing potential increases in amplitude and χ follows that behavior, in a clear deviation from standard GR which, as we will see, applies to all the $f(R)$ models discussed here. Inevitably, the enhancement in the perturbed potentials is suppressed by the background accelerated expansion when z approaches zero.

Lastly, we note that the difference in $\tilde{f}_{R0}$ between the sets of parameters translates into significant differences in the evolution of the perturbations. The evolution of the respective f_{RR} is crucial for understanding this. Looking at Fig. 3.5, one sees that the sooner f_{RR} starts to increase, the greater is the enhancement in the perturbed potentials. Hence, the evolution of the linear perturbations for the second set of potentials has a greater enhancement, translated to an actual growth in Φ_+. For the first set of parameters, not only does the enhancement kick in later, but the magnitude of f_{RR} remains very small throughout the evolution. Hence, for instance, Φ_+ will not necessarily grow, as the effect of the fifth force will suffice only to resist the expanding background. In either of the cases, nevertheless, the differences from the scale-invariant ΛCDM are noticeable by eye, particularly for the smaller scales.

3.3.2 Hu–Sawicki model

We start with Fig. 3.6, which shows the evolution of the Hubble expansion factor, the Ricci scalar and the effective equation of state of $f(R)$ as a function of z. We have used $c_1 = 0.190$, $d_1 = 0.0105$, $c_2 = 1.25 \times 10^{-3}$ and $d_2 = 6.56 \times 10^{-5}$, the latter defined as in Ref. [169]. As in the previous model, one can observe that the distinct sets of parameters yield two very similar background histories. Both the Hubble parameter, H, and the Ricci scalar, R, present an evolution as

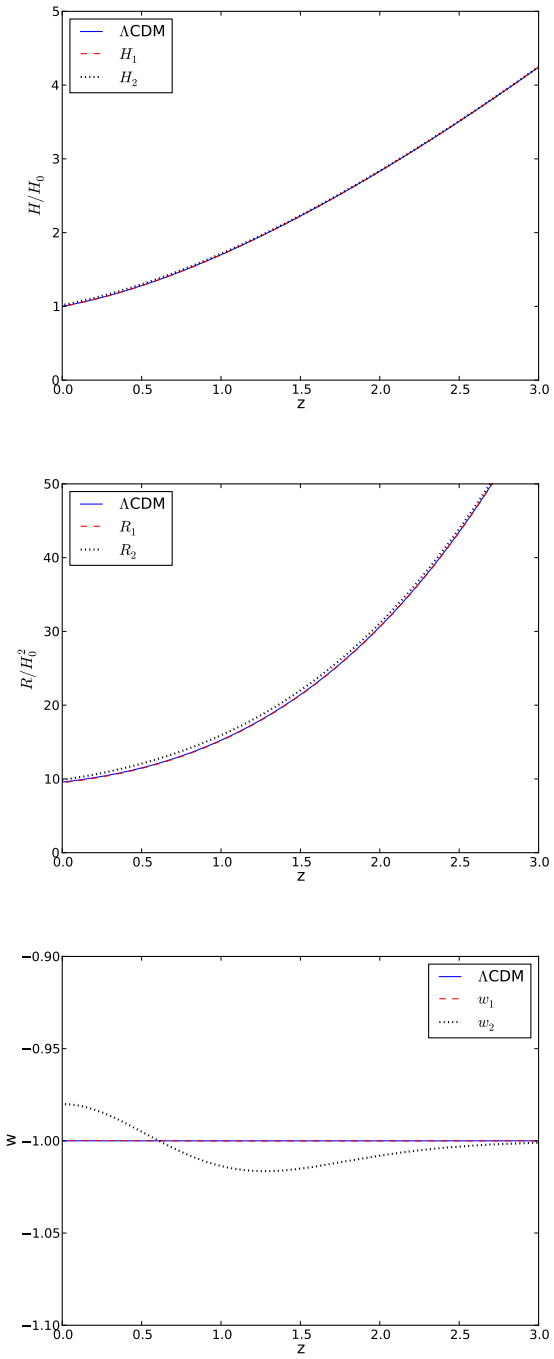

Figure 3.6 *The Hubble parameter, Ricci scalar, and $f(R)$ effective equation of state for the Hu–Sawicki model, compared to the ΛCDM model.*

a function of redshift that is very close to that predicted by ΛCDM. The main difference lies in the evolution of the effective equation of state, where we have the usual phantom crossing, which is particularly noticeable for the second set of parameters and negligible for the first set.

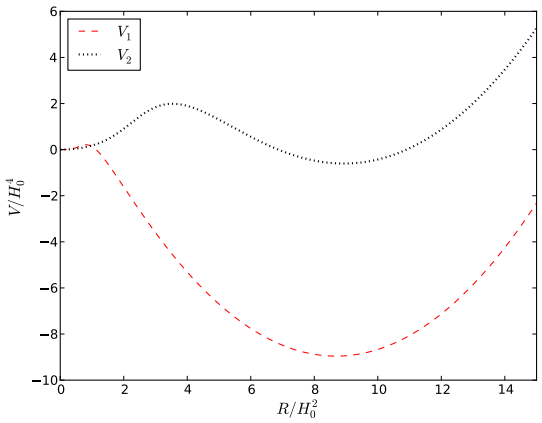

Figure 3.7 *The potential $V(R)$ for the two different cases considered in the Hu–Sawicki model.*

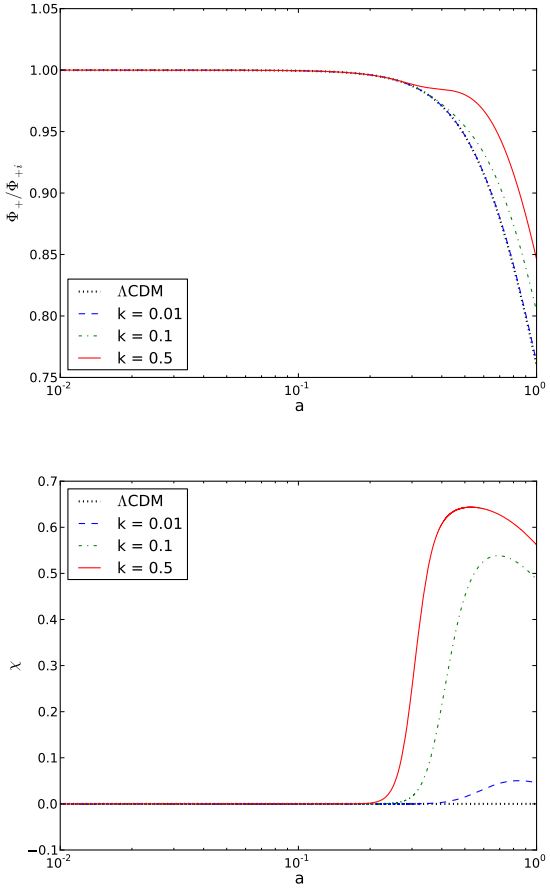

Figure 3.8 *The lensing potential Φ_+ and χ as a function of a for the Hu–Sawicki model, for the first set of parameters.*

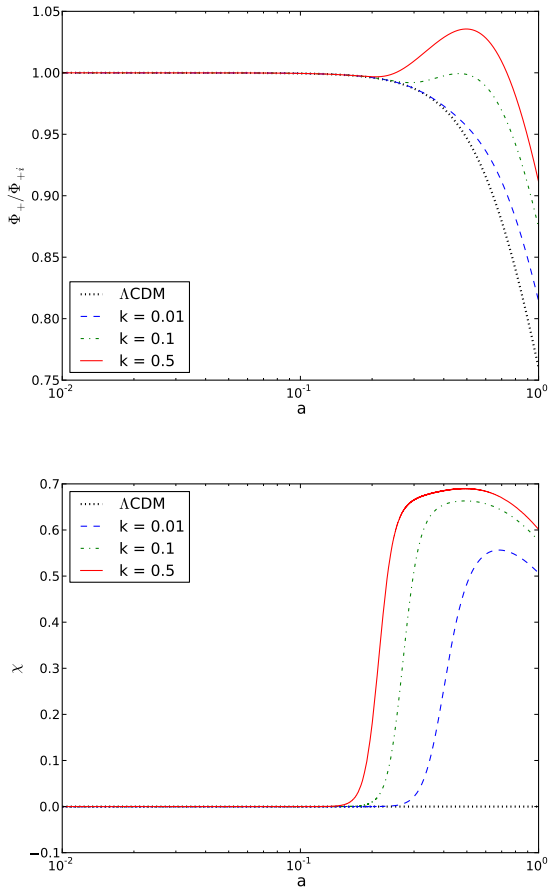

Figure 3.9 *The lensing potential Φ_+ and χ as a function of a for the Hu–Sawicki model, for the second set of parameters.*

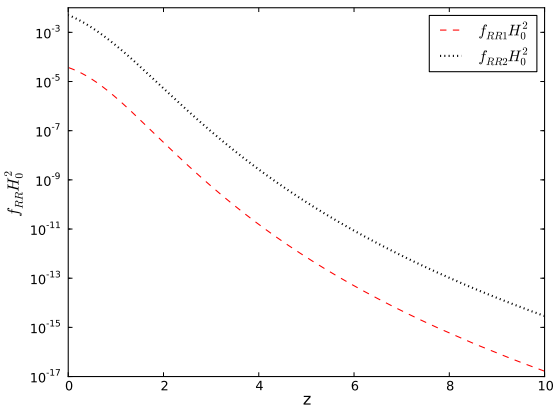

Figure 3.10 *The form of f_{RR} as a function of redshift for the two cases considered in the Hu–Sawicki model.*

Similarly to the previous model, both sets of parameters result in present-day values of H and R that closely agree. Since the minima of the respective $V(R)$ potentials, shown in Fig. 3.7, are located at almost equal R, it is expected that the background evolution of the models does not disagree much in the distant future.

In this model, we have $\Lambda_{\rm eff}^{\infty} \approx 2.2H_0^2$ and $\Lambda_{\rm eff}^{\rm de\,Sitter} \approx 2.2H_0^2$ for the first set, and $\Lambda_{\rm eff}^{\infty} \approx 2.3H_0^2$ and $\Lambda_{\rm eff}^{\rm de\,Sitter} \approx 2.2H_0^2$ for the second set of parameters. As for $\tilde{f}_{R0}$, we have $\tilde{f}_{R0} \approx -1 \times 10^{-4}$ for the first set of parameters, and $\tilde{f}_{R0} \approx -1 \times 10^{-2}$, recovering the result obtained in Ref. [169]. The stability of the solutions was guaranteed, as both f_{RR} and f_R remained definite positive throughout.

Figures 3.8 and 3.9 show that the linear evolution of perturbations in this model is almost identical to the previous model, the reason being the similarity in the evolution of f_{RR} of both models, seen for this model in Fig. 3.10. The subtle difference rests on the absolute value of this quantity, which is smaller for the Hu–Sawicki model. Therefore, the different modes will enter the range of the fifth force marginally later. Hence, the enhancement of the gravitational potentials is a bit smaller than in the Starobinsky model, which is noticeable when comparing Figs. 3.9 and 3.4.

3.3.3 Exponential model

For the Exponential model, we have chosen $\lambda_1 = 4.9$ and $R_{\star 1} = 0.9$, while $\lambda_2 = 1.5$ and $R_{\star 2} = 3.0$. We plot the evolution, as a function of redshift, of the background quantities H, R and $w_{\rm eff}$, for both sets of parameters, in Fig. 3.11. As in the previous models, the cases considered yield background histories very close to ΛCDM, with the exception of the effective equation of state. The latter presents the phantom crossing mentioned before, once again more noticeable for the second set of parameters, and negligible for the first.

Contrasting with the previous models, the present-day values of R and H obtained for the first set of parameters of this model are very close to the respective values of ΛCDM and the second set of parameters. This happens because, when evolution ends, the solution for R_1 is already close to the respective $V(R)$ potential's de Sitter minimum, which is located at a higher value than that of the second set of parameters, as one can see in Fig. 3.12. Since R_1 is expected to asymptotically settle at this value, one expects that, in the distant future, the respective evolution

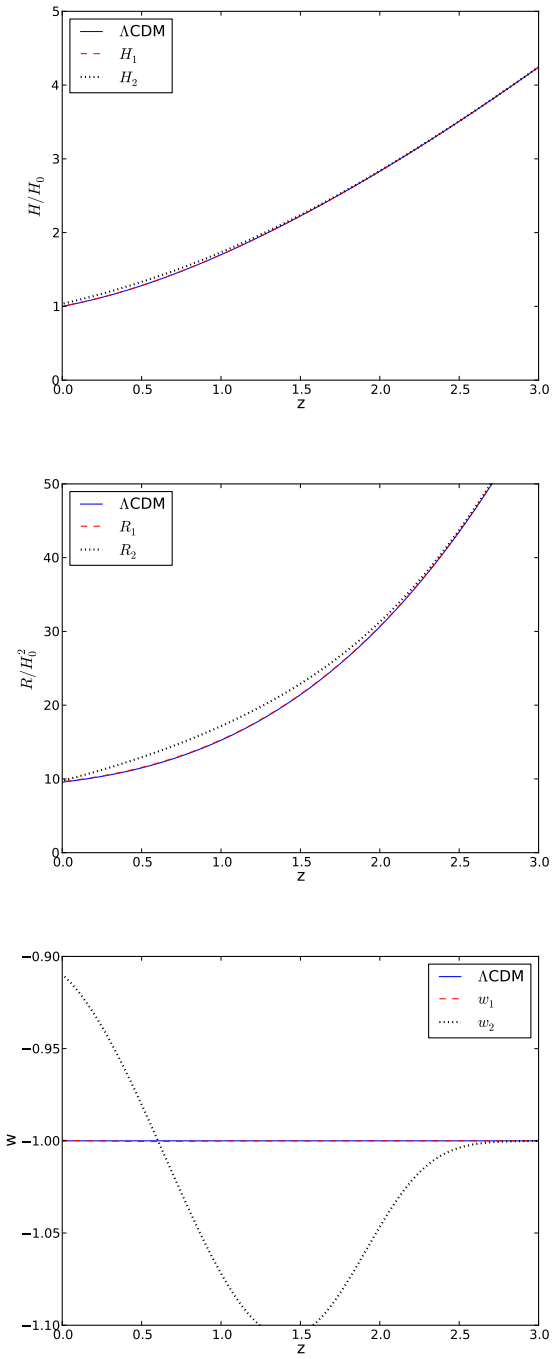

Figure 3.11 *The Hubble parameter, Ricci scalar, and $f(R)$ effective equation of state for the Exponential model, compared to the ΛCDM model.*

gradually differs from R_2, whose $V(R)$ minimum is located at a smaller value of R, and also differ from ΛCDM.

As for the values of the effective cosmological constants, for this model we have,

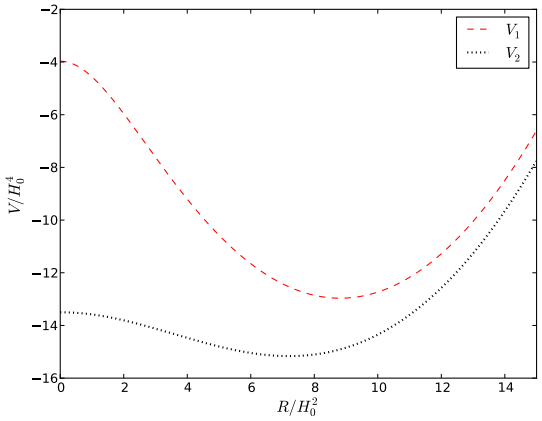

Figure 3.12 *The potential $V(R)$ for the two cases considered in the Exponential model.*

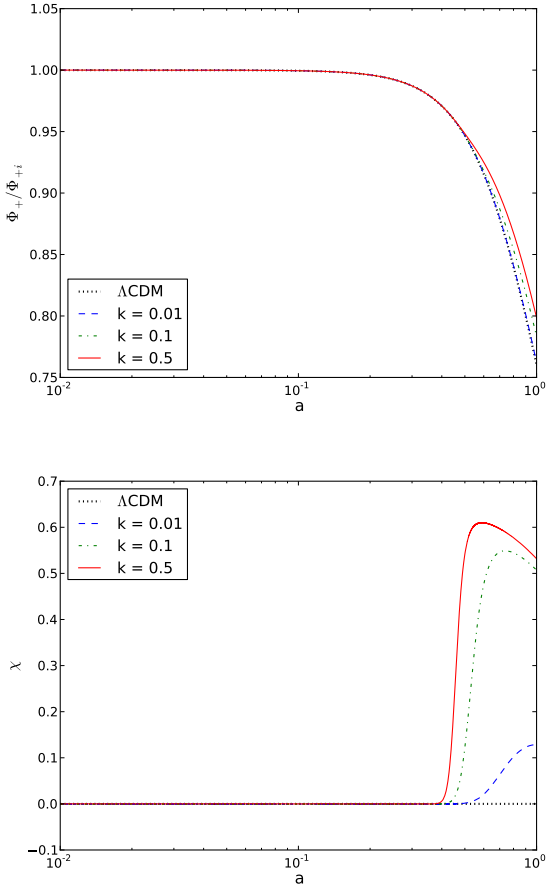

Figure 3.13 *The lensing potential Φ_+ and χ as a function of a for the Exponential model, for the first set of parameters.*

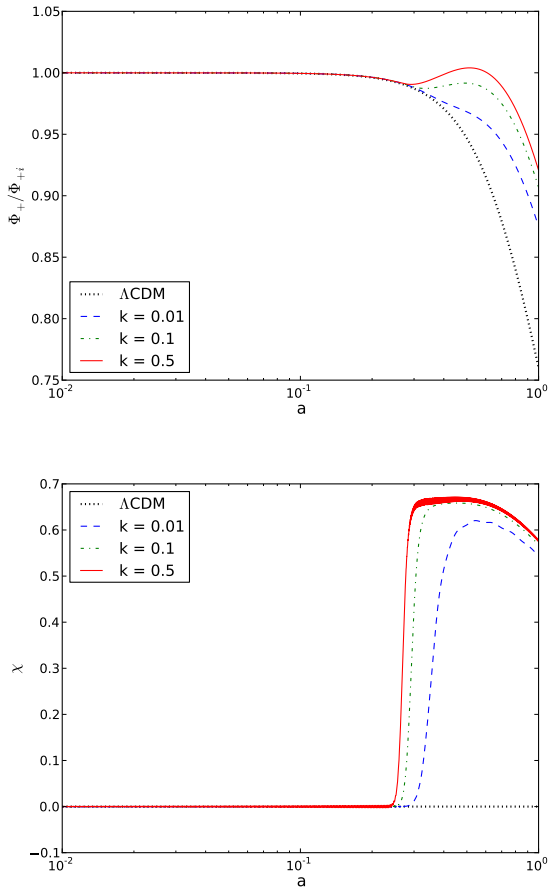

Figure 3.14 *The lensing potential Φ_+ and χ as a function of a for the Exponential model, for the second set of parameters.*

considering the first set of parameters, $\Lambda_{\rm eff}^{\infty} = 2.2H_0^2$ and $\Lambda_{\rm eff}^{\rm de\ Sitter} \approx 2.2H_0^2$, while for the second set we have $\Lambda_{\rm eff}^{\infty} = 2.2H_0^2$ and $\Lambda_{\rm eff}^{\rm de\ Sitter} \approx 1.8H_0^2$, in accordance with Ref. [159]. As for the values of $\tilde{f}_{R0}$, we have ensured that the first set of parameters results in a value of approximately -1×10^{-4}, while the second set results in approximately -6×10^{-2}.

Regarding the evolution of linear perturbations, this follows a similar pattern to that of the previous models, as can be seen in Figs. 3.13 and 3.14. However, for the Exponential model, f_{RR} is exponentially suppressed at high redshift. In Fig. 3.15 one sees that around $z = 3$ the magnitude of f_{RR} is still several orders of magnitude smaller than in the previous models. This means that the different k-modes will enter the fifth force range of action later and, consequently, the enhancement in the perturbations is much fainter for both sets of parameters. Note that, when we have $|\tilde{f}_{R0}| \approx 10^{-4}$, the difference between this model and

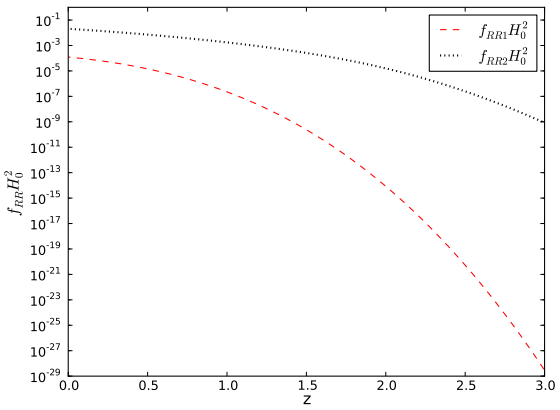

Figure 3.15 *The form of f_{RR} as a function of redshift for the two different cases considered in the Exponential model.*

ΛCDM is very small, even for the smallest scale considered. One final point regards the steep increase of χ particularly for the second set of parameters, which is related to the exponential growth of f_{RR} for decreasing redshift. Therefore, even though the modes enter the range of the fifth force later, these do so at a very rapid pace, leading to an abrupt enhancement of the perturbations, namely χ.

3.3.4 $w = -1$ $f(R)$ model

In this subsection, we present the evolution of the linearly-perturbed potentials for an $f(R)$ model with an effective equation of state identically equal to -1 throughout the cosmological evolution. Using the designer approach, we ensure that this model's background evolution is indistinguishable from the ΛCDM. We also tune the model such that the present-day value obtained for $\tilde{f}_{R0} \approx -1 \times 10^{-6}$. Hence, with this final model, we want to give an indication of what the evolution of the linear perturbations would be under more stringent viability constraints.

Figure 3.16 shows the evolution of the perturbations. One immediately observes that the enhancement in Φ_+ is almost negligible relative to the ΛCDM case. Only for the smallest scale can one detect by eye the difference between the models. Looking at the middle plot in Fig. 3.16, one sees that the difference between the $f(R)$ model and ΛCDM in Φ_+ ranges from 0 to a maximum to 4%. So, even though χ does present some enhancement, albeit smaller than in all of the previous cases, that does not translate to the observable lensing potential.

3.4 Discussion

In this work, we have focused on three viable $f(R)$ models. In spite of several, perhaps catastrophic, problem hovering over these theories regarding particle production and their weak-field limit [157, 174, 189, 190], they still receive a lot of attention because they provide insight into how simple modifications of the gravitational action can lead to departures from standard general relativity.

We have used two different parameterizations for each of the three models considered. One of them had already been used in previous work. We have recovered the obtained results which, inevitably, render them nonviable, even though these present cosmological evolutions that are very close to ΛCDM. The values obtained for $|\tilde{f}_{R0}|$ are way above the viability requirement. If this were the case, the linear evolution of perturbations would have definite signatures that would probably have been already observed, since the departure from ΛCDM is very accentuated. In this situation, the action of the fifth force is significant, and one can indeed observe a great enhancement of the perturbed potentials at the late stages of evolution, with even some growth on the lensing potential Φ_+, particularly on the smaller scales. Closer to the present, all of the scales end up succumbing to the effect of the expanding background and we see an inversion of the growth.

On the other hand, we have tried to fine-tune the other set of parameters such that the present-day value resulting from the cosmological evolution of the models would be within the observationally viability range, such that $\tilde{f}_{R0} \approx -10^{-4}$. In this case, we notice that the enhancement in the perturbations is more subtle for the Starobinsky and Hu–Sawicki model, and almost non-existent in Φ_+ for the Exponential model. For the last model, even though the growth in χ remains, the lateness of this leads to almost no enhancement in Φ_+, which offers close to no resistance to the background expansion. For the other models, one is able to detect some resistance to the background expansion in Φ_+.

The main differences in the evolution of the gravitational potentials between the different models are dependent on the evolution of f_{RR}. The latter, in turn, is related to the effective mass of the scalar degree of freedom associated to $f(R)$, the scalaron, which defines the range of action of the fifth force. Hence, it determines the moment when the different scales enter its range and, therefore, are enhanced. However, despite the differences amongst the models, the possible observational

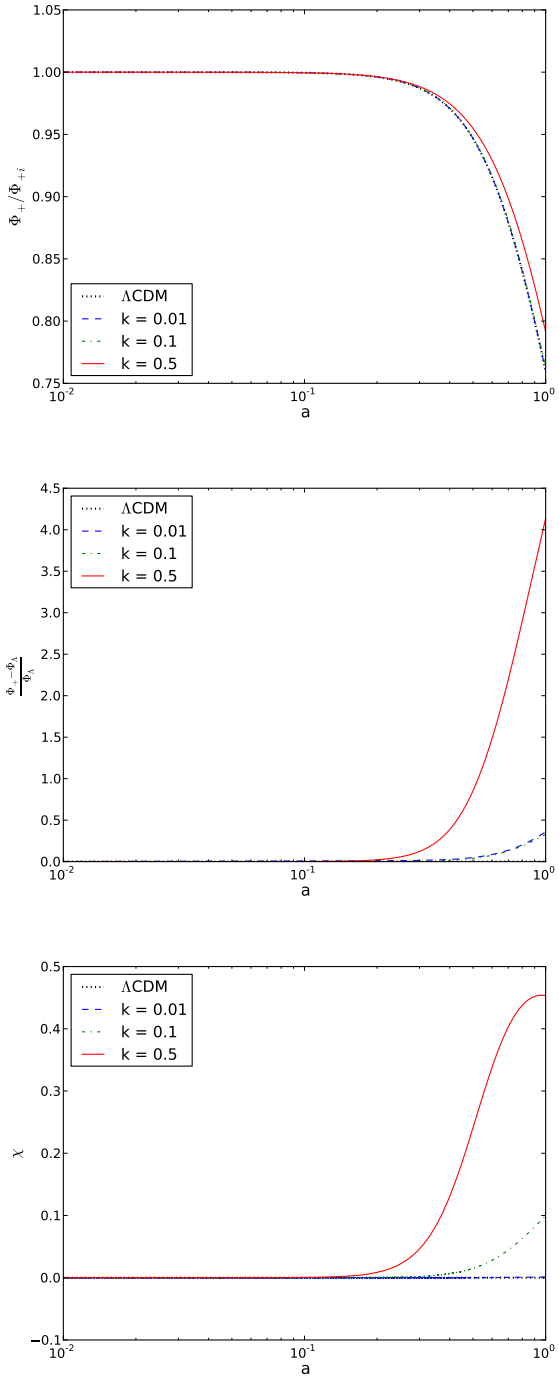

Figure 3.16 *The evolution of the linear perturbations as a function of the scale factor, a, for the $f(R)$ model with $w_{eff} = -1$, against the ΛCDM model. The middle plot shows the relative difference between both models in the evolution of Φ_+. The result for $k = 0.01h/\mathrm{Mpc}$ was enhanced by a factor of 100 to allow its visualization.*

signatures on the lensing potential become increasingly hard to detect compared to ΛCDM, particularly for the larger scales.

Lastly, we have considered the evolution of the perturbations for an $f(R)$ model with an effective equation of state $w_{\text{eff}} = -1$ and $\tilde{f}_{R0} \approx -10^{-6}$. This case is perfectly within both the observational and theoretical viability conditions and allows one to have an idea of the behavior of the gravitational potentials if all the three models respected these strict restrictions. For this case, we have used the designer approach to get a background history that is virtually indistinguishable from ΛCDM.

In that last approach, we were able to conclude that the evolution of linear perturbations when the viability conditions are completely satisfied follows very closely that of ΛCDM. Even though there is the usual evolution and growth in χ, this does not extend to Φ_+. We note that for the largest scale considered, $k = 0.5\,h/\text{Mpc}$, one gets the largest deviations from ΛCDM, at a maximum only of approximately 4%. Note, however, that $f(R)$ simulations have shown that the linear approach does not work particularly well for these models on the smaller scales, specially in those cases where the magnitude of the fifth force is smaller, hence for smaller $|\tilde{f}_{R0}|$. Nevertheless, the high non-linearity of the $f(R)$ equations seems to further suppress the effect of the fifth force and the deviations from ΛCDM [191].

Therefore, if indeed it is a particular $f(R)$ model driving cosmic acceleration, it may be extremely hard to extract any signature of it, since the observational precision, for instance in weak lensing experiments, available today and in the near future, will not allow detection of such a signal from ΛCDM.

Chapter 4

Dynamics of linear perturbations in the hybrid metric-Palatini theory of gravity

In this chapter, we focus on a novel model, the hybrid metric-Palatini gravity [192, 193]. In this type of theories, the usual Einstein-Hilbert Lagrangian is supplemented with an $f(\mathcal{R})$ Palatini term. This type of hybrid theory arises when perturbative quantization methods are considered on Palatini backgrounds [194], which are connected with non-perturbative quantum geometries [195].

Like the pure metric and Palatini cases, the hybrid theory has a dynamically equivalent scalar-tensor representation [192, 193]. Those authors have also shown that the scalar field need not be massive in order to pass the stringent solar system constraints [192], in contrast to the metric $f(R)$ theories, while possibly modifying the cosmological [196] and Galactic [197] dynamics due to its light, long-range interacting nature. In Ref. [196], the criteria for obtaining cosmic acceleration was discussed. Alongside that, several cosmological solutions were derived, depending on the form of the effective scalar field potential, describing both accelerating and decelerating Universes.

It has been shown that the hybrid metric-Palatini gravity shares some of the good properties of the pure Palatini formulation, such as not propagating an additional scalar degree of freedom in Minkowski flat spacetime, reducing to standard GR (plus a Cosmological Constant) in those regimes [198]. However, the additional

degree of freedom introduced in the hybrid metric-Palatini theory does propagate in curved spacetimes allowing it to avoid the microscopic matter instabilities known to the pure Palatini gravity with infrared corrections [192, 199]. Not only that, it has been shown that, for the hybrid theory, the scalar field fluctuations propagate at the speed of light on small scales, but the theory does not acquire an effective sound speed for matter perturbations [192, 196]. The last fact in particular is not verified in the pure Palatini approach which leads to instabilities in the growth of matter inhomogeneities [200].

In this work, we focus on cosmological perturbations in the hybrid metric-Palatini formalism in the Jordan frame. Therefore, in Section 4.1 we briefly introduce the hybrid metric-Palatini model and, in Section 4.2, we present the designer approach which allows us to retrieve a family of solutions for $f(\mathcal{R})$ whose effective equation of state is $w_{\text{eff}} = -1$. In Section 4.3 we derive the full set of perturbed cosmological equations and present them in the Newtonian and Synchronous gauges. Then, in Section 4.4 we derive the Poisson equation and re-express the perturbed potentials in terms of the lensing potential, Φ_+, and the slip, χ, which we numerically evolve. We finish in Section 4.5 with the conclusions of this work.

I would like to state that the work found in this chapter can be found in [3] and is of my sole authorship.

4.1 Description of the hybrid metric-Palatini gravity

The four-dimensional action describing the hybrid metric-Palatini gravity is given by

$$S = \frac{1}{2\kappa^2}\int d^4x\sqrt{-g}\,[R + f(\mathcal{R})] + S_m, \tag{4.1}$$

where $\kappa^2 = 8\pi G$ and we set $c = 1$. S_m is the standard matter action, R is the metric Einstein-Hilbert Ricci scalar and $\mathcal{R} = g^{\mu\nu}\mathcal{R}_{\mu\nu}$ is the Palatini curvature. The latter is defined in terms of the metric elements, $g^{\mu\nu}$, and a torsion-less independent connection, $\hat{\Gamma}$, through

$$\mathcal{R} \equiv g^{\mu\nu}\left(\hat{\Gamma}^{\alpha}_{\mu\nu,\alpha} - \hat{\Gamma}^{\alpha}_{\mu\alpha,\nu} + \hat{\Gamma}^{\alpha}_{\alpha\lambda}\hat{\Gamma}^{\lambda}_{\mu\nu} - \hat{\Gamma}^{\alpha}_{\mu\lambda}\hat{\Gamma}^{\lambda}_{\alpha\nu}\right). \tag{4.2}$$

Varying the action (4.1) with respect to the metric, one obtains the usual set of

Einstein equations, given by

$$G_{\mu\nu} + F(\mathcal{R})\mathcal{R}_{\mu\nu} - \frac{1}{2}f(\mathcal{R})g_{\mu\nu} = \kappa^2 T_{\mu\nu}, \tag{4.3}$$

where $G_{\mu\nu}$ is Einstein's tensor, and $F(\mathcal{R}) \equiv df(\mathcal{R})/d\mathcal{R}$. $T_{\mu\nu}$ is the matter field's stress–energy tensor, defined as

$$T_{\mu\nu} = -\frac{2}{\sqrt{-g}}\frac{\delta\left(\sqrt{-g}\mathcal{L}_m\right)}{\delta\left(g^{\mu\nu}\right)}, \tag{4.4}$$

where $\mathcal{L}_m \equiv \mathcal{L}_m\left[\chi_i, g_{\mu\nu}\right]$ is the minimally–coupled matter Lagrangian, dependent on the matter fields, χ_i, and the metric elements, $g_{\mu\nu}$. The trace of Eq. (4.3) is

$$F(\mathcal{R})\mathcal{R} - 2f(\mathcal{R}) = \kappa^2 + R \tag{4.5}$$

On the other hand, varying the action (4.1) with respect to the independent connection, $\hat{\Gamma}^{\alpha}_{\mu\nu}$, one gets the following equation,

$$\hat{\nabla}_{\alpha}\left(\sqrt{-g}F(\mathcal{R})g^{\mu\nu}\right) = 0, \tag{4.6}$$

which implies that $\hat{\Gamma}^{\alpha}_{\mu\nu}$ is the Levi–Civita connection of a metric $h_{\mu\nu} = F(\mathcal{R})g_{\mu\nu}$. Hence, one can verify that the Palatini Ricci tensor, $\mathcal{R}_{\mu\nu}$, is related to the metric one, $R_{\mu\nu}$, by the following relation

$$\begin{aligned}\mathcal{R}_{\mu\nu} &= R_{\mu\nu} + \frac{3}{2}\frac{1}{F^2(\mathcal{R})}F(\mathcal{R})_{,\mu}F(\mathcal{R})_{,\nu} \\ &\quad -\frac{1}{F(\mathcal{R})}\nabla_{\mu}F(\mathcal{R})_{,\nu} - \frac{1}{2}\frac{1}{F(\mathcal{R})}g_{\mu\nu}\Box F(\mathcal{R}).\end{aligned} \tag{4.7}$$

Introducing an auxiliary scalar field, ϕ, the action (4.1) can be recast into a scalar-tensor theory described by the following action [192]

$$S = \frac{1}{2\kappa^2}\int d^4x\sqrt{-g}\left[R + \phi\mathcal{R} - V(\phi)\right] + S_m, \tag{4.8}$$

where $\phi \equiv F(\mathcal{R})$ and $V(\phi) = \mathcal{R}F(\mathcal{R}) - f(\mathcal{R})$. Varying the latter action with respect to the metric $g_{\mu\nu}$, the scalar ϕ, and the independent connection $\hat{\Gamma}^{\alpha}_{\mu\nu}$, leads to

$$R_{\mu\nu} + \phi\mathcal{R}_{\mu\nu} - \frac{1}{2}\left(R + \phi\mathcal{R} - V\right)g_{\mu\nu} = \kappa^2 T_{\mu\nu}, \tag{4.9}$$

$$\mathcal{R} - V_\phi = 0, \tag{4.10}$$

$$\hat{\nabla}_\alpha \left(\sqrt{-g}\phi g^{\mu\nu}\right) = 0, \tag{4.11}$$

respectively. Equation (4.7) can be easily rewritten in terms of the auxiliary scalar field by using $F(\mathcal{R}) = \phi$ which, when traced, leads to the following relation between the metric and the Palatini Ricci scalars:

$$\mathcal{R} = R + \frac{3}{2\phi^2}\left(\partial\phi\right)^2 - \frac{3}{\phi}\Box\phi. \tag{4.12}$$

With this last relation, the action (4.8) can be rewritten as

$$S = \frac{1}{2\kappa^2}\int d^4x\sqrt{-g}\left[(1+\phi)R + \frac{3}{2\phi}\left(\partial\phi\right)^2 - V(\phi)\right] + S_m. \tag{4.13}$$

With the redefinition $(1+\phi) \equiv \varphi$, the action can be recast as that of a Brans-Dicke theory,

$$S = \frac{1}{2\kappa^2}\int d^4x\sqrt{-g}\left[\varphi R + \frac{3}{2\left(\varphi-1\right)}\left(\partial\phi\right)^2 - V(\phi)\right] + S_m, \tag{4.14}$$

where we can identify $\omega_{\rm BD} = -\frac{3\varphi}{2(\varphi-1)}$.

Using Eqs. (4.7) and (4.12), one can rewrite Eq. (4.9) as

$$\begin{aligned} G_{\mu\nu}\left(1+\phi\right) &= \kappa^2 T_{\mu\nu} - \frac{3}{2\phi}\partial_\mu\phi\partial_\nu\phi + \nabla_\mu\nabla_\nu\phi \\ &\quad -\frac{g_{\mu\nu}}{2}\left(V + 2\Box\phi\right) + \frac{3}{4\phi}g_{\mu\nu}\left(\partial\phi\right)^2. \end{aligned} \tag{4.15}$$

The latter equation can be recast in the usual GR form $G_{\mu\nu} = \kappa^2 T^{\rm hybrid}_{\mu\nu}$, such that

$$\begin{aligned} \left(1+\phi\right)T^{\rm hybrid}_{\mu\nu} &= T_{\mu\nu} + \frac{1}{\kappa^2}\Bigg[\nabla_\mu\nabla_\nu\phi - \frac{3}{2\phi}\partial_\mu\phi\partial_\nu\phi \\ &\quad - \frac{g_{\mu\nu}}{2}\left(V + 2\Box\phi\right) + \frac{3}{4\phi}g_{\mu\nu}\left(\partial\phi\right)^2\Bigg] \end{aligned} \tag{4.16}$$

Adopting a flat Friedmann-Robertson-Walker (FRW) metric, $ds^2 = -dt^2 +$

$a^2(t)d\vec{x}^2$, one can get the modified Friedmann equations:

$$3H^2 = \frac{1}{1+\phi}\left[\kappa^2\rho - 3H\dot{\phi} - \frac{3\dot{\phi}^2}{4\phi} + \frac{V(\phi)}{2}\right], \tag{4.17}$$

and,

$$2\dot{H} = \frac{1}{1+\phi}\left[-\kappa^2\left(\rho+p\right) + H\dot{\phi} - \ddot{\phi} + \frac{3\dot{\phi}^2}{2\phi}\right], \tag{4.18}$$

where a dot stands for a differentiation with respect to time, t, and $H = \dot{a}/a$ is the Hubble parameter.

Lastly, closing the set of cosmological equations, one can trace Eq. (4.9), getting

$$\frac{\phi}{3}\left[2V - (1+\phi)\frac{dV}{d\phi}\right] - \Box\phi + \frac{1}{2\phi}\left(\partial\phi\right)^2 = \frac{\kappa^2\phi}{3}T, \tag{4.19}$$

where we have used Eqs. (4.10) and (4.12), and T is the stress–energy tensor trace. Using the FRW metric, this equation takes the form

$$\ddot{\phi} + 3H\dot{\phi} - \frac{\dot{\phi}^2}{2\phi} + \frac{\phi}{3}\left[2V - (1+\phi)\frac{dV}{d\phi}\right] = \frac{\kappa^2\phi}{3}T, \tag{4.20}$$

describing the dynamical evolution of the additional degree of freedom introduced by this theory.

Solving Eq. (4.19) in the weak–field limit and far from matter sources, it has been shown that the scalar field behaves like [192, 193, 197]

$$\phi(r) \approx \phi_0 + \frac{2G\phi_0 M}{3r}e^{-m_\phi r}, \tag{4.21}$$

where the field's effective mass is defined as

$$m^2_{\phi|\phi=\phi_0} = \frac{2V - V_\phi - \phi\left(1+\phi\right)V_{\phi\phi}}{3}, \tag{4.22}$$

where ϕ_0 is the field's background value and M is the distant source's mass, determined assuming spherical symmetry. The authors of Refs. [192, 193] have also obtained the solutions to the metric perturbations, and defined an effective

Newton constant, $G_{\rm eff}$, and the post-Newtonian parameter, γ, as, respectively

$$G_{\rm eff} \equiv \frac{G}{1+\phi_0}\left[1-\frac{\phi_0}{3}e^{-m_\phi r}\right], \tag{4.23}$$

$$\gamma \equiv \frac{1+\phi_0/3e^{-m_\phi r}}{1-\phi_0/3e^{-m_\phi r}}. \tag{4.24}$$

From Eqs. (4.23) and (4.24), it becomes clear that $G_{\rm eff} \approx G$ and $\gamma \approx 1$ as long as ϕ_0 is small, regardless of the value of m_ϕ^2. Hence, contrary to what is seen in metric $f(R)$ theories, the hybrid metric-Palatini theory does not seem to need an evading mechanism, such as the chameleon mechanism, to pass the solar system tests. The previous two relations can also be derived from the Brans-Dicke identification made previously. In massive Brans-Dicke theory, we have in the weak-field limit [201]

$$G_{\rm eff} = \frac{G}{\varphi_0}\left[1+\frac{1}{2\omega_{\rm BD}+3}e^{-m_\varphi r}\right] \tag{4.25}$$

$$\gamma = \frac{1-\frac{e^{-m_\varphi r}}{2\omega_{\rm BD}+3}}{1+\frac{e^{-m_\varphi r}}{2\omega_{\rm BD}+3}}, \tag{4.26}$$

which go back to Eqs. (2.36) and (2.37) in the limit of $m_\varphi \to 0$. With the identification $\varphi_0 = 1+f_{\mathcal{R}0} \equiv 1+\phi_0$ and $\omega_{\rm BD} = -3(1+\phi_0)/2\phi_0$, one recovers the results of Eqs. (4.23) and (4.24).

4.2 ΛCDM designer approach

In this section, we present a way to numerically get a family of $f(\mathcal{R})$ functions that reproduce a ΛCDM-like background evolution. Starting from Eq. (4.3), it is clear one can define an effective stress–energy tensor for the hybrid metric-Palatini theory as

$$T_{\mu\nu}^{\rm hybrid} = T_{\mu\nu} + T_{\mu\nu}^{\rm eff}, \tag{4.27}$$

where $T_{\mu\nu}^{\rm eff}$ will be given by

$$T_{\mu\nu}^{\rm eff} = \frac{1}{\kappa^2}\left[f(\mathcal{R})\frac{g_{\mu\nu}}{2} - F\mathcal{R}_{\mu\nu}\right], \tag{4.28}$$

where we have omitted the dependence on $\mathcal{R}$ of F.

Using the relation between $R_{\mu\nu}$ and $\mathcal{R}_{\mu\nu}$ given by Eq. (4.7), one can define an

effective equation of state

$$w_{\rm eff} = \frac{f\left(\mathcal{R}\right) - 2F\left(\dot{H} + 3H^2\right) - 5H\dot{F} - \ddot{F}}{-f\left(\mathcal{R}\right) + 6F\left(\dot{H} + H^2\right) - 3\dot{F}^2/F + 3H\dot{F} + 3\ddot{F}}. \tag{4.29}$$

Taking $w_{\rm eff} = -1$ in order to get a background evolution that follows ΛCDM, one gets a nonlinear second–order differential equation for F

$$\ddot{F} - H\dot{F} + 2F\dot{H} - \frac{3}{2}\frac{\dot{F}^2}{F} = 0. \tag{4.30}$$

Changing to a logarithmic variable, i.e., $dt \to d\ln a$, such that $d/dt = Hd/d\ln a$, one gets

$$F'' + F'\left(\frac{E'}{2E} - 1\right) + F\frac{E'}{E} - \frac{3}{2}\frac{F'^2}{F} = 0, \tag{4.31}$$

where we have define $E\left(a\right) \equiv H^2/H_0^2 = \Omega_{\rm m}a^{-3} + \Omega_\gamma a^{-4} + \Omega_{\rm eff}a^{3\int_a^1(1+w_{\rm eff})d\ln a}$. In a flat Universe, $\Omega_{\rm eff} = 1 - \Omega_{\rm m} - \Omega_\gamma$ and, for $w_{\rm eff} = -1$, one recovers a ΛCDM-like cosmology. In order to set the initial conditions, we consider an initial redshift, $z_i \gg 0$, but after the matter–radiation equality epoch. In these circumstances, the contribution from the effective component is negligible, meaning $E \approx \Omega_{\rm m}a_i^{-3} + \Omega_\gamma a_i^{-4}$. Hence, E'/E is reduced to a constant, given by

$$\frac{E'}{E} = -\frac{3 + 4r_i}{1 + r_i}, \tag{4.32}$$

where $r_i = a_{\rm eq}/a_i$ and $a_{\rm eq} = \Omega_\gamma/\Omega_{\rm m}$. Therefore, at z_i, we have the following differential equation

$$F'' - F'\left[\frac{5 + 6r_i}{2\left(1 + r_i\right)}\right] - F\left[\frac{3 + 4r_i}{1 + r_i}\right] - \frac{3}{2}\frac{F'^2}{F} = 0, \tag{4.33}$$

which happens to have a simple solution for the initial value of F, given by

$$F_i = C_1 a_i^{-a}\left[\cos\left(\frac{1}{2}\left[\ln a_i + C_2\right]\sqrt{2b - a^2}\right)\right]^{-2}, \tag{4.34}$$

where a and b are the coefficients multiplying F' and F on equation (4.33), respectively, and C_1 and C_2 are constants that define the family of $f\left(\mathcal{R}\right)$ functions yielding a ΛCDM-like evolution. According to our assumptions, $0 \leq r_i \leq 1$, meaning that $2b - a^2$ will always be negative. Therefore, setting $2b - a^2 = -d$,

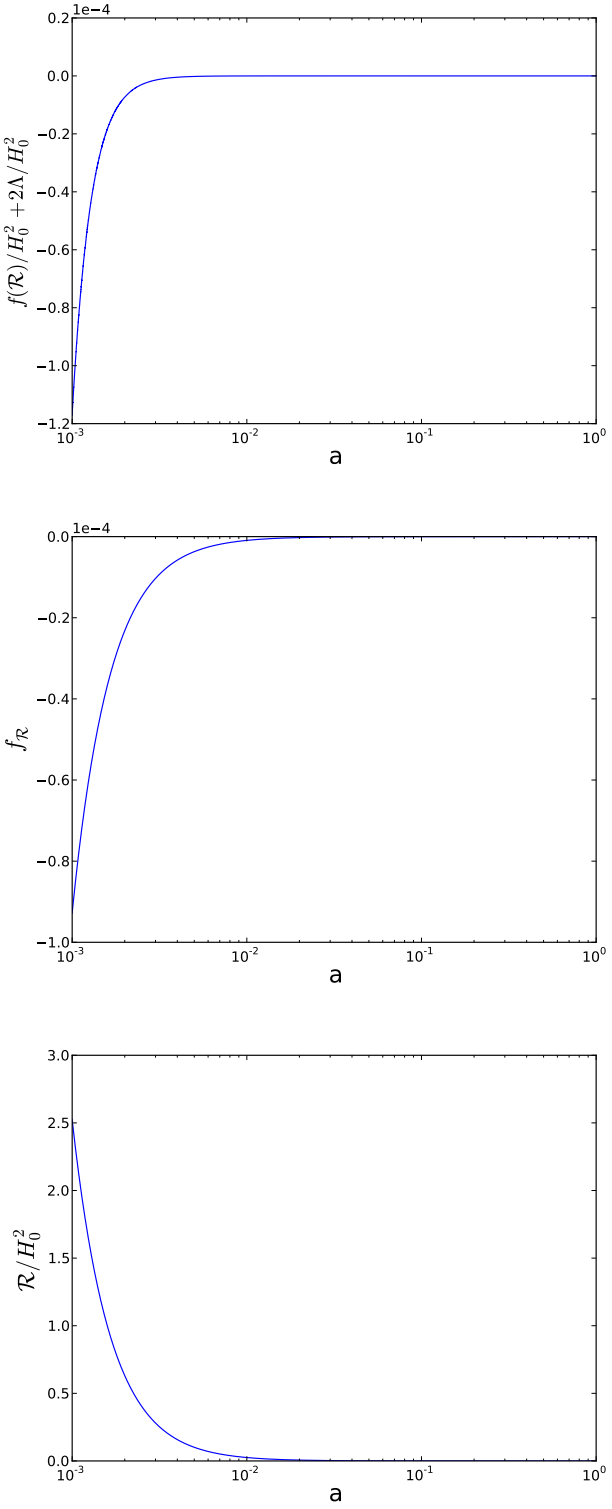

Figure 4.1 *Evolution of $f(\mathcal{R})$, $F(\mathcal{R})$ and $\mathcal{R}$, as a function of the scale factor, a, obtained using the designer approach for a model with $w_{eff} = -1$. We have set $C_1 = -1.0 \times 10^{-8}$ and $C_2 = -10.5$.*

where $d > 0$, our solution will, in fact, depend on a hyperbolic function,

$$F_i = C_1 a_i^{-a} \left[\cosh\left(\frac{1}{2} \left[\ln a_i + C_2 \right] \sqrt{d} \right) \right]^{-2} . \tag{4.35}$$

Finally, differentiating with respect to $\ln a_i$, one gets the initial condition for F'

$$F_i' = -C_1 \frac{a_i^{-a}}{\cosh\left(...\right)^2} \left[a + \sqrt{d} \tanh\left(...\right) \right] , \tag{4.36}$$

where we omitted the argument for the hyperbolic functions, defined in Eq. (4.35). Since $a > \sqrt{d}$, from Eq. (4.36) one can see that F_i' cannot be set to zero. Hence, we should expect some deviation from standard general relativity at the beginning of evolution.

In order to recover $f(\mathcal{R})$, at each step in the evolution, we compute $V(\phi)$ using Eq. (4.17). Then, we use the relation between $\mathcal{R}$ and R to compute the first which, with the fact that $V(\phi) = \mathcal{R}F - f(\mathcal{R})$, lets us determine $f(\mathcal{R})$. Figure 4.1 shows the evolution of $f(\mathcal{R})$, $F(\mathcal{R})$ and $\mathcal{R}$ for a model with $C_1 = -1.0 \times 10^{-8}$ and $C_2 = -10.5$. This particular choice of values ensures the modifications from GR in the distant past are not that significant, as well ensuring we have a positive definite effective mass for the scalar field.

We can clearly see in Fig. 4.1 that the modifications from standard GR, even though not large, are more significant in the distant past, as expected, with $f(\mathcal{R})$ hitting a maximum absolute deviation from Λ of 10^{-4}. And, as the evolution progresses, these differences start to vanish, with $f(\mathcal{R})$ tending to the exact Cosmological Constant value, and both $F(\mathcal{R})$ and $\mathcal{R}$ tending to zero.

4.3 Perturbation theory in the Jordan frame

In this section, we derive the equations governing the evolution of scalar perturbations in the hybrid metric-Palatini gravity theory. We will be working in the Jordan frame, following the notation of Kodama and Sasaki [202] for general perturbations. We will present the results in conformal time, τ, such that $dt = a\, d\tau$. Note that, now, $\mathcal{H} = aH$ will be the Hubble parameter in conformal time and an overdot will represent a differentiation with respect to conformal time.

Following Ref. [202], one can separate the spatial and time dependences of the perturbations of the metric. Therefore, for a given wave-number k, the metric can be decomposed into four time dependent perturbations A, B, H_L and H_T

$$\begin{aligned} g_{00} &= -a^2\left(1+2AY(k,x)\right), \\ g_{0i} &= -a^2 B Y_i, \\ g_{ij} &= a^2\left(\gamma_{ij}+2H_L Y\gamma_{ij}+2H_T Y_{ij}\right), \end{aligned} \tag{4.37}$$

where $Y(k,x)$ is the complete set of scalar harmonic functions and γ_{ij} is the spatial metric. In this work, we consider the case for which

$$Y \propto e^{i\vec{k}\cdot\vec{x}}, \tag{4.38}$$

$$Y_i = -\frac{1}{k}\nabla_i Y, \tag{4.39}$$

and,

$$Y_{ij} = \left(k^{-2}\nabla_i\nabla_j + \frac{\delta_{ij}}{3}\right) Y. \tag{4.40}$$

On the other hand, the stress-energy tensor perturbations can be decomposed into 4 components: density, $\delta\rho \equiv \rho\delta$; velocity, v; isotropic pressure, δp, and anisotropic stress, $\frac{3}{2}(\rho+p)\sigma$, as

$$\begin{aligned} T^0_0 &= -\rho\left(1+\delta Y\right), \\ T^0_i &= (\rho+p)\left(v-B\right)Y_i, \\ T^i_j &= p\,\delta^i_j + \delta p\,\delta^i_j + \frac{3}{2}(\rho+p)\,\sigma Y^i_j, \end{aligned} \tag{4.41}$$

where we have adopted the anisotropic stress notation of Ma and Bertschinger [203].

Since there is no dependence of the matter Lagrangian, $\mathcal{L}_m$, on the $f(\mathcal{R})$ modifications, in the Jordan frame, the matter conservation equations do not differ from those of standard general relativity, which are given by

$$\dot{\delta} + (1+w)\left(kv + 3\dot{H}_L\right) + 3\mathcal{H}\left(\frac{\delta p}{\delta\rho} - w\right)\delta = 0, \tag{4.42}$$

$$\begin{aligned} &\dot{v} - \dot{B} + \mathcal{H}\left(1-3w\right)\left(v-B\right) + \frac{\dot{w}}{1+w}\left(v-B\right) - \frac{\delta p/\delta\rho}{1+w}k\delta \\ &-kA + k\sigma = 0. \end{aligned} \tag{4.43}$$

The four perturbed field equations provide two additional independent equations. Here, we present all of the four equations and the perturbed equation of motion of the scalar field for completeness, leaving some intermediate results for Appendix C.1.

0 - 0 component

$$\begin{aligned} 2 \quad & (1+\phi)\left[A\left(3\mathcal{H}^2+\frac{3\dot{\phi}^2}{4\phi\,(1+\phi)}+\frac{3\mathcal{H}\dot{\phi}}{(1+\phi)}\right)-B\left(\mathcal{H}k+\frac{k\dot{\phi}}{2\,(1+\phi)}\right)\right. \\ - \quad & \left.\dot{H}_L\left(\frac{3\dot{\phi}}{2\,(1+\phi)}+3\mathcal{H}\right)-k^2\left(H_L+\frac{H_T}{3}\right)\right]-\dot{\delta\phi}\left(\frac{3\dot{\phi}}{2\phi}+3\mathcal{H}\right) \\ - \quad & \delta\phi\left(k^2+3\mathcal{H}^2-\frac{3\dot{\phi}^2}{4\phi^2}-a^2\frac{V_{,\phi}}{2}\right)=-\kappa^2a^2\rho\delta \end{aligned} \tag{4.44}$$

$i-i$ component

$$\begin{aligned} 2 \quad & (1+\phi)\left[A\left(\mathcal{H}^2+2\dot{\mathcal{H}}+\frac{\ddot{\phi}+\dot{\phi}\mathcal{H}}{(1+\phi)}-\frac{3\dot{\phi}^2}{4\phi\,(1+\phi)}-\frac{k^2}{3}\right)-\frac{k\dot{B}}{3}-\ddot{H}_L\right. \\ - \quad & B\left(\frac{2k\mathcal{H}}{3}+\frac{k\dot{\phi}}{3\,(1+\phi)}\right)-\dot{H}_L\left(\frac{\dot{\phi}}{(1+\phi)}+2\mathcal{H}\right)+\dot{A}\left(\mathcal{H}+\frac{\dot{\phi}}{2\,(1+\phi)}\right) \\ - \quad & \left.\frac{k^2}{3}\left(H_L+\frac{H_T}{3}\right)\right]-\delta\phi\left(\frac{3\dot{\phi}^2}{4\phi^2}+\frac{2k^2}{3}+2\dot{\mathcal{H}}+\mathcal{H}^2-a^2\frac{V_{,\phi}}{2}\right) \\ - \quad & \dot{\delta\phi}\left(\mathcal{H}-\frac{3\dot{\phi}}{2\phi}\right)-\ddot{\delta\phi}=\kappa^2a^2\delta p \end{aligned} \tag{4.45}$$

0 - i component

$$\begin{aligned} 2 \quad & (1+\phi)\left[A\left(\mathcal{H}+\frac{\dot{\phi}}{2\,(\phi+1)}\right)-\dot{H}_L-\frac{\dot{H}_T}{3}\right]+\delta\phi\left(\frac{3\dot{\phi}}{2\phi}+\mathcal{H}\right)-\dot{\delta\phi} \\ = \quad & \frac{\kappa^2a^2}{k}\,(\rho+p)\,(v-B) \end{aligned} \tag{4.46}$$

$i-j$ $(i\neq j)$ component

$$(1+\phi)\left[-k^2A - k\left(\dot{B}+2\mathcal{H}B\right)+\ddot{H}_T+2\mathcal{H}\dot{H}_T-k^2\left(H_L+\frac{H_T}{3}\right)\right]$$
$$-k^2\delta\phi-\dot{\phi}\left(kB-\dot{H}_T\right)=\frac{3}{2}\kappa^2a^2\left(\rho+p\right)\sigma \tag{4.47}$$

$\delta\phi$ equation

$$\begin{aligned}\ddot{\delta\phi} \quad &+\dot{\delta\phi}\left(2\mathcal{H}-\frac{\dot{\phi}}{\phi}\right)+\delta\phi\left(k^2+\frac{\dot{\phi}^2}{2\phi^2}-\frac{2}{3}a^2\phi V_{,\phi\phi}+a^2\frac{R}{3}\right)\\ + \quad &A\left(\frac{\dot{\phi}^2}{\phi}-2\ddot{\phi}-4\mathcal{H}\dot{\phi}\right)+\dot{\phi}\left(3\dot{H}_L-\dot{A}+kB\right)=-a^2\frac{\phi}{3}\delta R,\end{aligned} \tag{4.48}$$

where δR is the perturbed Ricci scalar, given by

$$\begin{aligned}\frac{a^2\delta R}{2Y} \quad &= \quad\Bigg[-6\frac{\ddot{a}}{a}A-3\mathcal{H}\dot{A}+k^2A+k\dot{B}+3k\mathcal{H}B+9\mathcal{H}\dot{H}_L+3\ddot{H}_L\\ &+ \quad 2k^2\left(H_L+\frac{H_T}{3}\right)\Bigg].\end{aligned} \tag{4.49}$$

4.3.1 Conformal newtonian gauge

In this particular gauge, one sets $H_T = B = 0$, $A = \Psi$ and $H_L = -\Phi$, following the notation of Ma and Bertschinger [203]. In this gauge, one can combine equations (4.42) and (4.43) for a Cold Dark Matter (CDM) and radiation overdensity, providing a set of single second–order differential equations, given by

$$\ddot{\delta}_c+\mathcal{H}\dot{\delta}_c+k^2\Psi-3\ddot{\Phi}-3\mathcal{H}\dot{\Phi}=0, \tag{4.50}$$
$$\ddot{\delta}_\gamma+\frac{1}{3}k^2\delta_\gamma+\frac{4}{3}k^2\Psi-4\ddot{\Phi}=0, \tag{4.51}$$

respectively. The Einstein equations, on the other hand, in this gauge, which have already been presented in Ref. [196], are given by

$0-0$ component

$$
\begin{aligned}
2 \quad & (1+\phi)\left[\Psi\left(3\mathcal{H}^2+\frac{3\dot{\phi}^2}{4\phi\,(1+\phi)}+\frac{3\mathcal{H}\dot{\phi}}{(1+\phi)}\right)+\dot{\Phi}\left(3\mathcal{H}+\frac{3\dot{\phi}}{2\,(1+\phi)}\right)+k^2\Phi\right] \\
- \quad & \dot{\delta\phi}\left(\frac{3\dot{\phi}}{2\phi}+3\mathcal{H}\right)-\delta\phi\left(k^2+3\mathcal{H}^2-\frac{3\dot{\phi}^2}{4\phi^2}-a^2\frac{V_{,\phi}}{2}\right)=-\kappa^2a^2\rho\delta
\end{aligned}
\tag{4.52}
$$

$i-i$ component

$$
\begin{aligned}
2 \quad & (1+\phi)\left[\Psi\left(\mathcal{H}^2+2\dot{\mathcal{H}}+\frac{\ddot{\phi}+\mathcal{H}\dot{\phi}}{(1+\phi)}-\frac{3\dot{\phi}^2}{4\phi\,(1+\phi)}\right)+\frac{k^2}{3}\left(\Phi-\Psi\right)\right. \\
+ \quad & \left.\dot{\Psi}\left(\mathcal{H}+\frac{\dot{\phi}}{2\,(1+\phi)}\right)+\dot{\Phi}\left(\frac{\dot{\phi}}{(1+\phi)}+2\mathcal{H}\right)+\ddot{\Phi}\right]-\dot{\delta\phi}\left(\mathcal{H}-\frac{3\dot{\phi}}{2\phi}\right) \\
- \quad & \delta\phi\left(\frac{3\dot{\phi}^2}{4\phi^2}+\frac{2}{3}k^2+2\dot{\mathcal{H}}+\mathcal{H}^2-a^2\frac{V_{,\phi}}{2}\right)-\ddot{\delta\phi}=\kappa^2a^2\delta p
\end{aligned}
\tag{4.53}
$$

$0-i$ component

$$
\begin{aligned}
2 \quad & (1+\phi)\left[\Psi\left(\mathcal{H}+\frac{\dot{\phi}}{2\,(\phi+1)}\right)+\dot{\Phi}\right]+\delta\phi\left(\mathcal{H}+\frac{3\dot{\phi}}{2\phi}\right)-\dot{\delta\phi} \\
= \quad & \frac{\kappa^2a^2}{k}\left(\rho+p\right)v
\end{aligned}
\tag{4.54}
$$

i - j $(i\neq j)$ component

$$
(1+\phi)\left(k^2\Phi-k^2\Psi\right)-k^2\delta\phi=\frac{3}{2}\kappa^2a^2\Sigma\left(\rho+p\right)\sigma. \tag{4.55}
$$

The last equation we show is the perturbed Klein-Gordon equation for the scalar field,

$\delta\phi$ equation

$$
\begin{aligned}
\ddot{\delta\phi} \quad & +\dot{\delta\phi}\left(2\mathcal{H}-\frac{\dot{\phi}}{\phi}\right)+\delta\phi\left(k^2+\frac{\dot{\phi}^2}{2\phi^2}-\frac{2}{3}a^2\phi V_{,\phi\phi}+a^2\frac{R}{3}\right) \\
+ \quad & \Psi\left(\frac{\dot{\phi}^2}{\phi}-2\ddot{\phi}-4\dot{\phi}\mathcal{H}\right)-\dot{\phi}\left(3\dot{\Phi}+\dot{\Psi}\right)=-\frac{\phi}{3}a^2\delta R,
\end{aligned}
\tag{4.56}
$$

where

$$\delta R = \frac{2}{a^2}\left[-6\frac{\ddot{a}}{a}\Psi - 3\mathcal{H}\dot{\Psi} + k^2\Psi - 9\mathcal{H}\dot{\Phi} - 3\ddot{\Phi} - 2k^2\Phi\right] Y. \tag{4.57}$$

4.3.2 Synchronous gauge

In this gauge, $A = B = 0$ and, adopting the notation of Ma and Bertschinger [203], $H_L = h/6$ and $H_T = -3\,(\eta + h/6)$. One may remove the remaining freedom and completely define the synchronous coordinates by setting that cold dark matter particles are at rest in this gauge, having zero peculiar velocity, v_m. Hence, the perturbed CDM and radiation evolution equations are written as

$$\dot{\delta}_c = -\frac{1}{2}\dot{h}, \tag{4.58}$$

$$\ddot{\delta}_\gamma + \frac{k^2}{3}\delta_\gamma - \frac{4}{3}\ddot{\delta}_c = 0, \tag{4.59}$$

respectively, while the perturbed Einstein equations and the perturbed field equation are given by

$\underline{0-0 \text{ component}}$

$$\begin{aligned} 2 \quad & (1+\phi)\left[k^2\eta - \frac{\dot{h}}{6}\left(3\mathcal{H} + \frac{3\dot{\phi}}{2\,(1+\phi)}\right)\right] - \delta\phi\left(k^2 + 3\mathcal{H}^2 - \frac{3\dot{\phi}^2}{4\phi^2} - a^2\frac{V_{,\phi}}{2}\right) \\ - \quad & \dot{\delta\phi}\left(3\mathcal{H} + \frac{3\dot{\phi}}{2\phi}\right) = -\kappa^2 a^2 \rho\delta \end{aligned} \tag{4.60}$$

$\underline{i-i \text{ component}}$

$$\begin{aligned} 2 \quad & (1+\phi)\left[-\frac{\dot{h}}{6}\left(2\mathcal{H} + \frac{\dot{\phi}}{(1+\phi)}\right) - \frac{\ddot{h}}{6} + \frac{1}{3}k^2\eta\right] - \dot{\delta\phi}\left(\mathcal{H} - \frac{3\dot{\phi}}{2\phi}\right) - \ddot{\delta\phi} \\ - \quad & \delta\phi\left(\frac{3\dot{\phi}^2}{4\phi^2} + \frac{2k^2}{3} + 2\dot{\mathcal{H}} + \mathcal{H}^2 - a^2\frac{V_{,\phi}}{2}\right) = \kappa^2 a^2 \delta p \end{aligned} \tag{4.61}$$

$\underline{0-i \text{ component}}$

$$2\left(1+\phi\right)\dot{\eta}+\delta\phi\left(\mathcal{H}+\frac{3\dot{\phi}}{2\phi}\right)-\delta\dot{\phi}=\frac{\kappa^2a^2}{k}\left(\rho+p\right)v \tag{4.62}$$

$\underline{i-j\ (i\neq j)\text{ component}}$

$$\begin{aligned}&\left(1+\phi\right)\left[k^2\eta-6\mathcal{H}\left(\dot{\eta}+\frac{\dot{h}}{6}\right)-3\ddot{\eta}-\frac{\ddot{h}}{2}\right]-3\dot{\phi}\left(\dot{\eta}+\frac{\dot{h}}{6}\right)\\&-k^2\delta\phi=\frac{3}{2}\kappa^2a^2\left(\rho+p\right)\sigma.\end{aligned} \tag{4.63}$$

$\underline{\delta\phi\text{ equation}}$

$$\begin{aligned}&\delta\ddot{\phi}+\delta\dot{\phi}\left(2\mathcal{H}-\frac{\dot{\phi}}{\phi}\right)+\delta\phi\left(k^2+\frac{\dot{\phi}^2}{2\phi^2}-\frac{2}{3}a^2\phi V_{,\phi\phi}+a^2\frac{R}{3}\right)\\&+\dot{\phi}\frac{\dot{h}}{2}=-a^2\frac{\phi}{3}\delta R,\end{aligned} \tag{4.64}$$

where δR is given by

$$\delta R=\frac{2}{a^2}\left[\frac{3}{2}\mathcal{H}\dot{h}+\frac{\ddot{h}}{2}-2\eta k^2\right]Y. \tag{4.65}$$

4.4 The lensing potential

In this section, we will be working in the Newtonian gauge with the anisotropy and Poisson equations. The former establishes a relation between the Newtonian potentials Ψ and Φ, while the latter describes the dependence of Φ, the curvature potential, on the matter comoving density perturbation

$$\Delta=\delta+3\frac{aH}{k}\mathcal{V}, \tag{4.66}$$

where $\mathcal{V}\equiv\left(1+w\right)v$.

As shown in Section 4.3.1, the anisotropy equation for theories described by the action (4.8) is given by Eq. (4.55). In order to obtain the Poisson equation, one has to write Eq. (4.46) in the Newtonian gauge and combine it with Eq. (4.52), the result being

$$\frac{k^2}{a^2H^2}\Phi = -\frac{3}{2}\frac{H_0^2}{H^2}\frac{E_i\Delta_i}{D(\phi)} - 3\Psi\left(\frac{\phi'^2}{4\phi D(\phi)} + \frac{\phi'}{2D(\phi)}\right) + \frac{3}{4}\frac{\phi'\delta\phi'}{\phi D(\phi)} - \frac{3}{2}\frac{\Phi'\phi'}{D(\phi)} + \frac{\delta\phi}{2D(\phi)}\left[\frac{k^2}{a^2H^2} + 3\left(2 - \frac{\phi'^2}{4\phi^2} + \frac{3\phi'}{2\phi}\right) - \frac{V_{,\phi}}{2H^2}\right], \quad (4.67)$$

where we have defined, for simplification, $D(\phi) \equiv 1 + \phi$, and introduced $E_i = \kappa^2\rho_i/3H_0^2$. The repeated indices represent a sum over the matter fields, and the prime indicates a differentiation with respect to $\ln a$.

Neglecting anisotropic contributions from matter fields (i.e. setting $\sigma_i = 0$), eq. (4.55) yields the following relation between the gravitational potentials

$$\Phi - \Psi = \frac{\delta\phi}{D(\phi)}. \quad (4.68)$$

This stands as a clear departure from standard general relativity where the anisotropy equation would be a simple constraint, $\Psi = \Phi$, reducing the number of independent perturbed variables. On the other hand, the Poisson equation would also just be an algebraic relation between the comoving matter density perturbation Δ_i and the curvature perturbation Φ.

However, in the hybrid metric-Palatini gravity, Eqs. (4.67) and (4.68) have extra dynamics. In the anisotropy equation, these are encoded in the slip between the Newtonian potentials. Following the work done in Refs. [2, 204] for $f(R)$ theories, we will choose to evolve the slip as one of the perturbed variables. And, alongside it, we choose to evolve another function of the Newtonian potentials Ψ and Φ, which facilitates the numerical treatment of the equations and the interpretation of the results. Namely, we evolve the following variables

$$\Phi_+ = \frac{\Phi + \Psi}{2} \quad (4.69)$$

$$\chi \equiv \delta\phi = D(\phi)(\Phi - \Psi), \quad (4.70)$$

along with the perturbations of matter fields. Now, eq. (4.68) becomes a constraint equation and any non-zero value of χ will signal a deviation from standard GR. The variable Φ_+ is the lensing potential, i.e. the combination of potentials responsible for such effects as the integrated Sachs–Wolfe effect in the CMB and weak lensing of distant galaxies. Ignoring any contribution from the radiation component, the momentum (4.54) and the Poisson (4.67) equations

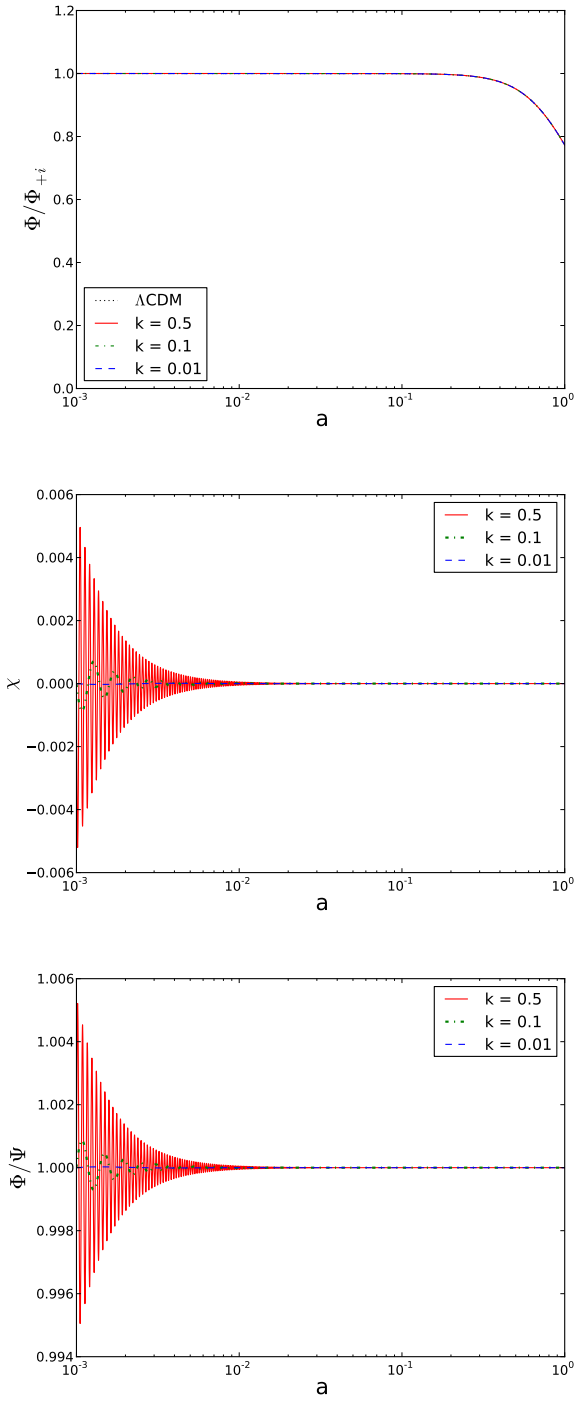

Figure 4.2 *The evolution of the lensing potential, Φ_+, χ and the ratio between the Newtonian potentials, Φ and Ψ, as a function of the scale factor, a, for the designer model with $w_{eff} = -1$ under analysis. Note that, for ΛCDM, $\chi = 0$ and $\Phi/\Psi = 1$ throughout the entire evolution. We plot this for three different k (h/Mpc) modes.*

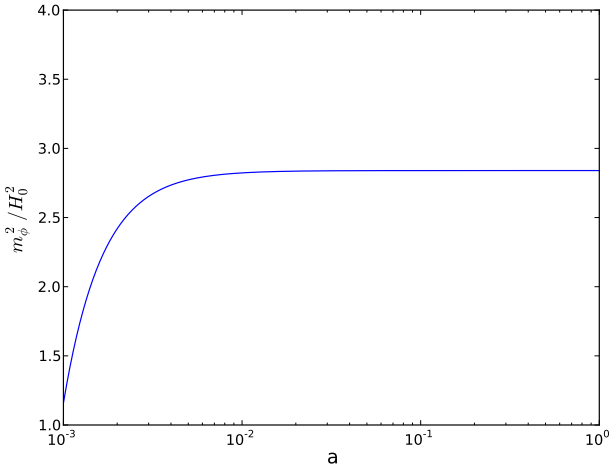

Figure 4.3 *The evolution of the effective scalar mass, m_ϕ^2, for the designer model $w_{eff} = -1$ considered in this analysis.*

provide a set of coupled first–order differential equations for Φ_+ and χ, given by

$$\Phi'_+ = \frac{3}{2}\frac{aH_0^2}{Hk D}E_i\mathcal{V}_i - \Phi_+\left(1+\frac{D'}{2D}\right) - \frac{3}{4}\frac{D'\chi}{\phi D^2} \tag{4.71}$$

$$\begin{aligned}\chi' &= 2\frac{H_0^2}{H^2}\frac{\phi D}{D'}E_i\Delta_i - 4\chi\left[\frac{\phi D}{D'} + \frac{D'}{8\phi D}\left(2\phi^2 - D\right) + \frac{1}{4}\left(3D+\phi\right) - \frac{V_{,\phi}}{12H^2}\frac{\phi D}{D'}\right] \\ &+ 2\Phi'_+\phi D + 2\Phi_+\left(\frac{DD'}{2} + \phi D + \frac{2}{3}\frac{k^2}{a^2H^2}\frac{\phi D^2}{D'}\right)\end{aligned} \tag{4.72}$$

The numerical evolution of the above equations is shown in Figure 4.2, for a model with $w_{\rm eff} = -1$ and a value of $|F(\mathcal{R})| \approx 10^{-4}$ at the start of evolution, which we have set at $z_i = 1000$. This ensures that, at this point, the deviations from general relativity are small and we can set the initial conditions as if that was the case. Therefore, we set $\Phi_+(z = z_i) = -1$ and $\chi(z = z_i) = 0$ and use the standard GR relations for the matter perturbations v_m and Δ_m,

$$v_m(z = z_i) = \frac{2k}{3aH}\Phi_+, \tag{4.73}$$

$$\Delta_m(z = z_i) = -\frac{2k^2}{3a^2H^2}\Phi_+. \tag{4.74}$$

In Fig. 4.2, one can clearly see oscillations in χ. This is expected since Equation (4.56) resembles that of a damped oscillator, whose frequency of oscillation will

increase with k. Also, we note that the deviations from ΛCDM are actually larger in the distant past. This is due to the behavior of the effective mass of the scalar field, m_ϕ, whose evolution for the model under analysis is plotted in Fig. 4.3. The latter, in turn, defines the range of action of the modifying fifth force: if we were to define a Compton wavelength for its range, this would be inversely proportional to m_ϕ. Hence, for $a \ll 1$, the range of action of the fifth force is quite significant, leading to a greater amplitude in the oscillations of χ, which is then damped with the evolution.

Of course, the amplitude of the slip oscillations is larger for the smaller scales (or larger k) as these begin their evolution deep within the range of action of the fifth force. Nevertheless, neither the enhancement or the oscillations in the slip are reflected on Φ_+, which remains almost indistinguishable from ΛCDM throughout the entire evolution, apart from a negligible increment at the beginning of it, for every scale considered. These oscillations in χ do, however, translate into rapid oscillations in the ratio between the Newtonian potentials, Φ and Ψ, which could potentially be discriminating between this particular model and GR.

We lastly note that the oscillations in $\chi \equiv \delta\phi$ arise from the homogeneous solution to the perturbed scalar field equation which will be that of a damped harmonic oscillator in the absence of an external force. Hence, their amplitude is set by the initial conditions we impose and are, thus, arbitrary. Therefore, we set the value of χ to zero at the initial redshift, which is not too restrictive since χ does oscillate quickly around zero. So, the overall maximum amplitude of the oscillations now depends on the values that ϕ and ϕ' take at z_i. As we will see in Chapter 5, this will allow us to infer constraints on ϕ at early-times by studying the imprint of these oscillations in the cosmic microwave background.

4.5 Discussion

In this paper, we have derived the full set of perturbed Einstein equations for the novel hybrid metric-Palatini theory of gravity and presented them in the Newtonian and synchronous gauges. The latter, in particular, open the possibility of implementing this model in CAMB [205] and give an in-depth analysis of the effects it can have at early times and even constrain its parameter space, which we leave for future work.

We have introduced a designer approach to obtain a family of functions $f(\mathcal{R})$ that reproduce a cosmology indistinguishable from ΛCDM, with an effective equation of state exactly equal to $w_{\text{eff}} = -1$. This particular approach leads to models where the modifications from standard reneral relativity are more significant in the distant past. And, even though one can tweak the free parameters to control such modifications in order that they are quite negligible at a redshift of $z_i \approx 1000$, this can prove problematic at even earlier times if the departure from GR gets increasingly larger, as it seems to do. Potentially, one could observe an inversion in the sign of G_{eff}, leading to an inversion of the effect of gravity. This was, however, avoided in our analysis. We would like to point out that, other background solutions were neglected, for now, due to the inability to consistently set the initial conditions for F when $w_{\text{eff}} \neq -1$. This is being explored for future work.

We also derived the Poisson equation, which is substantially different from standard GR, given the inclusion of several extra dynamical elements. We then introduced the lensing potential, Φ_+, and the slip between the Newtonian potentials, χ, which we numerically evolved using the designer approach. We note that the departure from GR is more noticeable at the beginning of evolution. More specifically, χ oscillates with a frequency proportional to the mode's wave number, and the oscillations' amplitude is the largest at this point. It is then gradually damped due to the evolution, tending to a GR value of 0.

Nevertheless, these oscillations never end up reflecting upon the lensing potential, Φ_+, which remains practically indistinguishable from ΛCDM apart from a negligible enhancement at the start of evolution. However, they do reflect upon the Newtonian potentials, translating into a signature on the ratio between them, which oscillates rather quickly, signaling a clear departure of this model from standard GR.

We also note that the evolution of χ and Φ_+ in the hybrid metric-Palatini theory is related, like in metric $f(R)$ models, to the effective mass of the additional scalar degree of freedom, m_ϕ^2. Since the latter is smaller at early times, the range of the action of the additional fifth force will be larger. Hence, the enhancement in the perturbations, specially χ, will be greater then. And it will be greater the smaller the scale under consideration is, since these scales start their evolution deep within the range of the additional force.

Chapter 5

Constraints on early-time decaying modified gravity from cosmological observations

The verification of GR at early-times is a large extrapolation from its consistency on the solar system scales. Early-time modifications of gravity are not very well tested, and we lack not only a better understanding of their effects on cosmological observables but also a consistent quantitative analysis of the constraining power existing surveys have over them. Most of the available information on our cosmos stems from either late-time observations or the imprint of early-time inhomogeneities on the cosmic microwave background. In this work, we explore to what extent early modifications of gravity, which become significant after recombination but then decay towards the present, can be constrained by current cosmological observations.

For this purpose, we consider the hybrid metric-Palatini gravity [192, 193], about which more details can be found in Chapter 4, where the specific $f(\mathcal{R})$ model we adopt for our study is also introduced. The model we chose is designed to yield a background evolution indistinguishable from ΛCDM. This recovery comes at the expense of a departure from the standard model at early times, with $f(\mathcal{R})$ differing from the actual Λ at high redshifts and tending indistinguishably closer to it towards the present. The same characteristics are observed for the scalar field: it tends to zero as it approaches the present from a maximum starting value at a specified initial high redshift after recombination. Designer $f(\mathcal{R})$

can therefore be considered a decaying early modified gravity model. A clear advantage of this model is that it enables a separation of the modifications introduced between linear perturbations and background effects. It has been shown in Ref. [3] that the ratio (and slip) between the metric potentials is expected to oscillate at high redshifts, but the respective observational effects have not yet been studied in detail.

While $f(R)$ gravity is a more frequently adopted toy model for the study of modified gravity effects, we opt for the hybrid theory instead. As will become clear in this chapter, in addition to the advantages already mentioned, the hybrid $f(\mathcal{R})$ theory provides a much cleaner modification of gravity on the smallest scales. We will derive the sub-horizon approximation for the $f(\mathcal{R})$ theory and show that the relative difference between the effective gravitational coupling to the actual Newtonian constant is very small at any scale and at the present, consistent with solar system tests. This contrasts with metric $f(R)$ theories, where we have $(G_{\rm eff} - G)/G = 4/3$ at linear order, requiring an additional screening chameleon mechanism to restore $G_{\rm eff}/G \to 1$ [68, 206–208].

Hence, the outline of this chapter is as follows. In Sec. 5.1, we briefly discuss the concept of early-time decaying modified gravity and introduce the hybrid metric-Palatini model we will investigate. In Sec. 5.1.1, we reproduce the relevant linearly perturbed modified Einstein equations in the Newtonian gauge. We explicitly show how the breakdown of the quasistatic approximation for the evolution of the scalar field fluctuation occurs at high redshifts. This failure motivates an analytic correction to the quasistatic approximation to accurately describe the evolution of the slip between the metric potentials in this high-curvature regime. In Secs. 5.1.2 and 5.1.3, we describe an embedding of the designer hybrid metric-Palatini model in the effective field theory (reviewed in Ref. [209]) of Horndeski scalar-tensor theory with a high-redshift decoupling of the modification to comply with stringent high-curvature constraints from the CMB. In Sec. 5.2, we infer constraints on the early-time decaying modified gravity model using current cosmological observations. Lastly, in Sec. 5.3 we conclude with some final thoughts and remarks, also providing an outlook for future cosmological constraints on the model. For completeness, in the appendices we provide details on our numerical computations and approximations adopted to describe oscillations in the scalar field fluctuations.

I would like to state that this work can be found in [4] and results of a collaboration with Vanessa Smer-Barreto and Lucas Lombriser. Vanessa helped

adapting my modified $f(\mathcal{R})$ MGCAMB code to work with the latest COSMOMC [210], contributed to the writing and independently checked the stability of the hybrid theory discussed in Sec. 5.1.3. Lucas originally suggested the implementation of the designer $f(\mathcal{R})$ model in MGCAMB, also contributed to the writing and obtained the results concerning future constraints from gravitational waves shown in Sec. 5.2.3.

5.1 A decaying early modification of gravity

The main purpose of this work is to explore constraints on early modified gravity, with modifications from GR arising at high redshifts and being suppressed as we approach the present time. We start by describing the general dynamics of the test model we will embed in Horndeski theory: the hybrid metric-Palatini gravity. This class of theories emanate from considering the metric and the connection as independent variables.

More specifically, we will adopt the designer hybrid-metric Palatini model first introduced in Ref. [3]. This model allows one to retrieve a family of $f(\mathcal{R})$ functions that produce a background evolution indistinguishable to ΛCDM. This is achieved by solving the second-order differential equation for $df(\mathcal{R})/d\mathcal{R} \equiv f_{\mathcal{R}}$ that arises from setting the effective equation of state to -1. More details on the general dynamics of the hybrid metric-Palatini theory and its designer model can be seen in Secs. 4.1 and 4.2 respectively.

Here, it will suffice to see the predicted evolution of the additional scalar field, $f_{\mathcal{R}}$, by the designer model. In Fig. 5.1 we plot its absolute value as a function of the scale factor a for different starting values of $f_{\mathcal{R}\mathrm{i}}$ at an initial redshift of 1000. We can see that the scalar field $f_{\mathcal{R}}$ decays with time and is strongly suppressed as we approach $a \to 1$. In Sec. 5.2 it will become evident that due to this suppression, $f(\mathcal{R})$ behaves like a decaying early-modified gravity model that satisfies solar system constraints [192].

Having a hybrid metric-Palatini model that recovers a ΛCDM-like background evolution allows to separate the modifications introduced between linear perturbations from background effects. In fact, possible deviations at the background level from ΛCDM have already been tested against observational data in Chapter 6 for other choices of the $f(\mathcal{R})$ function that do not recover the

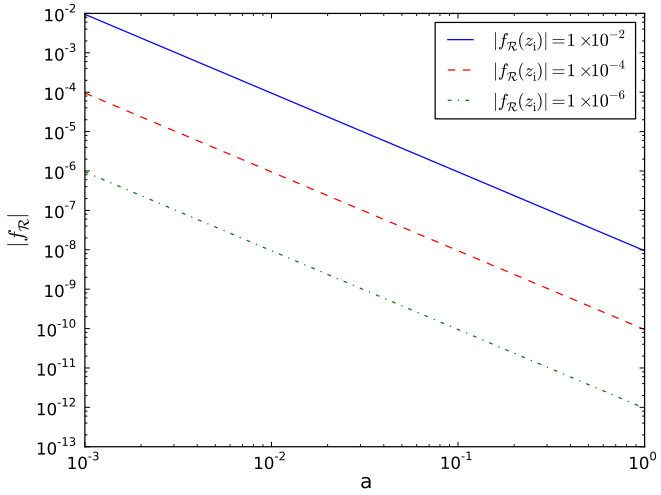

Figure 5.1 *Evolution of the absolute value of the additional scalar degree of freedom introduced in $f(\mathcal{R})$ theories, $f_{\mathcal{R}}$, as a function of the scale factor, a, with $z_{\rm i} = 1000$. We have fixed $\Omega_{\rm m} = 0.30$.*

ΛCDM expansion history. Modifications introduced in the linear cosmological perturbations have not yet been tested for $f(\mathcal{R})$ gravity. Hence, the designer model discussed here suits this purpose.

5.1.1 Linear perturbations in $f(\mathcal{R})$ gravity

We briefly review the main aspects concerning the evolution of linear perturbations in the hybrid metric-Palatini theory, first discussed in detail in Ref. [3]. For the full set of linearly perturbed Einstein and scalar field equations in the Newtonian gauge we direct the reader to Sec. 4.3.1. Typically for modified gravity theories (however, see Refs. [211, 212]), the hybrid metric-Palatini theory introduces a non-zero slip between the gravitational potentials in the Newtonian gauge, $\Phi = \delta g_{00}/(2g_{00})$ and $\Psi = -\delta g_{\rm ii}/(2g_{\rm ii})$. Neglecting any anisotropic contribution from matter fields, the anisotropy equation becomes

$$\Phi - \Psi = \frac{\delta f_{\mathcal{R}}}{1 + f_{\mathcal{R}}}\,, \tag{5.1}$$

where $\delta f_{\mathcal{R}}$ is the linear perturbation of the scalar field with its background value denoted by $f_{\mathcal{R}}$. This is the same as Eq. (4.68) but, given the scalar-tensor representation of the hybrid theory, we use the dynamically equivalent $f_{\mathcal{R}}$ instead of ϕ. Hence, $1 + f_{\mathcal{R}} \equiv D(\phi)$.

The evolution of $\delta f_{\mathcal{R}}$ is dictated by the linear perturbation of the scalar field equation of motion,

$$\delta\ddot{f}_{\mathcal{R}} + \delta\dot{f}_{\mathcal{R}}\left(2\mathcal{H} - \frac{\dot{f}_{\mathcal{R}}}{f_{\mathcal{R}}}\right) + \delta f_{\mathcal{R}}\left(k^2 + \frac{\dot{f}_{\mathcal{R}}^{\,2}}{2f_{\mathcal{R}}^{\,2}} + a^2 m_{f_{\mathcal{R}}}^2 - \frac{\kappa^2}{3}a^2 T\right)$$
$$+\Psi\left(\frac{\dot{f}_{\mathcal{R}}^{\,2}}{f_{\mathcal{R}}} - 2\ddot{f}_{\mathcal{R}} - 4\dot{f}_{\mathcal{R}}\mathcal{H}\right) - \dot{f}_{\mathcal{R}}\left(3\dot{\Phi} + \dot{\Psi}\right) = \frac{f_{\mathcal{R}}}{3}a^2\kappa^2\delta T, \tag{5.2}$$

where δT denotes the linear perturbation of the trace of the stress-energy tensor, $T = -\rho + 3p$, and *for this equation only*, the overdots represent derivatives with respect to conformal time τ with $dt = a\, d\tau$, and $\mathcal{H} \equiv aH$.

It has been shown in Ref. [3] and Sec. 4.4 that the evolution of $\delta f_{\mathcal{R}}$ is characterized by quick oscillations around zero, which end up reflecting in the ratio between the Newtonian potentials, $\gamma \equiv \Phi/\Psi$. These oscillations are scale dependent, oscillating faster and with larger amplitude at smaller scales. They can produce noticeable oscillations at near-horizon scales, depending on the initial value of the scalar field at early times that, for instance, have an impact on the Poisson equation. Due to the Hubble friction term (see Eq. (5.2)), these modifications eventually get damped as one approaches $a \approx 1$, becoming fairly negligible at the present with no signs of significant subhorizon modifications.

We will explore the behavior of $\delta f_{\mathcal{R}}$ further in the following sections, focusing on its subhorizon and early-time evolution, where we will develop accurate approximations for these regimes. In order to test our approximations, we follow Ref. [3] and solve the exact numerical evolution of the gravitational potentials and $\delta f_{\mathcal{R}}$, using the linearly perturbed conservation equations for the stress-energy tensor and the first-order differential equations for the lensing potential, $\Phi_+ \equiv (\Phi + \Psi)/2$.

Subhorizon approximation

We first consider wavemodes that are deep within the Hubble radius with wavenumber $k \gg aH$. To describe this limit, we adopt the quasistatic approximation, discarding time derivatives of perturbations when compared to their spatial variation. Generally, for Horndeski scalar-tensor theories, this is a good approximation on small scales [67]. In practice, this allows one to keep the terms proportional to $k^2/(a^2H^2)$ as well as those related to the matter

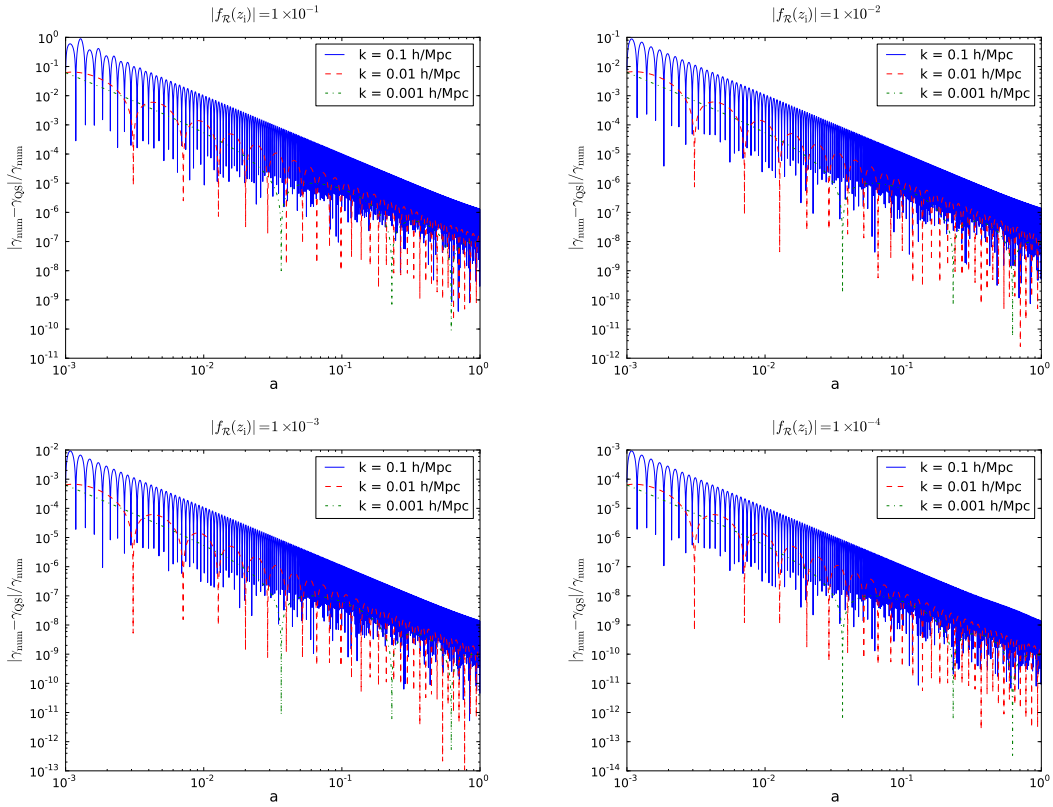

Figure 5.2 *Relative difference* $|\gamma_{\rm num} - \gamma_{\rm QS}|/\gamma_{\rm num}$ *between the numerical ratio* $\gamma \equiv \Phi/\Psi$ *and its quasistatic (QS) approximation given by Eq. (5.10). We have considered* $z_{\rm i} = 1000$ *and fixed* $\Omega_{\rm m} = 0.30$.

perturbation $\delta\rho_{\rm m}$ and the scalar field effective mass $m^2_{f_{\mathcal{R}}}$. The latter sets a modified length scale that can be compared to that of the perturbations.

From the $0-0$ linearly perturbed Einstein equation in the Newtonian gauge, we obtain in the subhorizon regime [3]

$$\frac{k^2}{a^2}\Phi \approx \frac{1}{2\,(1+f_{\mathcal{R}})}\left[\delta f_{\mathcal{R}}\left(\frac{k^2}{a^2}\right) - \kappa^2\delta\rho_{\rm m}\right], \tag{5.3}$$

where $\delta\rho_{\rm m} \equiv \rho_{\rm m}\delta_{\rm m}$. Using this approximation in the anisotropy equation we then get

$$\frac{k^2}{a^2}\Psi \approx -\frac{1}{2\,(1+f_{\mathcal{R}})}\left[\delta f_{\mathcal{R}}\left(\frac{k^2}{a^2}\right) + \kappa^2\delta\rho_{\rm m}\right]. \tag{5.4}$$

One can then calculate a similar approximation for $\delta f_{\mathcal{R}}$ from Eq. (5.2),

$$\delta f_{\mathcal{R}} \approx -\frac{H_0^2 E_{\rm m}}{k^2/a^2 + m^2_{f_{\mathcal{R}}}} f_{\mathcal{R}}\,\delta_{\rm m}\,, \tag{5.5}$$

which can be inserted back into Eqs. (5.3) and (5.4) such that

$$\frac{k^2}{a^2}\Phi \approx -\frac{H_0^2 E_{\rm m}\delta_{\rm m}}{2\left(1+f_{\mathcal{R}}\right)}\left[\frac{k^2/a^2\left(f_{\mathcal{R}}+3\right)+3m_{f_{\mathcal{R}}}^2}{k^2/a^2+m_{f_{\mathcal{R}}}^2}\right], \tag{5.6}$$

$$\frac{k^2}{a^2}\Psi \approx -\frac{H_0^2 E_{\rm m}\delta_{\rm m}}{2\left(1+f_{\mathcal{R}}\right)}\left[\frac{k^2/a^2\left(3-f_{\mathcal{R}}\right)+3m_{f_{\mathcal{R}}}^2}{k^2/a^2+m_{f_{\mathcal{R}}}^2}\right], \tag{5.7}$$

where $E_{\rm m} \equiv \Omega_{\rm m} a^{-3}$.

These approximations can, in turn, be used to obtain an expression for the lensing potential, Φ_+, in this regime:

$$\frac{k^2}{a^2}\Phi_+ \approx -\frac{3H_0^2 E_{\rm m}}{2\left(1+f_{\mathcal{R}}\right)}\delta_{\rm m} \tag{5.8}$$

whereas the slip between the potentials, $\delta f_{\mathcal{R}}$, is given by

$$\delta f_{\mathcal{R}} \approx \frac{2}{3}\frac{k^2}{a^2}\frac{f_{\mathcal{R}}\,\Phi_+}{k^2/a^2+m_{f_{\mathcal{R}}}^2}\,. \tag{5.9}$$

As mentioned in Sec. 4.1 and discussed in Refs. [192, 193], the background value of the scalar field is required to be small in order for the metric-Palatini theory to avoid solar system tests. In these circumstances, the quasistatic modifications will be almost unnoticeable, even if the range of the modifications, given by the effective Compton wavelength $\lambda_{\rm C} = 2\pi/m_{f_{\mathcal{R}}}$, is relevant. For instance, note that for $f_{\mathcal{R}} \to 0$, $\delta f_{\mathcal{R}} \to 0$ since $\delta f_{\mathcal{R}}$ is proportional to the background value of the scalar field $f_{\mathcal{R}}$ in the quasistatic regime, as can be seen in Eq. (5.9).

The $f(\mathcal{R})$ models that have been analyzed so far [3, 5] evolve towards smaller deviations from ΛCDM as we approach the present, with $f_{\mathcal{R}}$ tending to negligible values. This renders the modifications in the quasistatic regime subdominant, as was explicitly shown in Ref. [3] for the designer $f(\mathcal{R})$ model, with no mentionable enhancement of the perturbations in this regime when compared to ΛCDM.

In Fig. 5.2 we compare the numerical evolution of the ratio between the Newtonian potentials, γ, with its quasistatic approximation,

$$\gamma_{\rm QS} \equiv \frac{\Phi}{\Psi} = \frac{k^2/a^2\left(3+f_{\mathcal{R}}\right)+3m_{f_{\mathcal{R}}}^2}{k^2/a^2\left(3-f_{\mathcal{R}}\right)+3m_{f_{\mathcal{R}}}^2}\,. \tag{5.10}$$

We see that it is an accurate approximation at late times, as a consequence

of large $k/(aH)$ values. As we approach the present time in our models, the subhorizon modifications become suppressed, leading in turn to a very small difference between the compared values. This accuracy holds even when we consider larger initial displacements for the scalar field, $f_{\mathcal{R}\mathrm{i}}$.

For completeness, we also obtain the sub-horizon approximations for the perturbed potentials from Eqs. (2.32) and (2.34) imposing $\omega_{\mathrm{BD}} = -3\phi/\left(2\left[\phi-1\right]\right)$. Noting that $\phi = f_{\mathcal{R}} + 1$, we get

$$\gamma_{QSBD} = \frac{3 + f_{\mathcal{R}} - 2f_{\mathcal{R}}\left(1+f_{\mathcal{R}}\right)(Ma/k)^2}{3 - f_{\mathcal{R}} - 2f_{\mathcal{R}}\left(1+f_{\mathcal{R}}\right)(Ma/k)^2} \tag{5.11}$$

$$\frac{G_{\mathrm{eff}}}{G}_{\mathrm{QSBD}} = \frac{1}{1+f_{\mathcal{R}}}\frac{3 - f_{\mathcal{R}} - 2f_{\mathcal{R}}\left(1+f_{\mathcal{R}}\right)(Ma/k)^2}{3 - 2f_{\mathcal{R}}\left(1+f_{\mathcal{R}}\right)(Ma/k)^2}. \tag{5.12}$$

We note that the terms multiplying the mass term differ. This is due to the convention adopted by Ref. [144] for M^2, which yields different results than those obtained from the definition of the effective mass of the scalar field from the field's equation of motion. Hence, $M^2 \neq m^2_{f_{\mathcal{R}}}$. For Brans-Dicke theories, according to Ref. [144], $M^2 \approx V_{\phi\phi}$, which significantly differs from $m^2_{f_{\mathcal{R}}}$, not only in form but in sign. Nevertheless, the qualitative analysis of the results does not change, with $\gamma_{\mathrm{QSBD}} \to 1$ and $G_{\mathrm{eff}}/G_{\mathrm{QSBD}} \to 1$ as $f_{\mathcal{R}} \to 0$.

However, the quasistatic approximation breaks down at earlier times, due to the oscillatory behavior of $\delta f_{\mathcal{R}}$ discussed before and in detail in Sec. 4.4. This becomes more evident for the smaller scales, where the amplitude of the oscillations are larger. For large initial values of the scalar field the error can be of order unity and decreases as we consider smaller values for the initial displacement. Hence, for an accurate but computationally efficient description of the evolution of γ in the designer $f(\mathcal{R})$ model that is valid across a large range of redshifts and scales, some corrections must be applied to the subhorizon approximation (see Sec. 5.2.2). Lastly, we emphasize that in the hybrid metric-Palatini model $f_{\mathcal{R}}$ and $\delta f_{\mathcal{R}}$ are strongly suppressed at the present, and $(G_{\mathrm{eff}} - G)/G \ll 1$ at any scale, consistent with solar system tests. In contrast, in metric $f(R)$ gravity, for modes well within the Compton radius, we have $(G_{\mathrm{eff}} - G)/G = 4/3$ at linear order, and the model needs to employ a nonlinear chameleon mechanism [68, 206–208] to restore $G_{\mathrm{eff}}/G \to 1$ at the small scales probed by solar system tests. It is for this aspect that we adopt the decaying early-time gravitational modification characterized by the hybrid metric-Palatini model rather than the decaying mode of metric $f(R)$ gravity. Note that the suppression is also independent of environment and

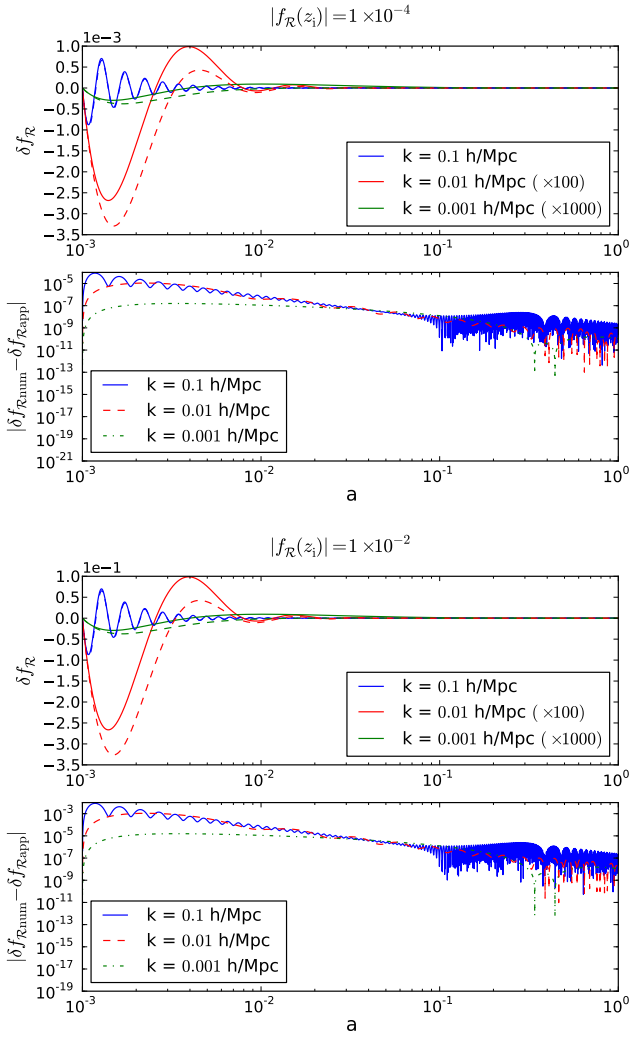

Figure 5.3 *The top panels show the numerical evolution (solid lines) of the perturbation $\delta f_{\mathcal{R}}$ against the evolution predicted by our analytical approximation (dashed lines) given by Eq. (5.14). The two largest scales have been enhanced by a factor of* 100 *and* 1000 *to be noticeable. The bottom panels show the absolute difference between the analytical approximation and the numerical results. We have fixed* $\Omega_{\mathrm{m}} = 0.30$.

cannot be unscreened by environment-dependent statistical measurements of the large-scale structure [66].

Early–time corrections

The dynamics of $\delta f_{\mathcal{R}}$ is dictated by Eq. (5.2), which is the equation of a damped harmonic oscillator with a driving force proportional to the matter perturbation.

The frequency of the oscillation depends on the mode wavenumber k, while the damping term is dominated by the Hubble parameter at early times, and $\delta f_{\mathcal{R}}$ quickly becomes negligible towards late times, where the oscillations are no longer observable. The driving term could deviate the equilibrium position of the oscillations. However, note that it is proportional to $f_{\mathcal{R}}$, which not only is fixed to a small value at early times as we study small deviations from GR, but also evolves towards zero at late times, rendering the external force term almost negligible.

Hence, rewriting Eq. (5.2) to depend on $\ln a$, assuming $f_{\mathcal{R}}, \dot{f_{\mathcal{R}}} \ll 1$, but not neglecting terms proportional to $\dot{f_{\mathcal{R}}}/f_{\mathcal{R}}$, we approximate it to

$$\delta f_{\mathcal{R}}'' + \delta f_{\mathcal{R}} \left(\frac{k^2}{a^2 H^2} + \frac{f_{\mathcal{R}}'^2}{2 f_{\mathcal{R}}^2} + \frac{H_0^2 \Omega_{\rm m} a^{-3}}{H^2} \right) + \delta f_{\mathcal{R}}' \left(3 + \frac{H'}{H} - \frac{f_{\mathcal{R}}'}{f_{\mathcal{R}}} \right) \approx 0 \,, \quad (5.13)$$

for which we attempt a solution under the Wentzel–Kramers–Brillouin (WKB) approximation given by

$$\delta f_{\mathcal{R}} \approx \frac{A}{\sqrt{2w}} a^{-\gamma_{\rm exp}} \cos \left(\int w \, d \ln a + \theta_0 \right) . \quad (5.14)$$

We expect the approximation to be valid as long as the adiabatic condition $|\dot{w}| \ll w^2$ holds, where w^2 is the term multiplying $\delta f_{\mathcal{R}}$ in Eq. (5.13); and $\gamma_{\rm exp}$ is the quantity multiplying the $\delta f_{\mathcal{R}}'$ term in Eq. (5.13). The constants θ_0 and A can be fixed by imposing suitable initial conditions for $\delta f_{\mathcal{R}}$ and $\delta f_{\mathcal{R}}'$ at a chosen redshift.

For the $f(\mathcal{R})$ designer model, the ratio between $f_{\mathcal{R}}'$ and $f_{\mathcal{R}}$ can be easily calculated at early times using the initial conditions presented in Sec. 4.1, using Eqs (4.35) and (4.36). This yields

$$\frac{f_{\mathcal{R}}'}{f_{\mathcal{R}}} \approx \sqrt{d} - a_{\rm aux} \,, \quad (5.15)$$

With this approximation, it is possible to simplify w and obtain an analytical solution for the integral $\int w \, d \ln a$. The details of this calculation may be found in Appendix C.1.

In Fig. 5.3 we set the initial conditions for $\delta f_{\mathcal{R}}$ by determining θ_0 such that $\delta f_{\mathcal{R}}$ is zero at the chosen initial redshift $z_{\rm i} = 1000$. We note that this is completely arbitrary, but not particularly relevant for the overall evolution of $\delta f_{\mathcal{R}}$ since it quickly oscillates around zero. We can then differentiate Eq. (5.14) with respect to $\ln a$ and compute A by calculating the numerical value of $\delta f_{\mathcal{R}}'$ using Eq. (67) of Ref. [3] at the same redshift. As discussed in Sec. 4.4, the amplitude of the

oscillations is solely determined by the initial conditions we set. Nevertheless, this gives us opportunity to constrain the allowed values of the scalar field $f_{\mathcal{R}}$ at high-redshifts, as it will dictate the overall amplitude of the oscillations of $\delta f_{\mathcal{R}}$ around zero and the impact on the observables we are considering.

We see in Fig. 5.3 that our analytical approximation works remarkably well, considering the complexity of the equation describing the dynamics of $\delta f_{\mathcal{R}}$. Even though it may fail in predicting the exact amplitude of the oscillations, the relative difference to the numerical results is insignificantly small compared to the precision available with current experiments. Also, it clearly encompasses the desired dependence on the scale of the modes of the perturbations, with a higher amplitude and frequency of oscillation the smaller scales (higher k) one considers.

Lastly, Fig. 5.3 serves as further confirmation of the viability of the subhorizon approximations derived in Sec. 5.1.1 at late times. As Eq. (5.9) dictates, $\delta f_{\mathcal{R}}$ should be strongly suppressed in the subhorizon regime following the behavior of the background scalar field value and with $k \gg aH$.

5.1.2 Decoupling at high redshifts

The hybrid metric-Palatini modification of gravity needs to decouple at high redshifts in order not to violate stringent high-curvature constraints from the CMB. However, we wish to determine below which redshift $z_{\rm on}$ the modification can be introduced and to which degree a decaying early-time modification motivated by the evolution of hybrid metric-Palatini gravity at $z \leq z_{\rm on}$ can be constrained by the CMB radiation observed today. In order to formulate an explicit realization of the decaying early modified gravity model, we embed the designer hybrid metric-Palatini scenario with high-redshift decoupling in Horndeski scalar-tensor theory [65] using the effective field theory of cosmic acceleration (see Ref. [209] for a review).

5.1.3 Embedding in Horndeski gravity and effective field theory

We now proceed to outline how the designer hybrid metric-Palatini model, detailed in Sec. 4.2, can be embedded in the Horndeski scalar-tensor theory. We

use the effective field theory of cosmic acceleration, where we adopt the notation of Ref. [213]. This allows us to express the designer $f(\mathcal{R})$ model in four time-dependent functions $\alpha_{\rm X}$ that, if turned off at a redshift higher than $z_{\rm on}$, allow to decouple the modifications introduced by the hybrid theory at high redshifts and not violate the stringent high-curvature constraints from the CMB. Using the EFT formalism also allows us to find the necessary conditions to ensure the stability of the model.

Given the ΛCDM background expansion history of our designer hybrid metric-Palatini model, its modifications are fully specified by the effective parameters characterizing the linear perturbations,

$$\alpha_{\rm M} = \frac{f'_{\mathcal{R}}}{1+f_{\mathcal{R}}}, \qquad \alpha_{\rm K} = -\frac{3}{2}\frac{f'_{\mathcal{R}}}{f_{\mathcal{R}}}\alpha_{\rm M}, \qquad \alpha_{\rm B} = -\alpha_{\rm M}, \tag{5.16}$$

where $\alpha_{\rm M} \equiv (M_*^2)'/M_*^2$ describes the running of the Planck mass $\kappa^2 M_*^2 \equiv 1+f_{\mathcal{R}}$; $\alpha_{\rm K}$ denotes the contribution of the kinetic energy of the scalar field; and $\alpha_{\rm B}$ determines the mixing of the kinetic contributions of the metric and scalar fields. The decaying early modifications of gravity constrained here are therefore realized in a Horndeski scalar-tensor model with

$$\alpha_{\rm X,model} = \begin{cases} \alpha_{\rm X}, & z \le z_{\rm on}, \\ 0, & z > z_{\rm on}, \end{cases} \tag{5.17}$$

where the $\alpha_{\rm X}$ are given by Eq. (5.16) according to hybrid metric–Palatini gravity. Note that $\alpha_{\rm X,model}(z > z_{\rm on}) = 0$ recovers a ΛCDM universe at high redshifts, avoiding the stringent high-curvature constraints at very early times.

Stability of the background solution of the Horndeski model with respect to the scalar mode requires [213]

$$Q_{\rm s} \equiv \frac{2M_*^2 D}{(2-\alpha_{\rm B})^2} > 0\,, \tag{5.18}$$

where

$$D \equiv \alpha_{\rm K} + \frac{3}{2}\alpha_{\rm B}^2 = -\frac{3(f'_{\mathcal{R}})^2}{2f_{\mathcal{R}}(1+f_{\mathcal{R}})^2}\,. \tag{5.19}$$

With the evolution of $f_{\mathcal{R}}$ given by hybrid metric-Palatini theory, we have

$$Q_{\rm s} = \begin{cases} < 0\,, & \text{for } f_{\mathcal{R}} > 0\,, \\ > 0\,, & \text{for } f_{\mathcal{R}} < 0\,. \end{cases} \tag{5.20}$$

Hence, we require $-1 < f_{\mathcal{R}} < 0$ to prevent ghost instabilities. To avoid a gradient instability or a superluminal sound speed $c_{\rm s}$ of the scalar field perturbation, we require that $0 < c_{\rm s}^2 \leq 1$. To check this, we compute $c_{\rm s}^2$ in the hybrid metric-Palatini theory,

$$\begin{aligned} D \cdot c_{\rm s}^2 &= \frac{\kappa^2}{H^2(1+f_{\mathcal{R}})}\left(\frac{4}{3}\rho_{\rm r}+\rho_{\rm m}\right)\left(f_{\mathcal{R}}+\frac{f'_{\mathcal{R}}}{2}\right) \\ &\quad +\frac{\alpha_{\rm M}}{2}\left(\frac{f'_{\mathcal{R}}+2(1+f_{\mathcal{R}})}{1+f_{\mathcal{R}}}\right)-\frac{f''_{\mathcal{R}}-(f'_{\mathcal{R}})^2}{1+f_{\mathcal{R}}}\,. \end{aligned} \tag{5.21}$$

Furthermore, note that for the designer model we use in this work

$$f'_{\mathcal{R}} = \begin{cases} >0\,, & \text{for } f_{\mathcal{R}}<0\,, \\ <0\,, & \text{for } f_{\mathcal{R}}>0\,, \end{cases} \tag{5.22}$$

and $|f'_{\mathcal{R}}| \gg |f_{\mathcal{R}}|$. Therefore, for $f_{\mathcal{R}} < 0$, $f_{\mathcal{R}} + f'_{\mathcal{R}}/2 > 0$. Also, $f''_{\mathcal{R}}$ will be negative-definite (as can be verified by differentiating Eq. (4.36)) for negative values of the scalar field. All of this, in conjunction with the fact that $\alpha_{\rm M} > 0$ and $D > 0$, ensures that $c_{\rm s}^2 > 0$ for $-1 < f_{\mathcal{R}} < 0$. We have also confirmed numerically that $c_{\rm s}$ is subluminal for the range of values we consider for $f_{\mathcal{R}{\rm i}}$. Note that whereas the condition for avoiding ghost instabilities applies to all hybrid metric-Palatini gravity models and should be respected when designing any other $f(\mathcal{R})$ models, the condition for avoiding gradient instabilities may be model dependent and should be studied in more detail for other choices of $f(\mathcal{R})$. For completeness, we also verify the stability of tensor modes [213] with $Q_{\rm T} \propto \kappa^2 M_\star^2 = 1 + f_{\mathcal{R}} > 0$ whenever $f_{\mathcal{R}} > -1$. Also note that in $f(\mathcal{R})$ models, the propagation speed of gravitational waves equals the speed of light $c_{\rm T} = 1$.

5.2 Observational constraints

Having fully specified a theoretically consistent decaying early modified gravity model in Sec. 5.1, we now determine the observational effects and constraints that can be set on early gravitational modifications with current cosmological data (Sec. 5.2.2). We also provide an outlook of constraints achievable with future surveys (Sec. 5.2.3).

5.2.1 Cosmological observables

To constrain our model parameters, we perform a MCMC search using a range of geometric probes and CMB measurements by Planck 2015.

Geometric probes

The comparison between the luminosity magnitudes of high-redshift to low-redshift supernovae Type Ia (SNe Ia) provides a relative distance measure affected by the Universe's expansion rate. Complementary absolute distance measures are obtained from measuring the local Hubble constant H_0 and the baryon acoustic oscillations (BAO) in the clustering of galaxies. These probes constrain the cosmological background evolution and since the $f(\mathcal{R})$ models considered here are designed to match the ΛCDM expansion history, they only serve to constrain the standard cosmological parameters and prevent degeneracies with the effect of the additional scalar degree of freedom on the fluctuations.

Cosmic microwave background

In addition to the geometic probes described in the previous section, the acoustic peaks in the CMB also contain information on the absolute distance to the last-scattering surface. These peaks are affected by early-time departures from GR at high curvature, i.e., in the case of $f(\mathcal{R})$ modifications, where $z_{\rm on}$ is sufficiently large. Gravitational modifications can generally further manifest themselves in the CMB temperature and polarization via secondary anisotropies. For details on the numerical computation of these effects in the designer hybrid metric-Palatini model, we refer the reader to Appendix C.

In Fig. 5.4, we show the predictions for the CMB temperature anisotropy power spectrum (TT) for three different choices of $z_{\rm on}$. Hence, we introduce the oscillations between the Newtonian potentials in distinct epochs of the cosmological evolution which in turn produces different effects in the observed power spectrum. The first immediate observation is that, the later we introduce these oscillations, the less significant is their impact on the TT power spectrum. This is mainly due to the fact that, at later epochs, the amplitude of the oscillations have already been considerably damped out, reducing their effect on the TT power spectrum.

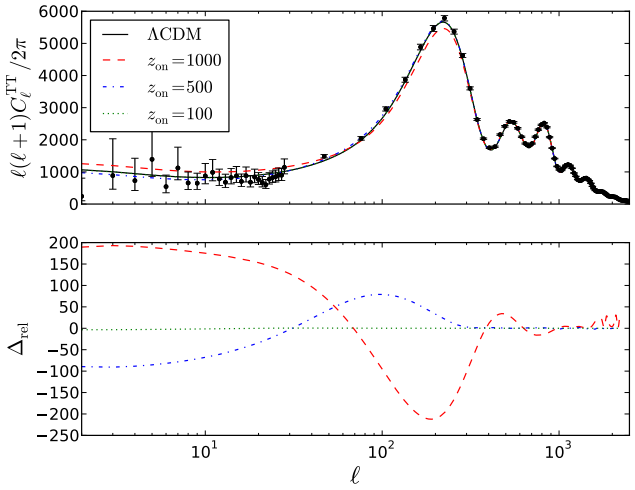

Figure 5.4 *The lensed CMB temperature anisotropy power spectrum predicted by the designer hybrid metric-Palatini model for* $|f_{\mathcal{R}}(z_{\rm i})| = 5\times10^{-2}$ *and different values of* $z_{\rm on}$ *as well as the prediction for the* Λ*CDM model (top panel). The lower panel shows the difference to* Λ*CDM,* $\Delta_{\rm rel} = \ell(\ell+1)\left(C_\ell^{TT,\rm hybrid} - C_\ell^{TT,\Lambda}\right)/(2\pi)$.

The second noticeable modification of the spectrum is in the Sachs-Wolfe plateau, on scales around $l < 100$, where we observe a shift towards higher or smaller values compared to ΛCDM. The Sachs-Wolfe effect, resulting from a combination of gravitational redshift and intrinsic temperature fluctuations at angular last-scattering, can lead to a variation of the temperature power spectrum like [214]

$$\frac{\Delta T}{T} \propto \delta\Phi, \tag{5.23}$$

where $\delta\Phi$ corresponds to the variation of the gravitational potential Φ. The designer hybrid-metric Palatini model introduces modifications close to the surface of last-scattering. Therefore, depending on the redshift we choose to start the oscillations, the Newtonian potential Φ will be displaced toward larger or smaller values compared to ΛCDM, leading to the shift we observe in the power spectrum. Then, at low ℓ, we have the traditional increase in power due to the integrated Sachs-Wolfe (ISW) effect in the presence of late-time dark energy. Our model clearly mimics ΛCDM due to the fact that we fix the background evolution to match the standard cosmological scenario, even if the power can be deviated toward lower or smaller values due to the Sachs-Wolfe effect discussed before.

Lastly, we have what is probably the most discerning effect on the CMB TT power spectrum. When we introduce the oscillations at $z_{\rm on} = 1000$, we notice

a significant decrease in the amplitude of the first peak. Traditionally, at early times, the non-negligible presence of radiation after the epoch of last-scattering can cause a decay of the gravitational potentials before these become constant, contributing to an early ISW effect that can influence the amplitude and position of the peaks. Therefore, if we allow modified gravity to be relevant close to the epoch of recombination, we not only modify this decay but also cause additional variation, influencing the acoustic phenomenology of the CMB. Of course, as we test lower valus of $z_{\rm on}$, this effect becomes increasingly negligible.

5.2.2 Cosmological constraints

Before presenting the current cosmological constraints on decaying early modified gravity, we briefly describe the cosmological datasets we use in our analysis. We then give an outlook on constraints that can be obtained with 21 cm surveys and gravitational wave observations.

Datasets

For the SN Ia luminosity-redshift relation, we use the dataset compiled in the Joint Lightcurve Analysis (JLA) [215]. This includes records from the full three years of the Sloan Digital Sky Survey (SDSS) survey plus the "C11 compilation" assembled by Conley et al. (2011); comprising supernovae from the Supernovae Legacy Survey (SNLS), the Hubble Space Telescope (HST) and several nearby experiments. This whole sample consists of 740 SNe Ia.
For H_0, we include information provided by the Wide Field Camera 3 (WFC3) on HST. The objective of this project was to determine the Hubble constant from optical and infrared observations of over 600 Cepheid variables in the host galaxies of 8 SNe Ia, which provide the calibration for a magnitude-redshift relation based on 240 SNe Ia [216]. Hence, we use the gaussian prior of $H_0 = 73.8 \pm 2.4$ km s^{-1} Mpc^{-1}.

We also use the BAO observations from the 6dF Galaxy Redshift Survey (6dFGRS) at low redshift $z_{\rm eff} = 0.106$ [217], as well as DR7 MGS from SDSS at $z_{\rm eff} = 0.15$, from the value-added galaxy catalogs hosted by NYU (NYU-VAGC) [218] and the BAO signal from the Baryon Oscillation Spectroscopic Survey (BOSS) DR11 at $z_{\rm eff} = 0.57$ [219].

$z_{\rm on}$	$\mathrm{sgn}(f_{\mathcal{R}})$	$\lvert f_{\mathcal{R}\rm i}\rvert \equiv \lvert f_{\mathcal{R}}(z_{\rm i})\rvert$	$\lvert f_{\mathcal{R}}(z_{\rm on})\rvert$	$\lvert f_{\mathcal{R}}(z=0)\rvert$
1000	$\pm$	$< 1.3 \times 10^{-2}$	$< 1.3 \times 10^{-2}$	$< 1.3 \times 10^{-8}$
500	$\pm$	$< 4.7 \times 10^{-2}$	$< 1.2 \times 10^{-2}$	$< 4.7 \times 10^{-8}$
100	$\pm$	—	—	—
1000	$-$	$< 1.1 \times 10^{-2}$	$< 1.1 \times 10^{-2}$	$< 1.1 \times 10^{-8}$
500	$-$	$< 4.8 \times 10^{-2}$	$< 1.2 \times 10^{-2}$	$< 4.8 \times 10^{-8}$
100	$-$	—	—	—

Table 5.1 *Current constraints (95% C.L.) on $f_{\mathcal{R}}(z_{\rm i} = 1000)$ from the combination of surveys discussed in Sec. 5.2.2. Note that models with a positive sign of $f_{\mathcal{R}}$ suffer from a ghost instability (see Sec. 5.1.3) and models with $z_{\rm on} = 100$ cannot be constrained within the prior $|f_{\mathcal{R}\rm i}| < 0.1$ required for the viability of the approximations performed in Sec. 5.1.1. However, a constraint of $|f_{\mathcal{R}\rm i}| \lesssim 10^{-3}$ on all models will be achievable with 21 cm intensity mapping (see Sec. 5.2.3). We also present constraints on the value of $f_{\mathcal{R}}$ at the redshift of decoupling, $z_{\rm on}$, and at the present time, $z = 0$.*

Lastly, we use the Planck 2015 data for the CMB. The Planck temperature and polarization and Planck lensing likelihood codes may be found in the Planck Legacy Archive [33].

Constraints

Using the datasets described in Sec. 5.2.2, we conduct an MCMC parameter estimation analysis with COSMOMC [210] (see Appendix C for details). We summarize our constraints on the early-time decaying modified gravity model of Sec. 5.1 in Table 5.1. It is easily noticeable that the constraining power of the data over the model changes significantly the later we introduce the oscillations between the Newtonian potentials ($z \leq z_{\rm on}$).

For $z_{\rm on} = 1000$, allowing both signs for $f_{\mathcal{R}\rm i} \equiv f_{\mathcal{R}}(z_{\rm i} = 1000)$, we infer a 1D-marginalized constraint of $|f_{\mathcal{R}\rm i}| < 1.3 \times 10^{-2}$ (95% C.L.), where we adopt a flat symmetric prior $f_{\mathcal{R}\rm i} \in [-0.1, 0.1]$. We stress, however, that positive values of $f_{\mathcal{R}\rm i}$ are affected by the ghost instability discussed in Sec. 5.1.3. Considering the stable branch only with a negative flat prior, we find $|f_{\mathcal{R}\rm i}| < 1.1 \times 10^{-2}$. These values are comparable to the constraints obtained in Chapter 6 on $f(\mathcal{R})$ models that deviate from the ΛCDM expansion history, using background data alone. Although we note that these constraints have been inferred for initial modifications at much higher redshift. ΛCDM is clearly the favored model and we find no evidence

for early-time modifications in the observations. The constraints we found are mostly driven by two prominent effects on the CMB that we have observed in Sec. 5.2.1: a modification of the Sachs-Wolfe plateau and of the amplitude of the first peak. However, there is also a non-negligible contribution of CMB lensing, which is sensitive to percent-level modifications at high ℓ [220] and can constrain the effects of $z_{\rm on} = 1000$ shown in Fig. 5.4. We also note that the present absolute value of the scalar field, $|f_{\mathcal{R}0}| \equiv |f_{\mathcal{R}}(z = 0)|$, is very small and of order 10^{-8}. This implies that modifications are strongly suppressed at the smallest scales, where these are proportional to the background value of the scalar field [192, 193] (see Sec. 5.1.1).

Finally, decreasing $z_{\rm on}$ leads to a considerable weakening of the constraints on the early-time deviation from GR. With $z_{\rm on} = 500$, constraints on the scalar field value at equal redshift weaken by a factor of approximately 4. For $z_{\rm on} = 100$, we can no longer constrain the scalar field value within the prior $|f_{\mathcal{R}\rm i}| < 0.1$. This is due to the oscillations on the slip between the gravitational potentials being significantly damped out by $z = 100$, hence only introducing very small deviations from GR.

5.2.3 Outlook: 21 cm and gravitational waves

Finally, we provide rough estimates of the constraints on early decaying modified gravity that will be achievable with 21 cm intensity mapping [221–223] and standard sirens [212, 224, 225] using gravitational waves emitted by events at cosmological distances. To estimate constraints obtainable with 21 cm surveys, we compare deviations in the matter power spectrum between the model and ΛCDM to bounds on modified gravity reported in Ref. [222] at $z = 11$ and Ref. [223] at $z = 2.5$. We find that $|f_{\mathcal{R}\rm i}| \lesssim 10^{-3}$ and $|f_{\mathcal{R}\rm i}| \lesssim 5 \times 10^{-2}$ for $z_{\rm on} = 1000$, which is competitive with the CMB constraints in Table 5.1. Standard sirens will constrain the luminosity distance at $z \sim (1 - 2)$ at the $\sim 1\%$ level, and at the $\sim 10\%$ level for $z \sim 7$ [226, 227]. In modified gravity models, this constraint can be used to set a bound on the evolution of the Planck mass [212], which for our model corresponds to a constraint of $|f_{\mathcal{R}\rm i}| \lesssim 10^3$, which will not be competitive with the constraints in Table 5.1.

5.3 Discussion

In this work we have explored the current cosmological constraints that can be inferred on modifications of gravity which may become significant at early times after recombination and decay towards the present. We have chosen the designer hybrid metric-Palatini model as a specific example of an early-time modification of gravity. Fixing the background evolution to exactly match ΛCDM, we are able to separate background constraints from constraints inferred from the modified dynamics of linear perturbations due to the impact that these have on the CMB. We also describe how this model can be realized in the more general context of the effective field theory formalism of Horndeski gravity, and study its stability. We conclude that the model is stable as long as the additional scalar degree of freedom introduced by the hybrid metric-Palatini theory remains negative with an amplitude smaller than unity, which implies an effective enhancement of the gravitational coupling.

In order to perform efficient numerical computations, we have developed an approximation for the evolution of the slip between the Newtonian potentials that is valid beyond the standard quasistatic subhorizon approximation. This extension becomes important at high redshifts, where we show that a quasistatic approach alone breaks down due to the known oscillations of the linear perturbations of the model [3].

Using a combination of observational data on the background evolution and of the CMB anisotropies, we infer constraints on the allowed early-time deviations from GR. The results we obtain are dependent on the redshift at which we introduce the oscillations in the slip between the gravitational potentials. If these are set at $z_{\rm on} = 1000$, we are able to constrain the absolute deviation from GR at $z_{\rm on}$ to $\lesssim 10^{-2}$ at the 95% confidence level. This result is comparable to the constraints obtained from background data alone in Chapter 6 for $f(\mathcal{R})$ models that depart from the ΛCDM expansion history.

The constraints we obtain at this redshift can be attributed to noticeable effects on the CMB power spectrum. We are able to observe a substantial shift in the Sachs-Wolfe plateau due to a modification of the Newtonian potential Φ at a time close to recombination. There is also a significant suppression of the first peak due to complementary variation of the gravitational potentials close to the epoch of recombination that, together with the non-negligible presence of radiation,

contributes to an early integrated Sachs-Wolfe effect that can alter the amplitude and position of the peaks. Smaller contributions to the constraints can be attributed to CMB lensing which is sensitive to the percent-level modifications we observe at high ℓ. Finally, we find that future 21 cm survey data will significantly improve upon the CMB constraints, whereas using gravitational wave events as standard sirens will not provide competitive bounds.

Chapter 6

Constraints on hybrid metric-Palatini gravity from background evolution

In this chapter we introduce two specific hybrid metric-Palatini models, respectively characterized by a quadratic and an exponential function $f(\mathcal{R})$ that modifies the standard Einstein–Hilbert gravitational action. For these models, we will explicitly show the background history they predict and how it deviates from the standard model ΛCDM. This is achieved by numerically evolving the Palatini Ricci scalar, $\mathcal{R}$, that is then used to compute the remaining background quantities. We then constrain the models free parameters against background data, including Supernovae, BAO and distance information from the CMB.

Therefore, in Section 6.1, we briefly review the hybrid metric-Palatini theory formalism, focusing on the background equations we will be using throughout this work. In Sec. 6.2, we introduce and dissect the two models we have used in this study, showing the background evolution predicted by these against ΛCDM. In Section 6.3 we present the background constraints on our models using a MCMC analysis, and finish in Sec. 6.4 with some concluding remarks on this work.

The work in this chapter can be seen in [5], and was done in collaboration with Vanessa Smer-Barreto. Vanessa contributed to the writing of the scientific text and wrote the Metropolis-Hastings MCMC code used to obtain the results, which I checked and tested alongside. We came up with the $f(\mathcal{R})$ models together, and

I devised their background implementation.

6.1 Cosmology in the hybrid metric-Palatini gravity

For more details on the hybrid metric-Palatini theory, namely its action, scalar-tensor formulation and background equations, we refer the reader to Sec. 4.1. For this work, it will suffice to reproduce the modified Friedmann equations adopting a flat Friedmann-Robertson-Walker (FRW) metric, $ds^2 = -dt^2 + a^2(t)d\vec{x}^2$, which will read:

$$3H^2 = \frac{1}{1+f_{\mathcal{R}}}\left[\kappa^2\rho - 3H\dot{f_{\mathcal{R}}} - \frac{3\dot{f_{\mathcal{R}}}^2}{4f_{\mathcal{R}}} + \frac{\mathcal{R}f_{\mathcal{R}} - f(\mathcal{R})}{2}\right], \tag{6.1}$$

and,

$$2\dot{H} = \frac{1}{1+f_{\mathcal{R}}}\left[-\kappa^2(\rho+p) + H\dot{f_{\mathcal{R}}} - \ddot{f_{\mathcal{R}}} + \frac{3\dot{f_{\mathcal{R}}}^2}{2f_{\mathcal{R}}}\right], \tag{6.2}$$

where a dot stands for a differentiation with respect to time, t, and $H = \dot{a}/a$ is the Hubble parameter; ρ and p are the total energy density and pressure of the Universe, while $f_{\mathcal{R}}$ and denotes a derivative of $f(\mathcal{R})$ with respect to the Palatini Ricci scalar. An equivalent equation for $\dot{H}$ can be taken from the trace of Eq. (4.3), yielding

$$\dot{H} = \frac{1}{6}\left[F(\mathcal{R})\mathcal{R} - 2f(\mathcal{R}) - \kappa^2 T - 12H^2\right], \tag{6.3}$$

where we have used $R = 6\left(\dot{H} + 2H^2\right)$.

A scalar-tensor description of this theory has been developed, where the additional scalar degree of freedom is identified as $\phi = F(\mathcal{R})$ [192, 193]. Eq. (11) in [192] is an effective Klein-Gordon equation for the scalar field. Using the FRW metric, it takes the form

$$\ddot{\phi} + 3H\dot{\phi} - \frac{\dot{\phi}^2}{2\phi} + \frac{\phi}{3}\left[2V - (1+\phi)\frac{dV}{d\phi}\right] = \frac{\kappa^2\phi}{3}T, \tag{6.4}$$

Equation (6.4) can be re-expressed as a dynamical equation for the Palatini Ricci scalar, $\mathcal{R}$. Recalling that $\phi \equiv F(\mathcal{R}) \equiv f_{\mathcal{R}}$, then one can set $\dot{F} = \dot{\mathcal{R}}f_{\mathcal{R}\mathcal{R}}$, where

$f_{\mathcal{R}\mathcal{R}}$ is the second derivative of $f(\mathcal{R})$ with respect to $\mathcal{R}$. A similar procedure can be done for higher order derivatives, allowing to rewrite Eq. (6.4) as

$$\begin{aligned}\ddot{\mathcal{R}} &= -\frac{1}{f_{\mathcal{R}\mathcal{R}}}\left[\dot{\mathcal{R}}^2\left(f_{\mathcal{R}\mathcal{R}\mathcal{R}}-\frac{f_{\mathcal{R}\mathcal{R}}^2}{2f_{\mathcal{R}}}\right)+3H\dot{\mathcal{R}}f_{\mathcal{R}\mathcal{R}}+\right.\\ &+ \left.\frac{f_{\mathcal{R}}}{3}\left[\mathcal{R}\left(f_{\mathcal{R}}-1\right)-2f(\mathcal{R})\right]-\kappa^2\frac{f_{\mathcal{R}}}{3}T\right]\end{aligned} \tag{6.5}$$

where we have used Eq. (5) in [192], and $f_{\mathcal{R}\mathcal{R}\mathcal{R}}$ is the third order derivative of $f(\mathcal{R})$ with respect to $\mathcal{R}$. From this equation, we can define an effective potential where the effective Palatini Ricci scalar will roll, since

$$\frac{dV_{\text{eff}}}{d\mathcal{R}}=\frac{f_{\mathcal{R}}}{3f_{\mathcal{R}\mathcal{R}}}\left[\mathcal{R}\left(f_{\mathcal{R}}-1\right)-2f(\mathcal{R})\right], \tag{6.6}$$

meaning $V(\mathcal{R})$ will be given by the indefinite integral

$$V(\mathcal{R})=\int^{\mathcal{R}}\frac{f_{\mathcal{R}}}{3f_{\mathcal{R}\mathcal{R}}}\left[\mathcal{R}\left(f_{\mathcal{R}}-1\right)-2f(\mathcal{R})\right]d\mathcal{R}. \tag{6.7}$$

It was shown that the hybrid metric-Palatini theory reduces to general relativity with a possible cosmological constant in vacuum, since it shares the property of pure Palatini $f(R)$ theories in Minkowski flat space-time [198]. Furthermore, the field's equation of motion have been analyzed as a dynamical system: it was explicitly shown that as long as one provides a suitable $V(\phi)$, or equivalently a function $f(\mathcal{R})$ such that the slope of the potential is downwards and its minimum happens for a small value of the scalar field ϕ, one should always obtain a natural transition from standard cosmological evolution to accelerated expansion close to the present while also avoiding any conflict with solar system constraints [196].

Hence, we use Eqs. (6.3) and (6.5) to numerically evolve the background quantities predicted by a specific $f(\mathcal{R})$ model. To set the initial conditions, we have fixed a very small value for $f_{\mathcal{R}}$ at a high redshift, z_{i}, such that the deviation from the Gravitational constant, G, is effectively small [3, 192, 193, 197] in the high curvature regime. Then, one can invert F to find $\mathcal{R}$ at that redshift.

Lastly, we set $\dot{\mathcal{R}}_{\text{i}}=0$ to minimize deviations from standard general relativity and use Eq. (6.1) to solve for the Hubble parameter at z_{i}. The Ricci scalar, R, can be computed using the GR relation, $R=6\left(\dot{H}+2H^2\right)$. Even though $\dot{\mathcal{R}}_{\text{i}}=0$ is a strong assumption, we have tested the models for a fairly broad range of

initial velocities, within a slow-roll regime, and observed that their qualitative behavior remained unaltered with the late-time evolution tending to an effective Cosmological Constant, and $\mathcal{R}$ asymptotically reaching the equilibrium position predicted by the effective potential we define in Eq. (6.7).

6.2 Models of hybrid metric-Palatini gravity

In this section, we introduce the models we defined for the hybrid metric-Palatini theory. While the general framework of this theory was derived in Refs. [192, 193, 196, 197], they did not write down specific models and explore their consequences. These were inspired in theories of $f(R)$ gravity, such as the Starobinsky [228] and the exponential [159] models, but are essentially phenomenological choices that are simply tested with the background evolution formalism displayed before.

6.2.1 The exponential model

The first model we introduce is defined by an exponential function, given by

$$f(\mathcal{R}) = \Lambda_\star \left(1 + e^{-\mathcal{R}/\mathcal{R}_\star}\right), \tag{6.8}$$

where $\Lambda_\star$ and $\mathcal{R}_\star$ are the model's parameters, both of order H_0^2, where H_0 is the present-day value of the Hubble parameter. We choose to define $\mathcal{R}_\star$ as a positive constant, while $\Lambda_\star$ should be a negative constant, since it should dominate over the other corrective terms introduced by our models. This is particularly relevant at late-times where, to recover standard GR with an effective Cosmological Constant, one should have $\Lambda_\star \approx -2\Lambda$. Hence, $\Lambda_\star < 0$ allows the effective Cosmological Constant to have the correct sign, which becomes clear, for instance, looking at Eq. (4.5) in vacuum.

The effective potential, $V(\mathcal{R})$, associated to this model, is given by doing the indefinite integral defined by Eq. (6.7), which has the simple form

$$\begin{aligned} V(\mathcal{R}) &= \frac{\mathcal{R}_\star}{3}\Bigg[2\Lambda_\star\mathcal{R} + \frac{1}{2}\mathcal{R}^2 - 2\Lambda_\star\mathcal{R}_\star e^{-\mathcal{R}/\mathcal{R}_\star} \\ &- e^{-\mathcal{R}/\mathcal{R}_\star}\left(\Lambda_\star\mathcal{R} + \Lambda_\star\mathcal{R}_\star\right)\Bigg]. \end{aligned} \tag{6.9}$$

We can see that the potential will be mostly dominated by its quadratic terms for order unit values of $\mathcal{R}_\star$. The minimum can then be estimated by

$$\mathcal{R}_{\rm min} \approx -2\Lambda_\star. \tag{6.10}$$

The effective cosmological constant value at which the Ricci scalar should sit in vacuum is given by the trace equation

$$\Lambda_{\rm eff} = \frac{1}{2}\left[-2\Lambda_\star f_{\mathcal{R}}(-2\Lambda_\star) - 2f(\Lambda_\star)\right] \approx -\Lambda_\star. \tag{6.11}$$

Hence, we do expect to obtain a ΛCDM like evolution in the distant future, if our solution for $\mathcal{R}$ is to settle at the minimum of its potential.

We choose a small value for $f_{\mathcal{R}}$ (less than unit), independently of the starting redshift $z_{\rm i}$. The reason for this is, as mentioned in the end of Sec. 6.1, that $f_{\mathcal{R}}$ sets the initial deviation from the actual gravitational constant in the high curvature regime. Therefore, higher values of $f_{\mathcal{R}}$ will either suppress gravity considerably or invert its sign if it is smaller than -1.

In Fig. 6.1, we plot the background evolution predicted by this model for a set of parameters as a function of redshift, z, using the prescription described at the end of Sec. 6.1. We use a Brent algorithm (see [229]) to find the correct $\Lambda_\star$ value that recovers a flat cosmology. Hence, the only true free parameters will be $\mathcal{R}_\star$ and $f_{\mathcal{R}}(z_{\rm i})$.

As we can see in Fig. 6.1, the evolution of the Palatini Ricci scalar starts at a position where the potential is tilted and one would expect for it to roll down towards the minimum. However, at early times, the evolution of $\mathcal{R}$ is dominated by the stress–energy tensor trace or, equivalently, by the matter energy density. Since the ratio $f_{\mathcal{R}}/f_{\mathcal{R}\mathcal{R}}$ is negative throughout the whole evolution, the matter density contribution pushes $\mathcal{R}$ upwards the effective potential, while its slope and the Hubble friction term exert the opposite effect. As matter ceases to dominate close to the present, $\mathcal{R}$ inverts its motion and starts evolving towards the minimum, where it will asymptotically settle in the distant future.

Lastly, in Fig. 6.1, we analyze the deceleration parameter q. We observe that our model predicts a Universe that will be expanding in an accelerated manner today, transitioning from a matter dominated decelerating phase at a redshift of around $z \approx 1$, as we have $q < 0$ at $z = 0$. This is a general result of this model,

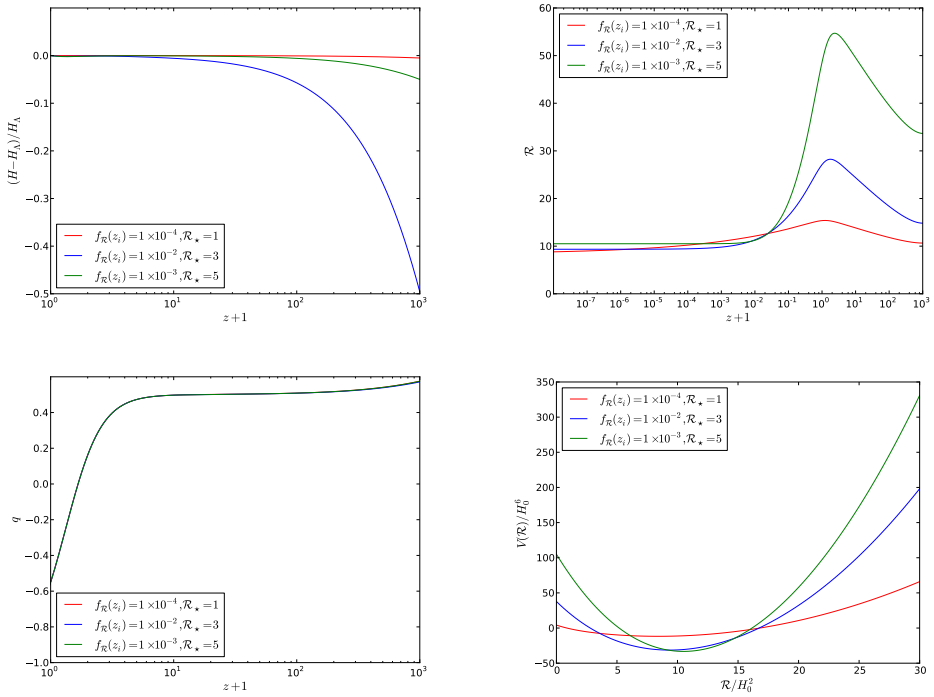

Figure 6.1 *The background evolution predicted by the exponential $f(\mathcal{R})$ model compared to ΛCDM. We choose to plot $\mathcal{R}$ far into the future ($z \to -1$), to explicitly show that our solution asymptotically tends to the minimum of the potential, $V(\mathcal{R})$, which we plot as well. We also plot the deceleration parameter q. The present-day matter energy density, $\Omega_{\rm m}$, is set to 0.30. $\mathcal{R}_\star$ is in units of H_0^2.*

as can be inferred from the deceleration parameter equation

$$q = -\frac{\dot{H}}{H^2} - 1, \tag{6.12}$$

where $\dot{H}$ is given by Eq. 6.3. Switching from physical time t to $\ln a$ we will have, at $z = 0$,

$$q = -\frac{1}{6H_0^2}\left[F(\mathcal{R})\mathcal{R} - 2f(\mathcal{R}) + 3H_0^2\Omega_{\rm m} - 12H_0^2\right] - 1. \tag{6.13}$$

As we observe in Fig.6.1, our model evolves towards small values of $F(\mathcal{R})$ today, as the exponential is suppressed by the larger values of $\mathcal{R}$. Therefore, in Eq. 6.13 we can neglect the $F(\mathcal{R})\mathcal{R}$ term. Then, from Eq. 6.8, we note that $f(\mathcal{R})$ will be dominated by $\Lambda_\star$. Since this parameter is determined from imposing a flat cosmology, $\Lambda_\star \approx -2\Lambda$, where $\Lambda \approx 2.1H_0^2$ is the actual cosmological constant. In

light of these arguments, Eq. 6.13 becomes

$$q \approx -\frac{2\Lambda}{3H_0^2} - \frac{\Omega_{\rm m}}{2} + 1 \approx -0.55. \tag{6.14}$$

We verify in Fig. 6.1 that our prediction matches remarkably well the numerical values of obtained for q today for different parameters of the exponential model. Hence, we conclude that this model should always predict an accelerated expansion today.

6.2.2 The quadratic model

The second model we introduce is the quadratic model, which we define by the function

$$f(\mathcal{R}) = \Lambda_\star \left(1 + \mathcal{R}^2/\mathcal{R}_\star^2\right), \tag{6.15}$$

where $\Lambda_\star$ and $\mathcal{R}_\star$ are a negative and positive constant of order H_0^2, just like in the previous model.

Computing the indefinite integral defined in Eq. (6.7) one can find the effective potential associated to this model:

$$V(\mathcal{R}) = -\frac{1}{3}\Lambda_\star \mathcal{R}^2 - \frac{1}{9}\mathcal{R}^3, \tag{6.16}$$

which clearly has a global minimum at $\mathcal{R} = 0$ and a maximum at $\mathcal{R} = 2\Lambda_\star$. Therefore, we expect the solution for $\mathcal{R}$ to asymptotically settle at the minimum in vacuum, leading to an effective cosmological constant value of

$$\Lambda_{\rm eff} \equiv \frac{1}{2}\left[-2\Lambda_\star f_{\mathcal{R}}(0) - 2f(0)\right] = -\Lambda_\star. \tag{6.17}$$

In Fig. 6.2, we can see the evolution predicted by the quadratic model for H, compared to ΛCDM's, for different values of $f_{\mathcal{R}}(z_{\rm i})$ and $\mathcal{R}_\star$. We have chosen a negative $f_{\mathcal{R}}(z_{\rm i})$ as this sets the initial $\mathcal{R}$ to be positive.

In Fig. 6.2 we observe that $\mathcal{R}$ rolls down the effective potential towards the minimum from the beginning of the evolution, asymptotically settling there. When compared to the behavior seen for the exponential model in Fig. 6.1, the different dynamics are linked to the ratio $f_{\mathcal{R}}/f_{\mathcal{R}\mathcal{R}}$ multiplying the stress–energy tensor in the dynamical equation for $\mathcal{R}$. For this particular setting of

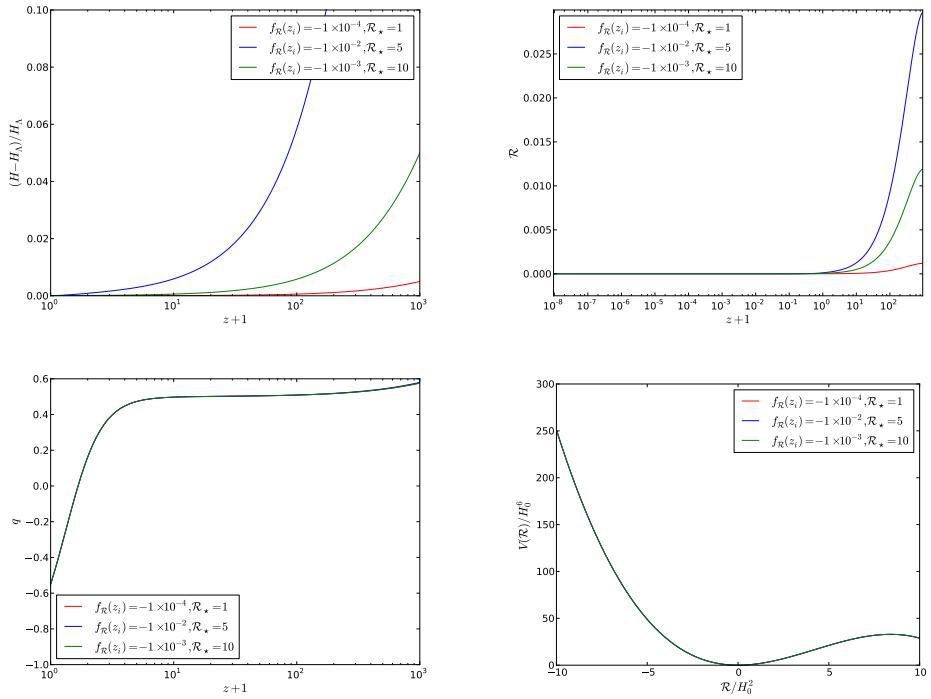

Figure 6.2 *The same as Fig. 6.1 for the quadratic $f(\mathcal{R})$ model. We have again fixed $\Omega_{\rm m} = 0.30$.*

the quadratic model, this ratio is positive at early times, meaning that $\mathcal{R}$ will be pulled down by the matter energy density term towards the minimum of the potential, asymptotically settling there when the matter contribution becomes negligible. Had we chosen $\mathcal{R}(z_{\rm i})$ to be positive instead, the behavior wouldn't qualitatively change, with the matter term dictating $\mathcal{R}$ to evolve towards the minimum in a symmetric manner, starting from $\mathcal{R} < 0$.

Also, note that by setting the initial conditions for $f_{\mathcal{R}}(z_{\rm i})$ such that deviations from standard GR are kept small, $\mathcal{R}$ starts its evolution already close to the minimum, guaranteeing that it settles onto the minimum of the effective potential $V(\mathcal{R})$. Had we started the evolution such that the initial value of $\mathcal{R}$ would be beyond the maximum observed for the effective potential in Fig. 6.2, $\mathcal{R}$ would roll indefinitely, jeopardizing the late-time achievement of an effective cosmological constant in this model.

Lastly, we have the evolution of the deceleration parameter q in Fig. 6.2 predicted by this model. We observe that, close to the present, $f(\mathcal{R})$ will be dominated by $\Lambda_\star$ as can be seen in Eq. 6.15, since $\mathcal{R}$ is tending to the minimum of the potential $V(\mathcal{R})$ located at zero. Hence, the analysis of the parameter q in Sec. 6.2.1 applies

in this case as well. Therefore, this model should always predict an accelerating Universe today.

6.3 Background constraints

6.3.1 Observables

I would like to state that this subsection was written by Vanessa Smer-Barreto.

To constrain our models parameters, we perform a Metropolis-Hastings analysis using several background-related observables: the luminosity distance from Supernova type Ia (SNIa); the baryon acoustic oscillations (BAO); the shift parameter, acoustic scale and redshift of decoupling from the cosmic microwave background.

SNIa luminosity–redshift relation

For the supernovae analysis, the luminosity distance, $d_{\rm L}$, is of the most relevance, and is given by

$$d_{\rm L}(z,\Theta) = c(1+z)\int_0^z \frac{dz'}{H(z',\Theta)}, \tag{6.18}$$

where c is the speed of light, and Θ holds the parameters of the model we are trying to constrain and the cosmology dependence of $d_{\rm L}$.

The expected distance moduli, m, of the i-th supernovae located at redshift $z_{\rm i}$ is given by

$$\mu^{\rm ex} \equiv m(z_{\rm i}) - M = 5\log_{10}\left[\frac{d_{\rm L}(z_{\rm d},\Theta)}{\rm Mpc}\right] + 25, \tag{6.19}$$

where m and M are the apparent and absolute magnitudes of the SNIa, respectively. Hence, one then obtains the statistical $\chi^2_{\rm SNIa}$ as

$$\chi^2_{\rm SNIa} \equiv \sum_{i=0}^{N_{\rm SNIa}} \frac{\left(\mu^{\rm ex}(z_{\rm i},\Theta) - \mu^{\rm obs}(z_{\rm i})\right)}{\sigma_{\rm i}}, \tag{6.20}$$

where $\mu^{\rm obs}(z_{\rm i})$ is the observationally measured distance moduli of the i-th supernovae and $\sigma_{\rm i}$ is the associated variance, and the sum is over all the available supernova in the data set.

In this work, we have used the Union 2.1 SNIa catalog from the "Supernova Cosmology Project" (SCP) [230]. This data set is a compilation of 580 type Ia Supernovae located over the redshift interval $0.623 < z < 1.415$. In our Metropolis-Hastings analysis, we have marginalized over the nuisance parameter H_0 using the procedure described in the appendix of Ref. [231].

Baryon acoustic oscillations peak

Baryon acoustic oscillations are found in the clustering of galaxy samples, showing as a peak in the two-point correlation function at a comoving separation, $r_{\rm s}$, equal to the sound horizon at the drag epoch, $z_{\rm d}$, when baryons were released from photons. $z_{\rm d}$ can be estimated using a fitting formula [232]

$$z_{\rm d} = \frac{1291\left(\Omega_{\rm m}\right)^{-0.419}}{1+0.659\left(\Omega_{\rm m}\right)^{0.828}}\left[1+b_1\left(\Omega_{\rm b}\right)^{b_2}\right], \tag{6.21}$$

where $\Omega_{\rm m} = \Omega_{\rm DM} + \Omega_{\rm b}$ is the sum of the present day energy densities of Dark Matter and Baryons; b_1 and b_2 are two fitting parameters, given by

$$b_1 = 0.313\left(\Omega_{\rm m}\right)^{-0.419}\left[1+0.607\left(\Omega_{\rm m}\right)^{0.674}\right], \tag{6.22}$$

$$b_2 = 0.238\left(\Omega_{\rm m}\right)^{0.223}. \tag{6.23}$$

The comoving sound horizon at the baryon drag epoch $r_{\rm s}$, which defines the scale of characteristic signatures of BAO on the large scale structure (as discussed in Sec. 1.4), can be determined by

$$r_{\rm s}\left(z,\Theta\right) = \frac{1}{\sqrt{3}}\int_0^{a(z)} \frac{dz'}{H\left(z',\Theta\right)\sqrt{1+\frac{3\rho_{\rm b}}{4\rho_\gamma}}}, \tag{6.24}$$

where $a(z) = 1/\left(1+z\right)$ and $\rho_{\rm b}$ and ρ_γ are, respectively, the baryon and photon energy density. We approximate the ratio between their densities as

$$\frac{3}{4}\frac{\rho_{\rm b}}{\rho_\gamma} \approx \frac{31500}{1+z}\Omega_{\rm b}h^2\left(\frac{T_{\rm CMB}}{2.7{\rm K}}\right)^{-4}, \tag{6.25}$$

where $h \equiv H_0/100$. In our calculations, we have assumed $T_{\rm CMB} = 2.7255$K. Lastly, since the comoving sound horizon calculation is very sensitive to early time effects, we have to consider the effect of radiation. We define its present-day

energy density, $\Omega_{\rm r}$, as

$$\Omega_{\rm r} = \frac{\Omega_{\rm m}}{1+z_{\rm eq}}, \tag{6.26}$$

where $z_{\rm eq}$ is the redshift at matter-radiation equality, which we approximate by

$$z_{\rm eq} \approx 25000\,\Omega_{\rm m}h^2\left(\frac{T_{\rm CMB}}{2.7{\rm K}}\right)^{-4}. \tag{6.27}$$

The peak position is dependent on the ratio of the distance measure, D_v, and the sound horizon at the drag epoch, $r_{\rm s}$. Since the latter is tightly constrained from CMB measurements, the observation of the BAO scales act as a standard ruler, allowing one to constrain the form of $D_{\rm v}$, which is determined by [232]

$$D_{\rm v}\left(z,\Theta\right) = \left[\left(\int_0^z \frac{dz'}{H\left(z',\Theta\right)}\right)^2 \frac{z}{H\left(z,\Theta\right)}\right]. \tag{6.28}$$

Hence, the expected distance ratio at redshift z is simply given by

$$d_z^{\rm ex}(\Theta) = \frac{r_{\rm s}(z_{\rm d},\Theta)}{D_{\rm v}\left(z,\Theta\right)}. \tag{6.29}$$

Therefore, having the observed $d_{\rm z}$, one can easily compute the BAO χ^2 as

$$\chi^2_{\rm BAO} = \left(d^{\rm ex}_{z_{\rm i}} - d^{\rm obs}_{\rm i}\right)^t \left(C^{-1}_{\rm BAO}\right)_{ij} \left(d^{\rm ex}_{z_{\rm j}} - d^{\rm obs}_{\rm j}\right), \tag{6.30}$$

where $\left(d^{\rm ex}_{z_{\rm i}}\left(\Theta\right) - d^{\rm obs}_{\rm i}\right)$ is the vector of the difference between the expected and theoretical values for $d_{z_{\rm i}}$, while $C_{\rm BAO}$ is the covariance matrix associated to the observations. Following the Planck analysis [233], we have used BAO observations from the 6dF Galaxy Redshift Survey (6dFGRS) at low redshift, $d^{\rm obs}(z=0.106) = 0.336 \pm 0.015$ [77], from the Luminous Red Galaxies (LRG) sample of the Sloan Digital Sky Survey (SDSS) 7-year data release at the median redshift, $d^{\rm obs}(z=0.35) = 0.1126 \pm 0.0022$ [234], and the BAO signal from BOSS CMASS DR9, $d^{\rm obs}(z=0.57) = 0.0732 \pm 0.0012$ [78]. We have considered a diagonal covariance matrix, therefore neglecting any possible correlations between the different measurements that were used.

Table 6.1 *Inverse covariance matrix for the distance information obtained from Planck in the ΛCDM framework.*

Planck				
	Best fit	$l_A(z_*)$	$R(z_*)$	z_*
$l_A(z_*)$	301.77	44.077	−383.927	−1.941
$R(z_*)$	1.7477	−383.927	48976.330	−630.791
z_*	1090.25	−1.941	−630.791	12.592

Cosmic microwave background

In this work, we use the cosmic microwave background distance information, including the the acoustic scale l_A, the "shift parameter" R, and the redshift at photon-decoupling $z_\star$. The first is a measurement of the ratio of the angular diameter distance to the photon-decoupling surface over the comoving sound horizon at decoupling [235]

$$l_A(z_\star) \equiv (1+z_\star)\,\frac{\pi D_A(z_\star)}{r_{\rm s}(z_\star)}, \tag{6.31}$$

where

$$D_A(z) = \frac{1}{1+z}\int_0^z \frac{dz'}{H(z')} \tag{6.32}$$

is the proper angular–diameter distance; $r_{\rm s}(z_\star)$ can be calculated using Eq. (6.24).

On the other hand, R is a measurement of the angular diameter distance at $z_\star$, and is given by [235]

$$R = \sqrt{\Omega_{\rm m} H_0^2}\,(1+z_\star)\,D_A(z_\star), \tag{6.33}$$

where $\Omega_{\rm m}$ is the present-day density of matter, as defined before. Lastly, the redshift at photon-decoupling can be estimated by the fitting formula [236]

$$z_\star = 1048\left[1+0.00124\left(\Omega_{\rm b}h^2\right)^{-0.738}\right]\left[1+g_1\left(\Omega_{\rm m}h^2\right)^{g2}\right], \tag{6.34}$$

where

$$g_1 = \frac{0.0783\left(\Omega_{\rm b}h^2\right)^{-0.238}}{1+39.5\left(\Omega_{\rm b}h^2\right)^{0.763}} \tag{6.35}$$

$$g_2 = \frac{0.560}{1+21.1\left(\Omega_{\rm b}h^2\right)^{1.81}}. \tag{6.36}$$

As usual, we compute the CMB distance χ^2 as follows

$$\chi^2_{\rm CMB} = \left(x_i^{\rm exp} - x_i^{\rm obs}\right)^t \left(C^{-1}\right)_{ij} \left(x_j^{\rm exp} - x_j^{\rm obs}\right), \tag{6.37}$$

where the vector $\left(x_i^{\rm exp}\left(\Theta\right) - x_i^{\rm obs}\right)$ measures the difference between the theoretical expectations and the observed values for the different quantities in analysis. In this work, we use the Planck distance information for the ΛCDM model to constrain our models. In table 6.1 it is possible to see the inverse covariance matrix and best-fit values obtained from Planck [237].

6.3.2 Metropolis - Hastings algorithm

I would like to state that part of this subsection was written by Vanessa Smer-Barreto.

Having described the procedure to calculate the χ^2 of each observable we consider in the previous section, we continue towards the calculation of the confidence contours by means of a Metropolis–Hastings algorithm, which is a Markov Chain Monte Carlo method based on a stochastic sampling technique [238]. The Metropolis-Hastings algorithm provides a method for sampling from some generic distribution, $P(x)$, and is particularly useful when the specific form of the distribution $P(x)$ is not known or depends on many parameters (i.e. is a multidimensional problem).

The idea is to define a Markov chain over possible x values (denoted x_1, x_2...x_n), in such a way that the stationary distribution of the Markov chain is in fact $P(x)$ as $n \to \infty$. The method is defined by an *acceptance/rejection* step. Suppose that the current state of the Markov chain is x_n, and we want to generate the x_{n+1} element. First, one generates an element $x^\star$ from a proposal distribution $Q(x^\star|x_n)$ that depends on the previous element (such as a Gaussian centered on x_n, for instance). Then, one computes the acceptance probability

$$A(x^\star \to x_n) = \min\left(1, \frac{\rm P(x^\star)}{\rm P(x_n)} \times \frac{\rm Q(x_n|x^\star)}{\rm Q(x^\star|x_n)}\right). \tag{6.38}$$

In a χ^2 analysis, $P(x) \propto e^{-\chi(x)^2}$. Hence, the ratio $P(x^\star)/P(x_n)$ will simply be given by $e^{\chi^2(x_n)-\chi^2(x^\star)}$. Also, if the proposal function is symmetric, the $\frac{Q(x_n|x^\star)}{Q(x^\star|x_n)}$ term will be equal to unity.

Lastly, all is left is to either accept or reject the candidate $x^\star$. To make this decision, a uniformly distributed random number is generated between 0 and 1 denoted u. The x_{n+1} element will be $x^\star$ if $A(x^\star \to x_n) \geq u$ or will remain x_n otherwise.

Another advantages of the Metropolis–Hastings algorithm is its treatment of marginalized variables. When considering a subset of the parameters that form a chain, the marginalization over the remainder of the parameters occurs immediately, therefore making the treatment of the chains a simple process.

6.3.3 Priors

I would like to state that this particular subsection was written by Vanessa Smer-Barreto.

In this section we discuss the range of variation of the parameters we use in our models, which are the flat priors we have chosen to impose over them. Our two $f(\mathcal{R})$ models have a set of three parameters they share. These are the present-day relative energy densities of matter and baryons, $\Omega_{\rm m}$ and $\Omega_{\rm b}$, and the present-day value of the Hubble parameter, H_0. The ranges we have chosen for them are, respectively, $[0.01, 0.99]$, $[0.001, 0.080]$ and $[40.0, 100.0]$.

Also for both models, $\Lambda_\star$ is determined by the background evolution, assuming we recover a flat cosmology today, at $a = 1$. As described in Sec. 6.2.1, this is achieved using a Brent algorithm (see [229]) which ensures that the present-day value of the numerical Hubble parameter we obtain coincides with H_0. We start our background evolution at a redshift of $z_i \approx 1 \times 10^8$, and neglect any relativistic effects. Hence, we take the equation of state for matter to be zero throughout, i.e. $\rho_{\rm m} \propto a^{-3}$.

For the exponential model, we study two situations. In the first case, we choose to keep $f_\mathcal{R}$ at $z_{\rm i}$ fixed to a very small value, 10^{-4}, and let $\mathcal{R}_\star$ vary between $[1.0, 10.0]$. We do so to test the data against a definitive modification of gravity where the ΛCDM limit is not explicitly attainable.

In the second case, we let $f_\mathcal{R}(z_{\rm i})$ vary between $[1 \times 10^{-6}, 0.1]$ and $\mathcal{R}_\star$ between $[0.01, 15.0]$. We can not consider $f_\mathcal{R}(z_{\rm i}) = 0$ due to the way we set the initial conditions in this model, as this would lead to a logarithmic divergence. Therefore, we can not set the deviations from standard GR plus ΛCDM at early

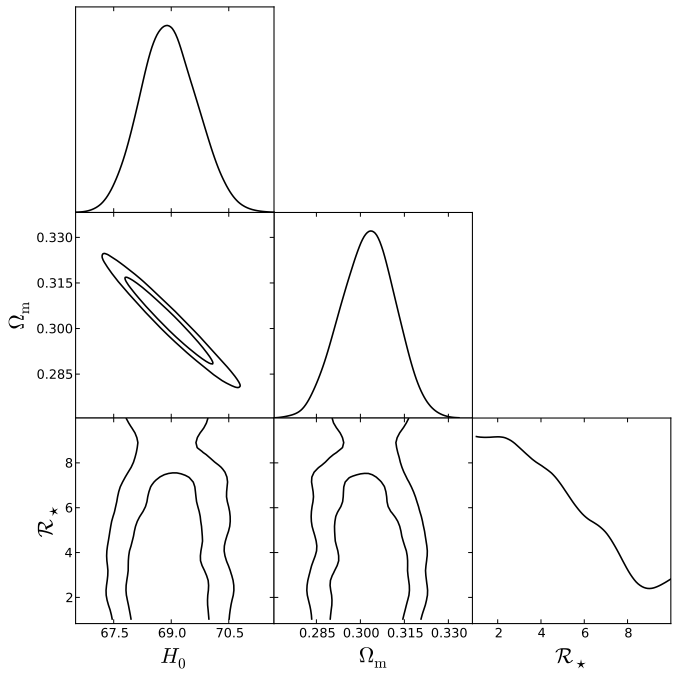

Figure 6.3 *The 2-d contours of the combined constraints from the background surveys we consider for the exponential $f(\mathcal{R})$ model with $f_{\mathcal{R}}(z_{\rm i})$ fixed to 10^{-4}. We also plot the individual marginalized posterior probability distributions of each parameter.*

times to zero, but only asymptotically minimize them by taking $f_{\mathcal{R}}(z_i) \to 0^+$. Nevertheless, we can test how large a deviation should be possible by considering an upper limit for $f_{\mathcal{R}}(z_{\rm i})$ of order 1×10^{-1}.

Lastly, for the quadratic model, we fix $\mathcal{R}_\star$ to a chosen value and let $f_{\mathcal{R}}$ at z_i vary between $[-0.1, 0.1]$. We chose to fix $\mathcal{R}_\star$ since the effective potential on which $\mathcal{R}$ evolves is independent of $\mathcal{R}_\star$ in the quadratic model, as seen in Eq. (6.16).

6.3.4 Results

In this section, we present the marginalized 2-d contours for the posterior probabilities distributions of our parameters which were calculated using a Metropolis-Hastings algorithm, as described in Sec. 6.3.2. The plots shown here exhibit the combined constraints of the three background surveys we described in Sec. 6.3.1. These plots were done using the plotting functions available in CosmoMC [210].

In Fig. 6.3 we have a triangular plot with the 2-d contours between H_0, $\Omega_{\rm m}$ and

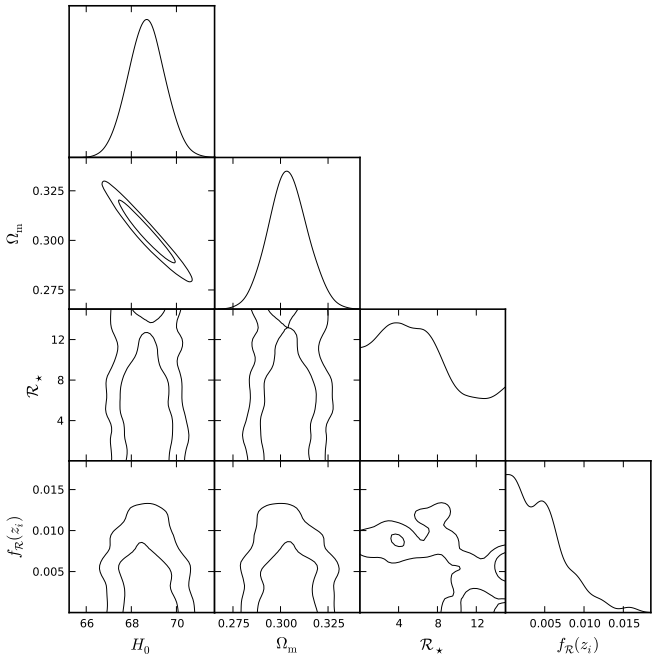

Figure 6.4 *The 2-d contours of the combined constraints from the background surveys we consider for the exponential $f(\mathcal{R})$ model by considering a prior range for $f_{\mathcal{R}}(z_{\rm i})$ between $[1 \times 10^{-6}, 0.1]$. We also plot the individual marginalized posterior probability distributions of each parameter.*

$\mathcal{R}_\star$, as well with the individualized posterior distributions of each parameter for the exponential model considering $f_{\mathcal{R}}(z_{\rm i})$ fixed to 10^{-4}. We obtain a slightly higher value of H_0 than the recent Planck result [233], but we do not perform such a complete analysis, limiting ourselves to background observables. We also observe a smaller $\Omega_{\rm m}$ value than in [233], which results from the combination of the different surveys we have considered, as the Union2.1 and BAO surveys do tend to prefer a slightly smaller $\Omega_{\rm m}$ value than Planck [230, 233]. The 1-σ limits on these parameters are $H_0 = 68.9 \pm 0.7$ and $\Omega_{\rm m} = 0.303 \pm 0.009$.

For the $\mathcal{R}_\star$ parameter we cannot clearly state the confidence limits, as these are completely prior determined. Interestingly, we do observe a preference towards smaller values of $\mathcal{R}_\star$, possibly extending all the way to 0 had we considered that limit. We set our initial conditions by imposing an initial $f_{\mathcal{R}}$ value at the starting redshift $z_{\rm i}$ that we invert to obtain the corresponding $\mathcal{R}_{\rm i}$. Hence, for this model, $\mathcal{R}_{\rm i} = -\mathcal{R}_\star \ln\left[-f_{\mathcal{R}}(z_{\rm i})\mathcal{R}_\star/\Lambda_\star\right]$. Therefore, we cannot have a pure GR plus ΛCDM for the exponential model because neither $f_{\mathcal{R}}(z_{\rm i})$ or $\mathcal{R}_\star$ can be set exactly to zero. However, the closest this model can get to ΛCDM, for a fixed $f_{\mathcal{R}}(z_{\rm i})$, is

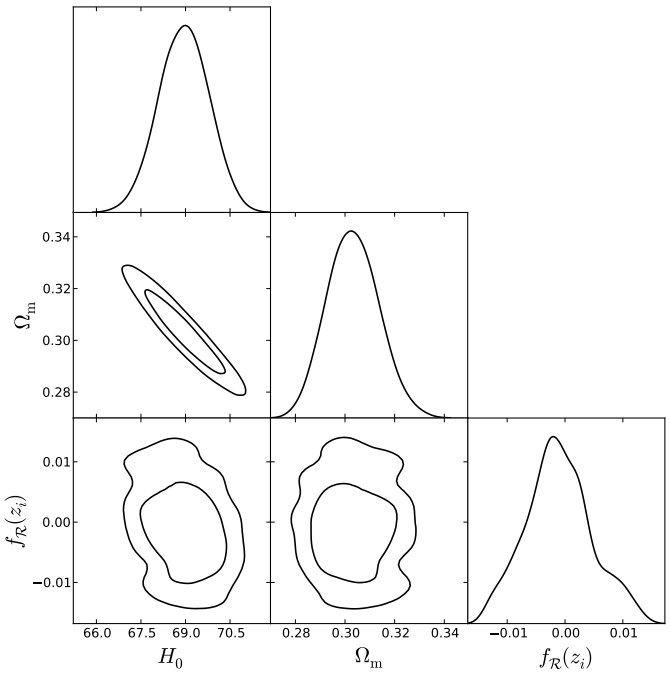

Figure 6.5 *Similar as Figs. 6.3 and 6.4 for the quadratic $f(\mathcal{R})$ model.*

when $\mathcal{R}_\star \to 0^+$: in this limit, we observe that $\mathcal{R}_{\rm i}$ tends to decreasingly smaller values as $\mathcal{R}_\star \to 0^+$, while keeping the $\mathcal{R}/\mathcal{R}_\star$ ratio considerably large such that $f(\mathcal{R}) \to \Lambda_\star$. Hence, we recover an almost ΛCDM like evolution, which can be understood looking at the trace equation, Eq. (4.5), which tends increasingly closer to the GR plus ΛCDM limit of $R + \kappa^2 T = 4\Lambda$.

Fig. 6.4 presents the combined constraints on the exponential model considering the flat prior on $f_{\mathcal{R}}(z_{\rm i})$ between $[1 \times 10^{-6}, 0.1]$. We can observe a clear upper limit on $f_{\mathcal{R}}(z_{\rm i})$ of around 10^{-2}, limiting, therefore, the maximum deviation from the actual gravitational constant G we can have at early times. However, now $\mathcal{R}_\star$ appears even more unconstrained by the data, as larger values of $\mathcal{R}_\star$ are also allowed since these can be compensated by the $f_{\mathcal{R}}(z_{\rm i}) \to 0^+$ values: this limit pushes the model closer to the standard GR plus ΛCDM limit even for large values of $\mathcal{R}_\star$. We reinforce that we can not set the deviation from standard GR exactly to zero because that would lead to a logarithmic divergence in the initial conditions of this model. However, the lower limit we have chosen for the $f_{\mathcal{R}}(z_{\rm i})$ prior is much smaller than the current precision with which one can measure early deviations from the gravitational constant [239, 240].

Lastly, in Fig. 6.5 we have the triangular plot with the confidence contours and 1-d marginalized posterior probability distributions for the $f(\mathcal{R})$ quadratic model.

We obtain very similar results for the standard cosmological parameters H_0 and $\Omega_{\rm m}$ as those observed in the exponential model in both situations, with the 1-σ limits on them being $H_0 = 68.9 \pm 0.8$ and $\Omega_{\rm m} = 0.303 \pm 0.010$.

For the quadratic model, we chose to keep $\mathcal{R}_\star$ fixed because it would not have a significant impact on the background evolution predicted by this model since it does not alter the shape of the potential on which $\mathcal{R}$ evolves. Hence, the third parameter we show constraints for is the initial value we impose for $f_\mathcal{R}$ at the starting redshift, $z_{\rm i}$. This, as detailed before, sets the maximum deviation from the standard gravitational constant G one can have at early times in this model, since $f_\mathcal{R}$ evolves asymptotically to 0 from its starting value.

It is clear that as $f_\mathcal{R}(z_{\rm i}) \to 0$ we get closer to a ΛCDM like evolution. Given it would be numerically hard to evolve the model if $f_\mathcal{R}(z_{\rm i}) = 0$, we made the approximation that, if the Metropolis–Hastings algorithm encountered such a value, we would have an exact ΛCDM background evolution. The results we have obtained show a preference for a standard GR plus ΛCDM scenario, as can be seen in the 1-d posterior probability distribution for $f_\mathcal{R}(z_{\rm i})$ in Fig. 6.5. The corresponding 1-σ confidence limits are $f_\mathcal{R}(z_{\rm i}) = -0.001 \pm 0.006$. We also observe a symmetry on the posterior distribution of this parameter, which could be expected given that the evolution of $\mathcal{R}$ is symmetric under the change of sign of $f_\mathcal{R}$ for, as discussed in Sec. 6.2.2.

6.4 Discussion

In this work, we explored a way to obtain the background evolution for two different models of the novel hybrid metric-Palatini theory of gravity. We re-wrote the dynamical equation for the additional degree of freedom introduced by this theory as a dynamical equation for the actual Palatini Ricci scalar $\mathcal{R}$. We define the initial conditions by imposing the deviation one has from standard GR at early times. Hence, we set a small value for $f_\mathcal{R}(z_{\rm i})$ and invert the latter to obtain $\mathcal{R}(z_{\rm i})$, while keeping $\dot{\mathcal{R}}(z_{\rm i}) = 0$.

We define an effective potential $V(\mathcal{R})$ where the Palatini Ricci scalar evolves and, if a minimum exists, $\mathcal{R}$ should asymptotically settle there in vacuum, so that one recovers standard GR plus an effective cosmological constant at late times. $V(\mathcal{R})$ could potentially have a complicated form. However, for the models we introduce

here, that is not the case.

We present the exponential and quadratic $f(\mathcal{R})$ models and show that the background evolution predicted by them does not deviate much from ΛCDM. This could be different, of course, had we decided to set the deviation from the gravitational constant G in the high-redshift regime to be large. Also, we explicitly show the effective potential $V(\mathcal{R})$ for both models and $\mathcal{R}$ asymptotically tending to its minimum at late times. This is less obvious in the exponential model as the matter term in Eq. (6.5) initially drives the Palatini Ricci scalar up the potential, only for it to later slowly fall down towards the minimum due to the potential slope.

We also study and present the evolution of the deceleration parameter q for our models. We verify, numerically, that they predict an accelerated expansion today for different values of their parameters. Furthermore, we perform a simple analytical analysis of q and conclude that our models yield a present-day value for it around $-1/2$, meaning they are suitable candidates for producing cosmological acceleration today.

We then use background CMB, BAO and Supernovae data to constrain the models. Keeping $f_{\mathcal{R}}(z_{\rm i})$ fixed to 10^{-4} for the exponential model, we cannot state an actual constraint on the $\mathcal{R}_\star$ parameter. However, we do note how the data, as expected, seems to tend towards the ΛCDM limit. We believe that, had we not chosen to restrict the prior range in order to have a definitive modification of gravity without the ΛCDM limit, we would see the lower range of our confidence contours in Fig. 6.3 tending to 0^+ in $\mathcal{R}_\star$.

Still for the exponential model, when we impose a flat prior on $f_{\mathcal{R}}(z_{\rm i})$ between $[1 \times 10^{-6}, 0.1]$ we observe a clear upper limit of order 10^{-2}. This value marks the maximum deviation one can have at early times from the actual gravitational constant G. Also, the data exhibits a marked tendency towards the lower limit of $f_{\mathcal{R}}(z_{\rm i})$, as $f_{\mathcal{R}}(z_{\rm i}) \to 0^+$ minimizes the early time deviations from the gravitational constant G, allowing the model to get asymptotically closer to the standard GR+ΛCDM limit.

For the quadratic model, we constrained the initial value of $f_{\mathcal{R}}$ while keeping $\mathcal{R}_\star$ fixed which means that, effectively, we are again constraining the maximum deviation one has from the gravitational constant at early times. As expected, the results indicate a preference towards no deviation at all, as in the standard GR plus Λ limit. We obtain $f_{\mathcal{R}}(z_{\rm i}) = -0.001 \pm 0.006$ as the confidence limits for

our parameter.

Hence, we see in this work that $f_{\mathcal{R}}(z_{\rm i})$ could play an important role in the constraining of this theory, as it sets the deviation one observes from standard GR at early times. The background data we have used permits a deviation around 1% from the actual gravitational constant G at early times, which is within constraints on $G_{\rm eff}/G$ coming from BBN and CMB data [239, 240].

This, combined with the fact that the Newtonian potentials also exhibit a departing behavior from ΛCDM at early times [3], suggests that it would be very interesting to constrain these models using the latest Planck data available by enhancing the formalism developed so far with the inclusion of perturbation observables.

Chapter 7

Conclusions

In this thesis we have looked into several scalar-tensor theories of gravity that introduce an additional degree of freedom in the gravitational action. All of the considered theories can be embedded in the generalized Horndeski action of scalar-tensor gravity theories that produce at most second order field equations [65].

It has been recently shown that self-accelerating theories, where the acceleration is driven by the actual modifications of gravity and not by a cosmological constant or dark energy contribution in the matter sector, originating from the Horndeski action can not be viable alternatives to ΛCDM as an explanation to cosmic acceleration [69]. Hence, in this work, we focus on the effects that the modifications to the gravitational sector of Einstein's field equations have over the large scale structure of the Universe, not worrying if these can genuinely produce cosmic acceleration on their own.

We start by looking into one of the first ever scalar-tensor modifications of gravity, the Brans-Dicke (BD) theory [117] in Chapter 2. We were able to apply a designer method in order to produce solutions of the BD scalar field that respect its well known attractor solutions in the matter dominated regime. This is achieved by fixing the background evolution to an effective wCDM cosmology with a dark energy equation of state $w_{\text{eff}} \geq -1$. The value of w_{eff} also parametrizes the scalar field potential $V(\phi)$, which is a simple constant for $w_{\text{eff}} = -1$. Hence, the ΛCDM background evolution is recovered for a Brans-Dicke parameter $\omega_{\text{BD}} \to \infty$ and $w_{\text{eff}} = -1$.

It has been long known that the BD theory modifies the ratio between the Newtonian potentials $\gamma \equiv \Phi/\Psi$, and also the quotient of the effective gravitational constant to its Newtonian value $G_{\rm eff}/G_{\rm N} \equiv \mu \equiv \xi$. This happens for modes of the perturbations that are well within the Hubble radius, i.e. such that the condition $k^2/a^2 \ll H^2$, which corresponds to subhorizon modes. Using analytic solutions we have obtained for the evolution of the BD scalar field, we were able to simplify the known expressions for γ and μ [144]. In particular, we were able to show that the effective mass parameter entering these expression could be neglected.

Hence, we have shown that γ does effectively remain constant and depends only on the Brans-Dicke parameter, while μ will depend mostly on the behavior of the term $1/\phi$. In the end, we obtained very simple and elegant solutions for the late-time evolution of μ, which grows toward larger deviations in the past. We have also shown that obtaining cosmological constraints on the BD parameter that are competitive with Solar system ones is an extraordinary challenge as it would require γ and μ to be measured to a precision of around 10^{-4}. However, since there could be a cumulative effect from measuring both of these quantities [146, 147], constraints on the growth rate (or weak lensing) of order 10^{-3} or even 10^{-2} might be sufficient to place competitive constraints on $\omega_{\rm BD}$.

Then, in Chapter 3, we studied the evolution of linear perturbations in what is possibly the most commonly considered modification of gravity, the metric $f(R)$ theory, where one modifies the gravitational action by introducing a function of the metric Ricci scalar R. Even though the behavior of the gravitational potentials had been analyzed before, this was usually focused on a single model and restricted its background evolution to that of ΛCDM using a designer approach. In this particular work, we extended the analysis to three viable and well known $f(R)$ models without fixing their background evolution.

With the numerical approach used in this chapter we were able to obtain the evolution of the Newtonian potentials from matter domination without running into divergence issues related to the rapidly oscillatory evolution of $w_{\rm eff}$ at high-redshifts that is common in $f(R)$ theories. This allowed a detailed comparison of the evolution of the lensing potential Φ_+ between the Starobinsky, Hu-Sawicki and exponential $f(R)$ models, as well as the behavior of the dynamical slip existent between Φ and Ψ, which is a clear departure from standard GR. Adopting limits on the models that were outside and on the limit of their viability according to existing constraints, we were able to show the clear effect that the evolution of the effective mass of the scalar field has on the linear potentials, as this sets

the range of action of the additional fifth force and thus the moment when the different scales enter it and are enhanced.

Lastly, we also adopted the designer method to study the evolution of the gravitational potentials in a model that had a background evolution indistinguishable from ΛCDM, but obeyed the strictest constraints existent on $f(R)$ theories from galactic and Solar system constraints that place an upper bound on the present-day value of $|f_{R0}| \approx 10^{-6}$. This allowed us to conclude that under these constraints the modifications from standard GR+ΛCDM are marginal and not even future weak lensing surveys like Euclid would be able to separate the theories. And, even though there are some questions on the validity of the linear approach on the smallest scales in $f(R)$ theories, the additional non-linearity of the $f(R)$ equations would even suppress more any additional modifications, according to simulations [191].

We then turn to the model that granted most attention in this thesis, the novel hybrid metric-Palatini theory [192, 193]. In this theory, you add to the metric Ricci scalar in the Einstein-Hilbert action a function of the Palatini Ricci scalar, $f(\mathcal{R})$. This hybrid theory shares some of the good properties of the pure Palatini theory while avoiding some of its known instabilities. Not only that, it has been shown that the additional scalar degree of freedom introduced by this theory need not to be massive in order to suppress the additional fifth-force. Hence, this theory can naturally avoid the tight Solar system tests as long as the background value of the scalar field is much smaller than unity. In Chapter 4 we studied the dynamics of linear perturbations in the hybrid theory, deriving the full set of linearized Einstein equations in both the Newtonian and conformal gauges and predicting their numerical evolution for a specific model from deep within matter domination.

In this chapter we introduced a designer model that matches the background evolution of ΛCDM exactly by solving a second order differential equation for the scalar field that arises from setting the effective dark energy equation of state $w_{\text{eff}} = -1$. This method allows for a consistent set of initial conditions at a high-redshift $z \approx 1000$ dependent on two parameters that define a family of solutions $f(\mathcal{R})$ matching the imposed background evolution. The scalar field always starts at a non-zero value in the high curvature regime and decays toward zero as we approach the present, ensuring its viability on Solar system scales.

We then use this model to obtain the numerical evolution of the lensing potential

Φ_+ and the slip between the gravitational potentials χ. Similarly to many modified gravity models, the latter is a dynamical quantity and quickly manifests as a clear modification from standard General Relativity. For the designer model we use we note that the modifications are larger in the past and are quickly damped toward the present. Even though the slip χ oscillates, the amplitude of its oscillations are not strong enough to manifest on the lensing potential. Nevertheless, we do note that the ratio between the gravitational potentials oscillates at high-redshifts, in what is a clear signature of this theory.

Following the work done in Chapter 4, we use the designer hybrid metric-Palatini model as the toy model adopted in Chapter 5 to study early time modifications of gravity. This model introduces a modification of gravity at high-redshift that decays toward the present, while yielding a background evolution that is indistinguishable from ΛCDM and having any possible modifications on the smallest scales suppressed. Hence, it is the perfect candidate to separate background from perturbations effects and thus study how modifications of gravity introduced after recombination can affect the cosmological observables we have such as the CMB temperature power spectrum. This also allows us to put quantitative constraints on these modifications using currently available data.

In order to perform this analysis we use the publicly available MGCAMB [241] code that parametrizes modifications on the linear perturbations using two functions of time and scale, μ and γ, that enter the modified Poisson equation and define the ratio between the Newtonian potentials, respectively. To mimic the oscillatory behavior observed in this theory for the ratio between the gravitational potentials at high-redshift, we develop an analytic approximation to describe the evolution of the slip between the potentials. We use this to extend the quasi-static subhorizon form of μ and γ (which we also derive for the $f(\mathcal{R})$ theory) to work in the high curvature regime.

We conclude that the constraints we obtain depend on the redshift at which we introduce the modifications, being better at the highest redshift we consider since it has the strongest changes: we obtain a constraint on the value of $|f_{\mathcal{R}}(z = 1000)| \approx 1 \times 10^{-2}$. This constraint can be attributed to noticeable effects on the CMB power spectrum. We are able to observe a substantial shift in the Sachs-Wolfe plateau due to a modification of the Newtonian potential at a time close to recombination. There is also a significant suppression of the first peak due to complementary variation of the gravitational potentials close to the epoch of recombination that, together with the non-negligible presence of radiation,

contributes to an early integrated Sachs-Wolfe eect that can alter the amplitude and position of the peaks. Smaller contributions to the constraints can be attributed to CMB lensing which is sensitive to the percent-level modifications we observe at high ℓ. Finally, we find that future 21 cm survey data will significantly improve upon the CMB constraints, whereas using gravitational wave events as standard sirens will not provide competitive bounds.

Lastly, in Chapter 6, we introduce two different models of the hybrid metric-Palatini theory inspired in some well known metric $f(R)$ models, the quadratic (Starobinsky) and exponential models. We devise a simple method to obtain the background evolution predicted by these models and show that the Palatini Ricci scalar evolves in an effective potential that, provided it has a minimum, will asymptotically settle in it and the models will behave as if they have an effective cosmological constant. Like the designer model, these tend to predict larger deviations from standard GR in the distant past.

We then use a Metropolis-Hasting MCMC algorithm to test the models against background observables alone, including the shift parameter of the CMB, baryonic acoustic oscillations and supernova luminosity-redshift information. We constrain the value of $f_{\mathcal{R}}(z_i \approx 10^8)$ with an upper bound of approximately 10^{-2}, comparable to the constraints obtained in Chapter 5 using cosmological observables. Furthermore, we note that the results we obtain are well within the allowed bounds placed on modifications of scalar-tensor theories of gravity at early-times coming from big bang nucleosynthesis and CMB [239, 240], since the background data we employ allows a deviation of the effective gravitational constant from its Newtonian value, $G_{\rm eff}/G$, of at most 1%.

Summing up, we have seen that the scalar degree of freedom introduced by the modified gravity theories we have studied in this thesis acts as a mediator of an additional fifth force that can modify the observable structure of our Universe. On the smallest scales, these modifications are extremely constrained by Solar system tests, demanding the existence of a screening mechanism that suppresses the extra interaction. However, on cosmological scales, changes to the evolution of the linearized Einstein equations can lead to different clustering patterns of the large scale structure, modify the growth rate of cosmological structure or even impact the propagation of traveling photons.

Therefore, in an epoch when so many surveys are being prepared with the intention of testing gravity on the largest scales, it is imperative to understand

exactly how these theories actually modify our observable Universe and what are the perspectives of constraining them. For instance, we have seen that, despite being a considerable challenge, it is possible to obtain cosmological constraints on the Brans-Dicke parameter $w_{\rm BD}$ that are competitive with the Solar system ones. On the other hand, on the metric $f(R)$ theories, from a weak lensing standpoint alone, it may be hard to improve on the already existing constraints with the accuracy we expect the Euclid survey to have. And, using the novel hybrid metric-Palatini theory, we have seen that the upcoming 21-cm data should be able to provide tight constraints over early-time modifications of gravity.

All the theories studied in this work fail, however, in one crucial aspect, and that is in providing a genuine self-accelerating alternative to the standard cosmological scenario. Despite being able to mimic ΛCDM perfectly at the background level, this is always done at the expense of a bare cosmological constant or a scalar potential. Moving forward, it is important to also focus on theories that are able to achieve acceleration from the gravitational modifications they actually introduce. Future work is already being developed in different collaborations on such theories such as the complete Brans-Dicke gravity [242] and the new gravitational scalar-tensor theories introduced in [243], with the intention of continuing to provide a clear understanding of how gravity can be modified and to what extent that may be done, if proven necessary.

Appendix A

Correction factor for V(ϕ)

In this appendix we show the correction factor one can add to the potential $V(\phi)$ in order to balance the scalar field dynamics in the exact numerical evolution of ρ_ϕ in order to recover a flat Universe today. Effectively, we want to solve the equation

$$-\frac{\phi'(a_0)}{\phi(a_0)}+\frac{\omega_{\rm BD}}{6}\left(\frac{\phi'(a_0)}{\phi(a_0)}\right)^2+\frac{1-D\Omega_{\rm m}}{\phi(a_0)}=(1-\Omega_{\rm m}), \tag{A.1}$$

where $a_0 = 1$ and D will be the correction factor such that $1 - D\Omega_{\rm m} \equiv \overline{\Omega}_\phi$, as discussed in Sec. 2.2. First we show that factor using our solution for $w_{\rm eff} = -1$ using Eq. (2.22):

$$D=\frac{1}{\Omega_{\rm m}}+K\frac{\left[3d\left(\Omega_{\rm m}-2\right)\left(8-6\Omega_{\rm m}+d\left(2-\Omega_{\rm m}\right)\left(1-\Omega_{\rm m}\right)\right)+2\omega_{\rm BD}\left(4-3\Omega_{\rm m}\right)^2\right]}{3\Omega_{\rm m}d^2\left(\Omega_{\rm m}-2\right)^2}, \tag{A.2}$$

where $K = \frac{\phi(a_i)g(a_0)}{g(a_i)}$, and $g(a)$ is defined in Eq. (2.23); $\phi(a_i)$ is the value of the scalar field at the starting redshift a_i. The parameter d is equal to $2\omega_{\rm BD} + 3$.

For the case $w_{\rm eff} > -1$, we use the late-time solution for ϕ given by Eq. (2.26):

$$\begin{aligned} D &= \frac{1}{\Omega_{\rm m}} - \frac{cd}{\Omega_{\rm m}}\left(\frac{1-\Omega_{\rm m}}{d} + \frac{3\sqrt{6}\sqrt{1-\Omega_{\rm m}}\,(1+w_{\rm eff})^{3/2}}{d\,(-2+3d\,(1+w_{\rm eff}))}\right. \\ &- \left.\frac{9\omega_{\rm BD}\,(1-\Omega_{\rm m})\,(1+w_{\rm eff})^{3}}{(2-3d\,(1+w_{\rm eff}))^{2}}\right), \end{aligned} \tag{A.3}$$

where $c = \phi(a_i)f(a_0)/f(a_i)$, and $f(a)$ is defined by Eq. (2.27).

Appendix B

Jordan frame perturbation equations

For completeness, we show here some of the components used for deriving the results presented in Section 6.1. The perturbations to the geometric quantities are unmodified in the hybrid metric-Palatini theory. Hence, as in standard GR, for the Christoffel symbols we have:

$$\delta\Gamma^0_{00} = \dot{A}Y, \quad \delta\Gamma^0_{0j} = -\left[kA + \mathcal{H}B\right]Y_j, \tag{B.1}$$

$$\begin{aligned}\delta\Gamma^0_{ij} &= \left[-\mathcal{H}A + \frac{k}{3}B + 2\mathcal{H}H_L + \dot{H}_L\right]\gamma_{ij}Y \\ &\quad + \left[-kB + 2\mathcal{H}H_T + \dot{H}_T\right]Y_{ij},\end{aligned} \tag{B.2}$$

$$\delta\Gamma^j_{00} = -\left[kA + \dot{B} + \mathcal{H}B\right]Y^j, \tag{B.3}$$

$$\delta\Gamma^i_{0j} = \dot{H}_L\delta^i_j Y + \dot{H}_T Y^i_j, \tag{B.4}$$

$$\begin{aligned}\delta\Gamma^i_{jk} &= -kH_L\left(\delta^i_j Y_k + \delta^i_k Y_j - \delta_{jk}Y^i\right) + \mathcal{H}B\gamma_{jk}Y^i \\ &\quad + H_T\left(Y^i_{j,k} + Y^i_{k,j} - Y^{,i}_{jk}\right).\end{aligned} \tag{B.5}$$

As for the Ricci scalar and the Ricci tensor, we have

$$\begin{aligned}
\delta R &= \frac{2}{a^2}\Bigg[-6\frac{\ddot{a}}{a}A - 3\mathcal{H}\dot{A} + k^2 A + k\dot{B} + 3k\mathcal{H}B + 9\mathcal{H}\dot{H}_L + 3\ddot{H}_L \\
&\quad +2k^2\left(H_L + \frac{H_T}{3}\right)\Bigg]Y, \qquad \text{(B.6)} \\
\delta R_{00} &= -\left[k^2 A - 3\mathcal{H}\dot{A} + k\left(\dot{B} + \mathcal{H}B\right) + 3\ddot{H}_L + 3\mathcal{H}\dot{H}_L\right]Y, \qquad \text{(B.7)} \\
\delta R_{jk} &= \Bigg[-2A\left(\frac{\ddot{a}}{a} + \mathcal{H}^2\right) - \mathcal{H}\dot{A} + \frac{k^2}{3}A + \frac{k}{3}\left(\dot{B} + 5\mathcal{H}B\right) + \ddot{H}_L + 5\mathcal{H}\dot{H}_L \\
&\quad +2\left(\frac{\ddot{a}}{a} + \mathcal{H}^2\right)H_L + \frac{4k^2}{3}\left(H_L + \frac{H_T}{3}\right)\Bigg]\delta_{jk}Y \\
&\quad +\Bigg[-k^2 A - k\left(\dot{B} + \mathcal{H}B\right) + \ddot{H}_T + \mathcal{H}\dot{H}_T + 2\left(\frac{\ddot{a}}{a} + \mathcal{H}^2\right)H_T \\
&\quad -k^2\left(H_L + \frac{H_T}{3}\right) + \mathcal{H}\left(\dot{H}_T - kB\right)\Bigg]Y_{jk}, \qquad \text{(B.8)} \\
\delta R_{0j} &= \left[-\left(\frac{\ddot{a}}{a} + \mathcal{H}^2\right)B - 2k\mathcal{H}A + 2k\dot{H}_L + \frac{2}{3}k\dot{H}_T\right]Y_j \qquad \text{(B.9)}
\end{aligned}$$

The main additional components come from the perturbations to the covariant derivatives of ϕ that appear in eq. (4.15)

$$\delta\left(\nabla_\mu\nabla_\nu\phi\right) = \nabla_\mu\nabla_\nu\delta\phi - \delta\Gamma^\alpha_{\mu\nu}\partial_\alpha\phi \qquad \text{(B.10)}$$

$$\delta\left(\nabla^\mu\nabla_\nu\phi\right) = \nabla^\mu\nabla_\nu\delta\phi - \delta g^{\mu\alpha}\nabla_\alpha\nabla_\nu\phi - g^{\mu\alpha}\delta\Gamma^\beta_{\alpha\nu}\partial_\beta\phi \qquad \text{(B.11)}$$

We are considering our scalar degree of freedom to be a function such that $\phi = \phi\left(t\right) + \delta\phi\left(x,t\right)$, and so we get

$$\delta\left(\nabla^i\nabla_i\phi\right) = \frac{Y}{a^2}\left[-k^2\delta\phi - 3\mathcal{H}\dot{\delta\phi} + \dot{\phi}\left(6\mathcal{H}A - kB - 3\dot{H}_L\right)\right] \tag{B.12}$$

$$\delta\left(\nabla^0\nabla_0\phi\right) = \frac{Y}{a^2}\left[-\ddot{\delta\phi} + \mathcal{H}\dot{\delta\phi} + 2\ddot{\phi}A - 2A\mathcal{H}\dot{\phi} + \dot{\phi}\dot{A}\right] \tag{B.13}$$

$$\delta\left(\nabla^0\nabla_i\phi\right) = \frac{Y_i}{a^2}\left[k\dot{\delta\phi} - \mathcal{H}k\delta\phi - kA\dot{\phi}\right] \tag{B.14}$$

$$\delta\left(\nabla^i\nabla_k\phi\right) = \frac{Y^i_k}{a^2}\left[k^2\delta\phi + \dot{\phi}\left(kB - \dot{H}_T\right)\right] \tag{B.15}$$

$$\begin{aligned}\delta\left(\nabla_i\nabla_j\phi\right) = \frac{\delta_{ij}Y}{a^2}&\left[-\frac{k^2}{3}\delta\phi - \mathcal{H}\dot{\delta\phi} + \dot{\phi}\left(2\mathcal{H}A - \frac{k}{3}B - 2\mathcal{H}H_L - \dot{H}_L\right)\right] \\ &+\frac{Y_{ij}}{a^2}\left[k^2\delta\phi + \dot{\phi}\left(kB - 2\mathcal{H}H_T - \dot{H}_T\right)\right]\end{aligned} \tag{B.16}$$

$$\delta\left(\nabla_0\nabla_j\phi\right) = \frac{Y_j}{a^2}\left[-k\dot{\delta\phi} + k\mathcal{H}\delta\phi + \dot{\phi}\left(kA + \mathcal{H}B\right)\right]. \tag{B.17}$$

Appendix C

Implementation in MGCAMB

In order to compute the CMB observables, we implement our early decaying modified gravity model in the publicly available MGCAMB code [241], a modified version of the also public CAMB code [205] that allows to study the effects of modified gravity models on the CMB through modifications of the linear equations describing the growth of perturbations. MGCAMB works by parameterizing the evolution of the gravitational potentials simply through two time- and scale-dependent functions: the ratio of the metric potentials $\gamma(a,k) \equiv \Phi/\Psi$ and the effective modified gravitational coupling in the Poisson equation, $\mu(a,k) = G_{\rm eff}/G$. The framework of MGCAMB is general enough to include possible early-time effects, hence it is well-suited for testing the hybrid metric-Palatini theory. Moreover, we chose to work with MGCAMB as it allows us to use the approximations described in Secs. 5.1.1 and 5.1.1 to improve computational efficiency without loss of accuracy.

We implement our model by modifying both γ and μ in the code. For γ we use the subhorizon approximation described in Eq. (5.10) and add an oscillatory term described by $\delta f_{\mathcal{R}}$ to account for the early-time oscillations. From Ref. [3] we note that the gravitational potentials can be expressed as

$$\Phi = \Phi_+ + \frac{\delta f_{\mathcal{R}}}{2(1+f_{\mathcal{R}})}\,, \quad \Psi = \Phi_+ - \frac{\delta f_{\mathcal{R}}}{2(1+f_{\mathcal{R}})}\,, \tag{C.1}$$

which uses the observation that the early-time oscillations in $\delta f_{\mathcal{R}}$ do not affect the lensing potential Φ_+ for small-enough values of the amplitude of the oscillations. Φ_+ has an approximately constant value of unity throughout the

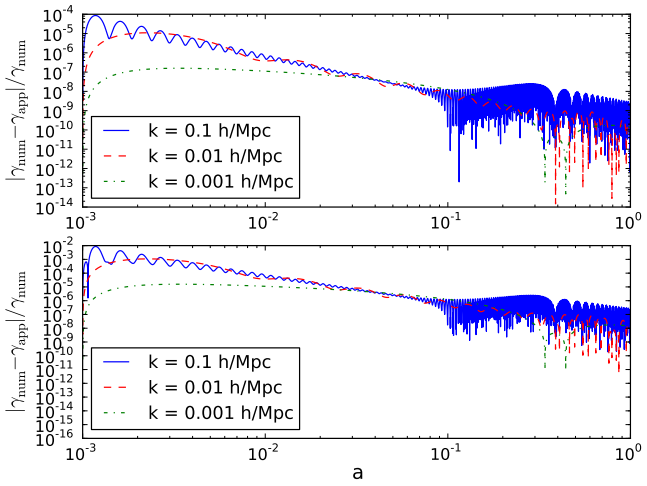

Figure C.1 *Relative difference between the numerical evolution of* $\gamma \equiv \Phi/\Psi$ *and the approximation in Eq. (C.2). The top panel shows* $|f_{\mathcal{R}\mathrm{i}}| = 10^{-4}$ *and the lower panel shows* $|f_{\mathcal{R}\mathrm{i}}| = 10^{-2}$*. We have again fixed* $\Omega_\mathrm{m} = 0.30$.

matter dominated era. Therefore, with $\Phi_+ \gg \delta f_\mathcal{R}$ one can perform a Taylor expansion on the ratio between the potentials that results in

$$\gamma = \frac{\Phi}{\Psi} \approx 1 - \frac{\delta f_\mathcal{R}}{(1 + f_\mathcal{R})}\,. \tag{C.2}$$

We compare this approximation against numerical results in Fig. C.1, finding good agreement between the two, at an accuracy comparable to that observed in Fig. 5.3 for the slip between the metric potentials. Given this result, we generalize γ_QS with the simple modification

$$\gamma_\mathrm{MG} \approx \gamma_\mathrm{QS} + \frac{\delta f_\mathcal{R}}{1 + f_\mathcal{R}}, \tag{C.3}$$

where γ_QS can be found in Eq. (5.10). Correspondingly, we modify μ to include the effect of the oscillations in the Poisson equation such that

$$\mu_\mathrm{MG} = \mu_\mathrm{QS} + \frac{\delta f_\mathcal{R}}{2(1 + f_\mathcal{R})}\,, \tag{C.4}$$

where μ_QS is given in Eq. (5.7).

Finally, note that the initial conditions required to solve for the background evolution of our models are always set at the redshift $z_\mathrm{i} = 1000$. As described

in Secs. 5.1.2 and 5.1.3 through an embedding in the effective field theory of Horndeski gravity, the model is designed to behave as ΛCDM at the level of linear perturbations down to a redshift $z_{\rm on}$, at which point the modifications are introduced. At redshift $z_{\rm i}$ we set $\delta f_{\mathcal{R}} = 0$, with its subsequent evolution being determined by Eq. (5.14).

C.1 Analytic solution for the integrated spring term

Using Eq. (5.15), we can simplify the w term of Eq. (5.14) as

$$w \approx \left[\frac{k^2 a^{-2}}{H_0^2 E} + \frac{\left(a_{\rm aux} - \sqrt{d}\right)^2}{2} + \frac{\Omega_{\rm m}}{\Omega_{\rm m} + \Omega_\Lambda a^3} \right]^{1/2} , \tag{C.5}$$

where we have neglected the presence of radiation in the Hubble factor $H \equiv H_0\sqrt{E}$ since applying this approximation only for redshifts deep within the matter-dominated era. For $k \gg aH$, Eq. (C.5) can be further approximated by

$$w \approx \left(\frac{k^2}{a^2 H_0^2 E} \right)^{1/2} \left(1 + \frac{b a^2 H_0^2 E}{2k^2} \right) , \tag{C.6}$$

where $b = \left(a_{\rm aux} - \sqrt{d}\right)^2 /2 + \Omega_{\rm m}/\left(\Omega_{\rm m} + \Omega_\Lambda a^3\right)$, which allows us to perform an analytic integration of Eq. (5.14). The result depends on hypergeometric functions that can, however, be approximated as unity. For simplicity, we therefore present the result without the presence of these functions:

$$\begin{aligned} \int w d\ln a \;\approx 2\; & \left(\frac{k^2 a}{H_0^2 \Omega_{\rm m}} \right)^{1/2} + \frac{\left[a_{\rm aux} - \sqrt{d}\right]^2}{4} \left(\frac{\Omega_{\rm m} H_0^2}{k^2 a} \right)^{1/2} \left(\sqrt{\frac{\Omega_{\rm m}}{\Omega_\Lambda} a^3 + 1} - 3 \right) \\ & - \Omega_{\rm m} \left(\frac{H_0^2}{k^2 a} \right)^{1/2} . \end{aligned} \tag{C.7}$$

In the limit of $k \ll aH$, we can instead approximate w as

$$w \approx \sqrt{b} \left(1 + \frac{1}{2} \frac{k^2}{a^2 H_0^2 E b} \right) . \tag{C.8}$$

To perform an analytic integration, we use the approximation $b \approx 1/2 \left(a_{\rm aux} - \sqrt{d}\right)^2 + 1$, which results in

$$\int w d \ln a \approx \sqrt{b} + \frac{1}{2\sqrt{b}} \frac{k^2 a}{H_0^2 \Omega_{\rm m}} \,. \tag{C.9}$$

We compare the implementation of the approximations in Eqs. (C.8) and (C.9) against numerical results in Fig. 5.3, finding good agreement between the two.

Bibliography

[1] N. A. Lima and P. G. Ferreira, JCAP **01**, 10 (2016).

[2] N. A. Lima and A. R. Liddle, Phys. Rev. D **88**, 043521 (2013).

[3] N. A. Lima, Phys. Rev. D **89**, 083527 (2014).

[4] N. A. Lima, V.-S. Barreto, and L. Lombriser, Phys. Rev. D **94**, 083507 (2016).

[5] N. A. Lima and V.-S. Barreto, Astroph. J. **818**, 186 (2016).

[6] A. Einstein, Annalen der Physik **49**, 769 (1916).

[7] S. S. Shapiro, J. L. Davis, D. E. Lebach, and J. S. Gregory, Phys. Rev. Lett. **92**, 121101 (2004).

[8] S. B. Lambert and C. L. Poncin-Lafitte, A&A **499**, 331 (2009).

[9] S. B. Lambert and C. L. Poncin-Lafitte, **529**, A70 (2011).

[10] B. Bertotti, L. Iess, and P. Tortora, Nature **425**, 374 (2003).

[11] G. M. Clemence, Rev. Mod. Phys. **19**, 361 (1947).

[12] A. P. Abbott *et al.*, Phys. Rev. Lett. **116**, 061102 (2016).

[13] C. M. Will, Liv. Rev. Rel. **17**, 4 (2014).

[14] C. M. Will, ApJ **163**, 611 (1971).

[15] C. M. Will, ApJ **177**, 757 (1972).

[16] C. M. Will, (Cambridge University Press, New York, 1993).

[17] I. I. Shapiro, Phys. Rev. Lett. **13**, 789 (1964).

[18] H. M. Antia, S. M. Chitre, and D. O. Gough, A&A **477**, 657 (2008).

[19] A. S. Konopliv, S. W. Asmar, W. M. Folkner, O. Karatekin, D. C. Nunes, S. E. Smrekar, C. F. Yoder, and T. M. Zuber, Icarus **211**, 401 (2011).

[20] A. G. Riess *et al.*, Astron. J. **116**, 1009 (1998).

[21] S. Perlmutter *et al.*, Astrophy. J. **517**, 565 (1999).

[22] A. G. Riess *et al.*, Astroph. J. **659**, 98 (2007).

[23] R. Amanullah *et al.*, Astroph. J. **716**, 712 (2010).

[24] J. R. G. III *et al.*, ApJ **624**, 463 (2005).

[25] 2dF Galaxy Team, "The 2df galaxy redshift survey," `http://www.2dfgrs.net/` (2004).

[26] O. Lahav, Liv. Rev. Rel. **7**, 8 (2004).

[27] D. G. York *et al.*, The Astronomical Journal **120**, 1579 (2000).

[28] F. S. Labini, N. L. Vasilyev, L. Pietronero, and Y. V. Baryshev, Europhys. Lett. **86**, 49001 (2009).

[29] M. Scrimgeour, T. Davis, and C. Blake, MNRAS **425**, 116 (2012).

[30] Planck Collaboration, arXiv e-prints (2015), arXiv:1507.02704 .

[31] C. L. Bennett *et al.*, ApJ. Supp. Series **148**, 1 (2003).

[32] M. Tegmark *et al.*, ApJ **606**, 702 (2004).

[33] P. Ade *et al.*, arXiv e-prints (2015), arXiv:1502.01582 .

[34] S. Weinberg, Rev. Mod. Phys. **61:1-23** (1989).

[35] T. Padmanabhan, Phys. Rept. **380**, 235 (2003).

[36] A. Padilla, arXiv e-prints (2015), arXiv:1502.05296 .

[37] E. J. Copeland, M. Sami, and S. Tsujikawa, Int. J. Mod. Phys. D **15:1753-1936** (2006).

[38] R. R. Caldwell, R. Dave, and P. J. Steinhardt, Phys. Rev. Lett **80**, 1582 (1998).

[39] R. R. Caldwell and E. V. Linder, Phys. Rev. Lett **95**, 141301 (2005).

[40] C. Wetterich, A&A **303**, 321 (1995).

[41] E. J. Copeland, A. R. Liddle, and D. Wands, Phys. Rev. D **57**, 4686 (1998).

[42] B. Ratra and P. J. E. Peebles, Phys. Rev. D **37**, 3406 (1988).

[43] T. Chiba, T. Okabe, and M. Yamaguchi, Phys. Rev. D **62**, 023511 (2000).

[44] C. Armendariz-Picon, V. F. Mukhanov, and P. J. Steinhardt, Phys. Rev. D **63**, 103510 (2001).

[45] G. Dvali, G. Gabadadze, and M. Porrati, Phys. Lett. B **485**, 208 (2000).

[46] C. Deayet, Phys. Lett. B **502**, 199 (2001).

[47] C. Deayet, G. R. Dvali, and G. Gabadadze, Phys. Rev. D **65**, 044023 (2002).

[48] M. A. Luty, M. Porrati, and R. Rattazzi, JHEP **0309**, 029 (2003).

[49] D. Gorbunov, K. Koyama, and S. Sibiryakov, Phys. Rev. D **73**, 044016 (2006).

[50] K. Koyama, Phys. Rev. D **72**, 123511 (2009).

[51] C. de Rham and G. Gabadadze, Phys. Rev. D **82**, 044020 (2010).

[52] C. de Rham, G. Gabadadze, and A. J. Tolley, Phys. Rev. Lett. **106**, 231101 (2011).

[53] S. F. Hassan and R. A. Rosen, Phys. Rev. Lett. **108**, 041101 (2012).

[54] T. Clifton, P. G. Ferreira, A. Padilla, and C. Skordis, Phys. Rept. **513**, 1 (2012).

[55] A. Joyce, L. Lombriser, and F. Schmidt, arXiv e-prints (2016), arXiv:1601.06133 .

[56] C. H. Brans and R. H. Dicke, Phys. Rev. **124**, 925 (1961).

[57] T. P. Sotiriou and V. Faraoni, Rev. Mod. Phys. **82**, 451 (2010).

[58] P. Brax, A.-C. Davis, B. Li, and H. A. Winther, Phys. Rev. D **86**, 044015 (2012).

[59] J. Khoury and A. Weltman, Phys. Rev. Lett. **93**, 171104 (2004).

[60] J. Khoury and A. Weltman, Phys. Rev. D **69**, 044026 (2004).

[61] K. Hinterbichler and J. Khoury, Phys. Rev. Lett. **104**, 231301 (2010).

[62] E. Babichev, C. Deayet, and R. Ziour, Int. J. Mod. Phys. D **18**, 2147 (2009).

[63] A. I. Vainshtein, Phys. Lett. B **39**, 393 (1972).

[64] A. Nicolis, R. Rattazzi, and E. Trincherini, Phys. Rev. D **79**, 064036 (2009).

[65] G. W. Horndeski, Int.J.Theor.Phys. **10**, 363 (1974).

[66] L. Lombriser, F. Simpson, and A. Mead, Phys. Rev. Lett. **114**, 251101 (2015).

[67] L. Lombriser and A. Taylor, JCAP **1511**, 040 (2015).

[68] J. Khoury and A. Weltman, Phys. Rev. Lett. **93** (2004).

[69] L. Lombriser and N. A. Lima, arXiv e-prints (2016), arXiv:1602.07670 .

[70] E. V. Linder, Rept. Prog. Phys. **71**, 056901 (2008).

[71] A. Silvestri and M. Trodden, Rept. Prog. Phys. **72**, 096901 (2009).

[72] A. Joyce, B. Jain, J. Khoury, and M. Trodden, Phys. Rept. **568**, 1 (2015).

[73] W. Hu and M. J. White, ApJ **471**, 30 (1996).

[74] D. J. Eisenstein and W. Hu, ApJ **496**, 605 (1998).

[75] C. Blake and K. Glazebrook, ApJ **594**, 665 (2003).

[76] D. J. Eisenstein *et al.*, ApJ **633**, 560 (2005).

[77] F. Beutler *et al.*, Mon. Not. Roy. Astron. Soc. **416**, 3017 (2011).

[78] L. Anderson *et al.*, Mon. Not. Roy. Astron. Soc. **428**, 1036 (2013).

[79] B. Boisseau, Esposito-Ferése, D. Polarski, and A. A. Starobinski, Phys. Rev. Lett. **85**, 2236 (2000).

[80] S. Tsujikawa, Phys. Rev. D **76**, 023514 (2007).

[81] E. Bertschinger, ApJ **648**, 797 (2006).

[82] E. V. Linder, Phys. Rev. D **72**, 043529 (2005).

[83] M. Ishak, A. Upadhye, and D. N. Spergel, Phys. Rev. D **74**, 043513 (2006).

[84] R. Caldwell, A. Cooray, and A. Melchiorri, Phys. Rev. D **76**, 023507 (2007).

[85] L. Amendola, M. Kunz, and D. Sapone, JCAP **0804**, 013 (2008).

[86] L. Pogosian, A. Silvestri, K. Koyama, and G.-B. Zhao, Phys. Rev. D **81**, 104023 (2010).

[87] L. Pogosian and A. Silvestri, arXiv e-prints (2016), arXiv:1606.05339 .

[88] A. Hojjati, G.-B. Zhao, L. Pogosian, A. Silvestri, R. Crittenden, and K. Koyama, Phys. Rev. D **85** (2012).

[89] S. Asaba, C. Hikage, K. Koyama, G.-B. Zhao, A. Hojjati, and L. Pogosian, JCAP **1308**, 029 (2013).

[90] R. K. Sachs and A. M. Wolfe, ApJ **147**, 73 (1967).

[91] L. Amendola *et al.*, Liv. Rev. Rel. **16**, 6 (2012).

[92] M. Kilbinger, Rep. Prog. Phys. **78**, 086901 (2015).

[93] M. White and C. S. Kochanek, ApJ **560**, 539 (2001).

[94] O. Doré *et al.*, arXiv e-prints arXiv:0712.1599 .

[95] F. Simpson *et al.*, MNRAS **429**, 2249 (2013).

[96] N. Kaiser, MNRAS **227**, 1 (1987).

[97] A. J. S. Hamilton, arXiv (1997), astro-ph/9708102 .

[98] W. J. Percival *et al.*, MNRAS **353**, 1201 (2004).

[99] M. Tegmark *et al.*, Phys. Rev. D **74**, 123507 (2006).

[100] C. Blake *et al.*, MNRAS **436**, 3089 (2013).

[101] Y.-S. Song and O. Dore, JCAP **0903**, 025 (2009).

[102] P. Zhang, M. Liguori, R. Bean, and S. Dodelson, Phys. Rev. Lett **99**, 141302 (2007).

[103] LSST Dark Energy Science Collaboration, arXiv e-prints (2012), arXiv:1211.0310 .

[104] Y.-Seon and K. Koyama, JCAP **0901**, 048 (2009).

[105] S. F. Daniel, E. V. Linder, T. L. Smith, R. R. Caldwell, A. Cooray, *et al.*, Phys. Rev. D **81**, 123508 (2010).

[106] G.-B. Zhao, T. Giannantonio, L. Pogosian, A. Silvestri, D. J. Bacon, and other, Phys. Rev. D **81**, 103510 (2010).

[107] Y.-S. Song, G.-B. Zhao, D. Bacon, K. Koyama, R. C. Nichol, *et al.*, Phys. Rev. D **84**, 083523 (2011).

[108] F. Simpson, C. Heymans, D. Parkinson, C. Blake, M. Kilbinger, *et al.*, MNRAS **429**, 2249 (2013).

[109] P. A. R. Ade *et al.* (Planck collaboration), arXiv e-prints (2015), arXiv:1502.01590 .

[110] J. Liu and J. C. Hill, Phys. Rev. D **92**, 063517 (2015).

[111] D. Spergel *et al.*, arXiv e-prints (2013), arXiv:1305.5422 .

[112] R. Maartens, F. B. Abdalla, M. Jarvis, and M. G. Santos, arXiv e-prints (2015), arXiv:1501.04076v1 .

[113] T. Baker, P. G. Ferreira, and C. Skordis, Phys. Rev. D **87**, 024015 (2013).

[114] R. A. Battye and J. A. Pearson, JCAP **1207**, 019 (2012).

[115] G. Gubitosi, F. Piazza, and F. Vernizzi, JCAP **1302**, 032 (2013).

[116] J. Gleyzes, D. Langlois, F. Piazza, and F. Vernizzi, JCAP **1308**, 025 (2013).

[117] C. H. Brans and R. H. Dicke, Phys. Rev. **124**, 925 (1961).

[118] P. G. Bergmann, Int. J. Theor. Phys. **1**, 25 (1968).

[119] J. Nordtvedt, Astroph. J. **161**, 1059 (1970).

[120] R. V. Wagoner, Phys. Rev. D **1**, 3209 (1970).

[121] J. D. Bekenstein, Phys. Rev. D **15**, 1458 (1977).

[122] J. D. Bekenstein and A. Meisels, Phys. Rev. D **18**, 4378 (1978).

[123] N. Banerjee and D. Pavon, Phys. Rev. D **63**, 043504 (2001).

[124] A. A. Sen, S. Sen, and S. Sethi, Phys. Rev. D **63**, 107501 (2001).

[125] C. M. Will, Liv. Rel. Rev. **9**, 3 (2006).

[126] B. Bertotti, L. Iess, and P. Tortora, Nature **425**, 374 (2003).

[127] Y.-C. Li, F.-Q. Wu, and X. Chen, Phys. Rev. D **88**, 084053 (2013).

[128] A. Avilez and C. Skordis, Phys. Rev. Lett. **113**, 011101 (2014).

[129] O. Bertolami and P. J. Martins, Phys. Rev. D **61**, 064007 (2000).

[130] M. K. Mak and T. Harko, Europhys. Lett. **60**, 155 (2002).

[131] S. Sen and A. A. Sen, Phys. Rev. D **63**, 124006 (2001).

[132] W. Chakraborty and U. Debnath, Int. J. Theor. Phys. **48**, 232 (2008).

[133] J. P. Uzan, Phys. Rev. D **59**, 123510 (1999).

[134] N. Bartolo and M. Pietroni, Phys. Rev. D **61**, 023518 (1999).

[135] A. R. Liddle and R. J. Scherrer, Phys. Rev. D **59**, 023509 (1998).

[136] C. Santos and R. Gregory, Ann. Phys. **258**, 111 (1997).

[137] D. S. Salopek, J. R. Bond, and J. M. Bardeen, Phys. Rev. D **40**, 1753 (1989).

[138] H. Nariai, Prog. of Theor. Phys. **40**, 49 (1968).

[139] H. Nariai, Prog. of Theor. Phys. **42**, 544 (1969).

[140] L. E. Gure-vich, A. M. Finkelstein, and V. A. Ruban, Astrophys. Space Sci. **98**, 101 (1973).

[141] T. Clifton, D. F. Mota, and J. D. Barrow, MNRAS **358**, 601 (2005).

[142] A. R. Liddle, A. Mazumdar, and J. D. Barrow, Phys. Rev. D **58**, 027302 (1998).

[143] V. Acquaviva and L. Verde, JCAP **12**, 001 (2007).

[144] A. D. Felice, T. Kobayashi, and S. Tsujikawa, Phys. Lett. B **706**, 123 (2011).

[145] S. Tsujikawa, Phys. Rev. D **76**, 023514 (2007).

[146] T. Baker, P. G. Ferreira, and C. Skordis, Phys. Rev. D **89**, 024026 (2014).

[147] C. D. Leonard, T. Baker, and P. G. Ferreira, Phys. Rev. D **91**, 083504 (2015).

[148] R. P. Woodard, Lect. Notes Phys. **720**, 403 (2007).

[149] R. P. Woodard, Lect. Notes Phys. **720**, 403 (2007).

[150] D. Langlois and K. Noui, JCAP **02**, 34 (2016).

[151] I. Ayuso, J. B. Jimenez, and A. C. Dombriz, Phys. Rev. D **91**, 104003 (2014).

[152] A. A. Starobinsky, Phys. Lett. B **91**, 90 (1980).

[153] S. Capozziello, S. Nojiri, S. D. Odintsov, and A. Troisi, Phys. Lett. B **639**, 135 (2006).

[154] S. Nojiri and S. D. Odintsov, Int. J. Geom. Meth. Mod. Phys. **4**, 115 (2007).

[155] G. Cognola, E. Elizalde, S. Nojiri, S. D. Odintsov, L. Sebastiani, and S. Zerbini, Phys. Rev. D **77**, 046009 (2008).

[156] J.-h. He and B. Wang, Phys. Rev. D **87**, 023508 (2013).

[157] A. A. Starobinsky, JETP Lett. **86**, 157 (2007).

[158] W. Hu and I. Sawicki, Phys. Rev. D **76**, 064004 (2007).

[159] L. Jaime, M. Salgado, and L. Patino, Springer Proc. Phys. **157**, 363 (2012).

[160] Y.-S. Song, W. Hu, and I. Sawicki, Phys. Rev. D **75**, 044004 (2007).

[161] R. Bean, D. Bernat, L. Pogosian, A. Silvestri, and M. Trodden, Phys. Rev. D **75**, 064020 (2007).

[162] L. Pogosian and A. Silvestri, Phys. Rev. D **77**, 023503 (2008).

[163] B. Li and J. D. Barrow, Phys. Rev. D **75**, 084010 (2007).

[164] A. de la Cruz-Dombriz, A. Dobado, and A. L. Maroto, Phys. Rev. D **77**, 123515 (2008).

[165] S. Tsujikawa, R. Gannouji, B. Moraes, and D. Polarski, Phys. Rev. D **80**, 084044 (2009).

[166] R. Gannouji, B. Moraes, D. F. Mota, D. Polarski, S. Tsujikawa, and H. A. Winther, Phys. Rev. D **82**, 124006 (2010).

[167] A. Hojjati, L. Pogosian, A. Silvestri, and S. Talbot, Phys. Rev. D **86**, 123503 (2012).

[168] T. Abbott *et al.* (Dark Energy Survey Collaboration), arXiv e-prints (2005), arXiv:astro-ph/0510346 .

[169] L. Jaime, L. Patino, and M. Salgado, arXiv e-prints (2012), arXiv:1206.1642 .

[170] D. Wands, Class. Quant. Grav. **11**, 269 (1994).

[171] T. P. Sotiriou, Class. Quant. Grav. **23**, 5117 (2006).

[172] D. J. Fixsen and J. C. Mather, Astroph. J. **581**, 817 (2002).

[173] N. Jarosik *et al.*, Astroph. J. Supp. Series **192**, 14 (2011).

[174] S. Capozziello and M. D. Laurentis, Phys. Rept. **509**, 167 (2011).

[175] L. Amendola, R. Gannouji, D. Polarski, and S. Tsujikawa, Phys. Rev. D **75**, 083504 (2007).

[176] L. Amendola, , D. Polarski, and S. Tsujikawa, Phys. Rev. Lett. **98**, 131302 (2007).

[177] G. J. Olmo, Phys. Rev. D **75**, 023511 (2007).

[178] T. Chiba, T. L. Smith, and A. L. Erickcek, Phys. Rev. D **75**, 124014 (2007).

[179] A. D. Dolgov and M. Kawasaki, Phys. Lett. B **573**, 1 (2003).

[180] A. Nunez and S. Solganik, arXiv e-prints (2004), arXiv:hep-th/0403159 .

[181] V. T. Gurovich and A. A. Starobinsky, Sov. Phys. JETP **50**, 844 (1979).

[182] L. Lombriser, A. Slosar, U. Seljak, and W. Hu, Phys. Rev. D **85**, 124038 (2012).

[183] B. Jain, V. Vikram, and J. Sakstein, JCAP **779**, 1 (2012).

[184] A. Hall, C. Bonvin, and A. Challinor, Phys. Rev. D **87**, 064026 (2013).

[185] S. Capozziello and M. D. Laurentis, Ann. Phys. **524**, 545 (2012).

[186] E. Elizalde, S. D. Odintsov, L. Sebastiani, and S. Zerbini, Eur. Phys. J. C **72**, 1843 (2012).

[187] K. Bamba, A. Lopez-Revelles, R. Myrzakulov, S. Odintsov, and L. Sebastiani, TSPU Bulletin **13:128**, 22 (2012).

[188] H. Motohashi, A. A. Starobinsky, and J. Yokoyama, Prog. of Theor. Phys. **123**, 5 (2010).

[189] T. Clifton, P. Dunsby, R. Goswami, and A. M. Nzioki, Phys. Rev. D **87**, 063517 (2013).

[190] A. L. Erickcek, N. Barnaby, C. Burrage, and Z. Huang, Phys. Rev. Lett. **110**, 171101 (2013).

[191] B. Li, W. A. Hellwing, K. Koyama, G.-B. Zhao, E. Jennings, and C. M. Baugh, MNRAS **428**, 743 (2012).

[192] T. Harko, T. S. Koivisto, F. S. N. Lobo, and G. J. Olmo, Phys. Rev. D **85**, 084016 (2012).

[193] S. Capozziello, T. Harko, F. S. N. Lobo, and G. J. Olmo, Int. J. Mod. Phys. D **22**, 1342006 (2013).

[194] E. E. Flanagan, Class. Quant. Grav. **21**, 417 (2003).

[195] G. J. Olmo and P. Singh, JCAP **0901**, 030 (2009).

[196] S. Capozziello, T. Harko, T. S. Koivisto, F. S. N. Lobo, and G. J. Olmo, JCAP **1304**, 011 (2013).

[197] S. Capozziello, T. Harko, T. S. Koivisto, F. S. N. Lobo, and G. J. Olmo, JCAP **07**, 024 (2013).

[198] T. S. Koivisto and N. Tamanini, Phys. Rev. D **87**, 104030 (2013).

[199] G. J. Olmo, Int. J. Mod. Phys. D **20**, 413 (2011).

[200] T. Koivisto and H. K.-Suonio, Class. Quant. Grav. **23**, 2355 (2006).

[201] L. Perivolaropoulos, Phys. Rev. D **81**, 047501 (2010).

[202] H. Kodama and M. Sasaki, Prog. Theor. Phys. Suppl. **78**, 1 (1984).

[203] C. P. Ma and E. Bertschinger, Astroph. J. **455**, 7 (1995).

[204] L. Pogosian and A. Silvestri, Phys. Rev. D **77**, 023503 (2008).

[205] A. Lewis, A. Challinor, and A. Lasenby, Astroph. J. **538**, 473 (2000).

[206] W. Hu and I. Sawicki, Phys. Rev. **D76**, 064004 (2007).

[207] P. Brax, C. van de Bruck, A.-C. Davis, and D. J. Shaw, Phys. Rev. **D78**, 104021 (2008).

[208] L. Lombriser, Annalen Phys. **526**, 259 (2014).

[209] J. Gleyzes, D. Langlois, and F. Vernizzi, Int. J. Mod. Phys. **D23**, 3010 (2014).

[210] A. Lewis and S. Bridle, Phys. Rev. D **66**, 103511 (2002).

[211] L. Lombriser and A. Taylor, Phys. Rev. Lett. **114**, 031101 (2015).

[212] L. Lombriser and A. Taylor, JCAP **1603**, 031 (2016).

[213] E. Bellini and I. Sawicki, JCAP **07**, 050 (2014).

[214] R. K. Sachs and A. M. Wolfe, ApJ **147**, 73 (1967).

[215] M. Betoule *et al.*, Astron. Astrophys. **568**, A22 (2014).

[216] A. G. Riess *et al.*, ApJ **730**, 119 (2011).

[217] F. Beutler *et al.*, Mon. Not. Roy. Astron. Soc. **416**, 3017 (2011).

[218] A. Ross *et al.*, Mon. Not. Roy. Astron. Soc. **449**, 835 (2015).

[219] L. Anderson *et al.*, MNRAS **441**, 24 (2013).

[220] E. Calabrese *et al.*, Phys. Rev. D **80**, 103516 (2009).

[221] P. Madau, A. Meiksin, and M. J. Rees, ApJ **475**, 429 (1997).

[222] P. Brax, S. Clesse, and A.-C. Davis, JCAP **1301**, 003 (2013).

[223] A. Hall, C. Bonvin, and A. Challinor, Phys. Rev. **D87**, 064026 (2013).

[224] B. F. Schutz, Nature **323**, 310 (1986).

[225] D. E. Holz and S. A. Hughes, Astrophys. J. **629**, 15 (2005).

[226] C. Cutler and D. E. Holz, Phys. Rev. **D80**, 104009 (2009).

[227] N. Tamanini, C. Caprini, E. Barausse, A. Sesana, A. Klein, and A. Petiteau, arXiv e-prints (2016), arXiv:1601.07112 .

[228] A. A. Starobinsky, JETP Lett. **86**, 157 (2007).

[229] R. P. Brent, *Algorithms for Minimization without Derivatives* (Prentice-Hall, 1972).

[230] N. Suzuki *et al.*, ApJ **746**, 85 (2012).

[231] R. Giostri *et al.*, JCAP **027**, 1203 (2012).

[232] D. Eisenstein *et al.*, Astrophys. J. **633**, 560 (2005).

[233] P. A. R. Ade *et al.*, A&A **571**, A16 (2013).

[234] N. Padmanabhan *et al.*, Mon. Not. Roy. Astron. Soc. **427**, 2132 (2012).

[235] Y. Wang and P. Mukherjee, Phys. Rev. D **76**, 103533 (2007).

[236] W. Hu and N. Sugiyama, ApJ **471**, 542 (1996).

[237] Y. Wang and S. Wang, Phys. Rev. D **88**, 043522 (2013).

[238] D. D. L. Minh and D. L. P. Minh, arXiv e-prints (2014), arXiv:1408.4438 .

[239] K. Umezu, K. Ichiki, and M. Yahiro, Phys. Rev. D **72**, 044010 (2005).

[240] S. Galli, A. Melchiorri, G. F. Smoot, and O. Zahn, Phys. Rev. D **80**, 023508 (2009).

[241] A. Hojjati, L. Pogosian, and G.-B. Zhao, JCAP **08**, 005 (2011).

[242] G. Kofinas, arXiv e-prints (2015), arXiv:1510.06845 .

[243] A. Naruko, D. Yoshida, and S. Mukohyama, Class. Quant. Grav. **33**, 9 (2015).